10

Keller, M., D. Bohnsack, R. Koch, M. Hinderer, J. Hornung, H. Al Ajmi, and B. Abu Amarah, 2019, Outcrop analog studies of the Wasia-Biyadh and Aruma aquifers in the Kingdom of Saudi Arabia, *in* H. R. AlAnzi, R. A. Rahmani, R. J. Steel and O. M. Soliman, eds., Siliciclastic reservoirs of the Arabian plate: AAPG Memoir 116, p. 317–382.

Outcrop Analog Studies of the Wasia–Biyadh and Aruma Aquifers in the Kingdom of Saudi Arabia

Martin Keller[1]

GeoZentrum Nordbayern, Universität Erlangen, Schlossgarten 5, D-91054 Erlangen (e-mail: martin.keller@fau.de)

Daniel Bohnsack[2] **and Roman Koch**

GeoZentrum Nordbayern, Universität Erlangen, Schlossgarten 5, D-91054 Erlangen (e-mail: daniel.bohnsack@web.de; roman.koch@fau.de)

Matthias Hinderer and Jens Hornung

Institut für Angewandte Geowissenschaften, TU Darmstadt, Schnittspahnstrasse 9, D-64287 Darmstadt (e-mail: hornung@geo.tu-darmstadt.de; hinderer@geo.tu-darmstadt.de)

Hussain Al Ajmi

Ministry of Environment, Water and Agriculture, Riyadh, KSA (e-mail: hussain.alajmi@yahoo.com)

Bassam Abu Amarah

Department of Geological Sciences, King Saud University, Riyadh, KSA (e-mail: babuamarah@ksu.edu.sa)

ABSTRACT

In recent years, outcrop analogue studies have become a powerful tool in sedimentology for the assessment of reservoirs, both in hydrocarbon and aquifer studies. Data from exploratory drilling campaigns can be augmented significantly by observations on the outcrop of the corresponding stratigraphical interval with the objective to validate the borehole information through direct observation. In addition, through the physical separation of the outcrop area and the subsurface, the increased spatial coverage of a reservoir and its equivalents provides additional information about facies and their changes and thus on reservoir properties.

This chapter presents results of a study on the Cretaceous sedimentary aquifers in Saudi Arabia (Wasia–Biyadh–Aruma) in order to better assess the storage volume of fossil groundwater, which is of fundamental importance for the hyper-arid kingdom.

Besides the regional 3-D stratigraphic framework, the focus was on measurements of porosity and permeability of approximately 150 samples and the interpretation of reservoir quality in terms of sedimentary facies and its diagenetic overprint. In general, both porosity

[1] *Current address: National Center for Water Research, Ministry of Environment, Water and Agriculture, Riyadh, KSA*

[2] *Current address: Department of Civil, Geo and Environmental Engineering, Technical University of Munich, Arcisstrasse 33, D-80333 Munich*

DOI:10.1306/13642171M1183514

and permeability are varying on a high level (Biyadh: 1–36% / 2100–6500 mD; Wasia: 3–42% / 2100–6500 mD; Aruma: 1–38% / 10^{-6}–0.15 Darcy). Apparently, the storage volume and hydraulics of these regional aquifers are controlled not only by their fracturing but also by their matrix porosity. Permeability varies by about an order of magnitude among samples or between vertical and horizontal permeability within some samples. This variation can be well explained by heterogeneity due to sedimentary facies, for example, cross-bedding and bioturbation. In some areas, the kind of cementation and its intensity have a large effect on the permeability. The data obtained enhance the quality of the hydraulic interpretations of this aquifer system.

Spectral gamma-ray logs proved to be useful for a regional correlation and the correlation of aquifers and aquicludes. This is based on the recognition of the major unconformities in the logs but also on the identification of various paleosol horizons, which regularly show high emissions of U and Th radionuclides. Intensive weathering during the Cretaceous is responsible for dominantly kaolinitic clay mineralogy and consequently negligible K emissions.

INTRODUCTION

In recent years, outcrop analogue studies have become a powerful tool in sedimentology for the assessment of reservoirs, both in hydrocarbon (e.g., Pöppelreiter et al., 2011; Koehrer et al., 2012; Obermaier et al., 2012, 2015) and aquifer studies (e.g., Hornung and Aigner, 1999, 2002a, b, 2004). Data from exploratory drilling campaigns can be augmented significantly by observations on the outcrop of the corresponding stratigraphical interval with the objective to validate the borehole information through direct observation. In addition, through the physical separation of the outcrop area and the subsurface, the increased spatial coverage of a reservoir and its equivalents provides additional information about facies and their changes and thus on reservoir properties.

A typical workflow starts with detailed lithologic logging of a section and the subsequent mapping of the facies across the outcrop. Together with bedding and bed forms, these are the basic elements of a 3-D architectural framework of the depositional environment. In addition, the spectral gamma-ray emissions are usually logged at an interval of 30 cm (12 in.). In a subsequent step, samples are taken for the measurement of porosity and permeability and for the detailed lithologic description of the sediment under the microscope.

The permeability and storage capacity for groundwater in siliciclastic sedimentary rocks are linked to the porosity of the rock and to a network of openings corresponding to bedding planes, joints, faults, and other fractures. Shape, spacing, number, and distribution of these are often controlled by the sedimentary facies and architecture (Gross et al., 1995; Gross, 2003; Di Naccio et al., 2005).

In carbonate rocks, karstification, dolomitization, diagenetic dissolution of carbonate minerals, and dissolution of evaporites are additional sources for porosity and may enhance the storage capacity significantly. Both small-scale and large-scale variations in sedimentary facies and architecture are of importance for the definition and zonation of hydrofacies units.

In recent years, the Ministry of Water and Electricity of the Kingdom of Saudi Arabia, now Ministry of Electricity, Water, and Agriculture, started to evaluate the entire groundwater resources of the kingdom, regardless whether they are trapped in principal or secondary aquifers and regardless of whether they are exploited presently or not. In this context, the main objective of the present study is to provide the geological and the hydraulic information from outcrops for the project: "Detailed Water Resources Studies of the Wasia–Biyadh and Aruma Aquifers, Kingdom of Saudi Arabia," carried out by GTZ/Dornier on behalf of the Ministry of Water and Electricity of Saudi Arabia. A detailed restudy and reinterpretation of the succession of the data given by Moshrif (1979, 1980, 1983), Vaslet et al. (1991) and Le Nindre et al. (2008) is beyond the scope of this study. Instead, their observations will be taken as a baseline and complemented by our own observations from those outcrops that are suitable for the purpose of this study. Consequently, only the most important lithologs are shown in this chapter, and their inventory is collated to the observations of Moshrif (1979, 1980, 1983), Vaslet et al. (1991) and Le Nindre et al. (2008).

METHODS

Fieldwork

Fieldwork was carried out mainly in the outcrops of the Cretaceous rock formations in the Ar Riyadh quadrangle. Outcrops of the Cretaceous in central Arabia

are already known from former investigations. Powers et al. (1966) and Le Nindre et al. (2008) provided a great number of GPS coordinates, which helped to access some of the more remote outcrops. Coordinates given by Philip et al. (2002) were used for outcrops of the Aruma Group. Additional sections were found through the evaluation of satellite images (Google Earth) and on the geological map of the Ar Riyadh quadrangle (Vaslet et al., 1991).

Field work was also carried out on the siliciclastic rocks in the Sakaka area (Figure 1). However, as these rocks are biostratigraphically poorly dated and as the

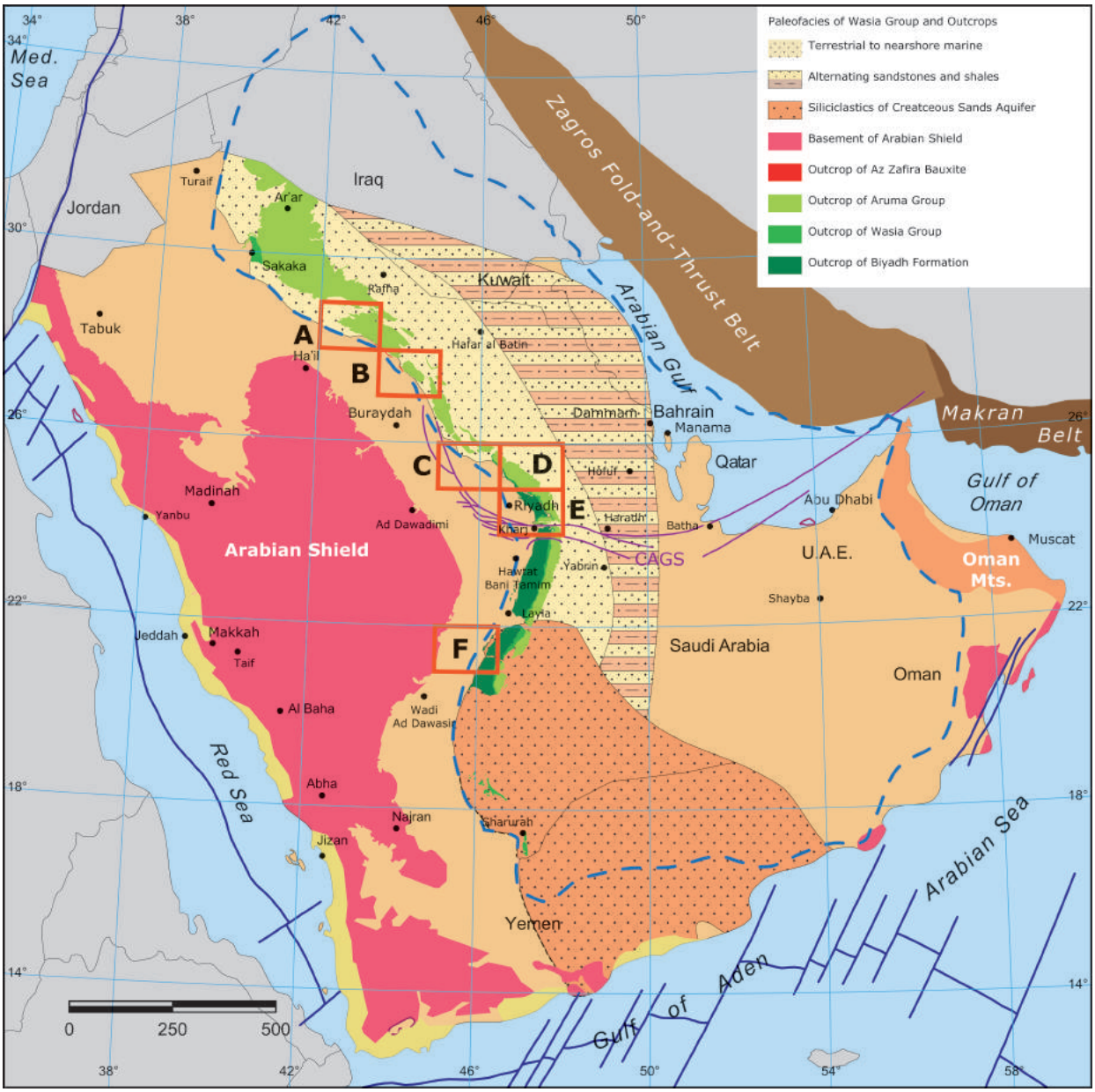

Figure 1. Plate-tectonic setting of the Arabian plate and paleogeography of the Wasia Group during the Aptian–Albian. The map shows the repeated (K100 MRS through K110 MRS of Sharland et al., 2001) easternmost progradation of the Wasia sands during maximum regression and the westernmost retrogradation of the finer siliciclastic sediment. The stacking of progradational and retrogradational sediments ("alternation of sandstones and shales") leads to a rapid decrease in the quality of the Wasia aquifer (modified from Davies et al., 2002). Area of the Wasia–Biyadh–Aruma groundwater project outlined in blue. A to F: Geological quadrangle maps mentioned in the text. A = Turabah; B = Qibah; C = Shaqra; D: Rumah; E = Riyadh; F = Sulayyimah. CAGS = Central Arabian Graben System.

facies cannot easily be correlated to those of the Ar Riyadh quadrangle, the results of the study in that area are not considered here.

Most of the outcrops are located at the prominent escarpments striking from northeast of Ar Riyadh toward the southeast near the Kharj area (Figure 2). The resistant ledge-forming cuestas of the Upper Cretaceous Aruma Group served as a protector for the poorly cemented siliciclastic rocks of the Wasia Group that are prone to erosion. Hence, the best preserved outcrops for logging vertical sections are located near these escarpments.

The sections were logged from the base to the top. Because of the slight dip of the strata toward the northeast (0.5°–2°), sections could be logged at different localities and later were combined to cover the entire formations.

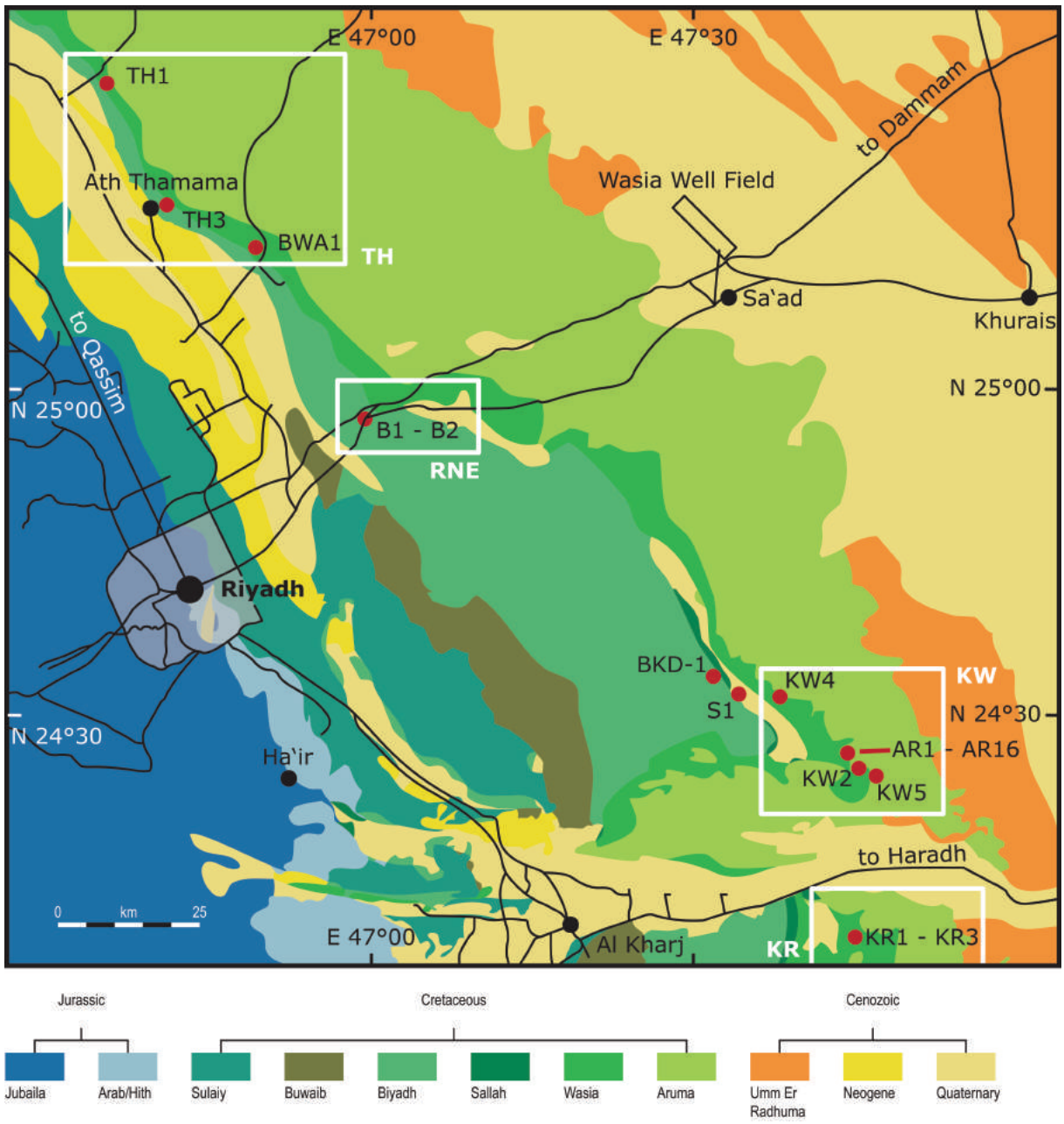

Figure 2. Geological map of the study area (Rumah and Riyadh quadrangles) and locations of sections. KR = Khushaym Radi area; KW = Khashm Wisi area; TH = Ath Thumama area; RNE = Sections northeast of Riyadh. Red dots indicate measured sections.

Gamma Radiation

General Remarks and Main Target of Investigation

The natural gamma radiation log (NGR) of rocks shows the sum of radioactive emissions of the different minerals constituting the succession. In sedimentary rocks, the most important elements are uranium (U), potassium (K), and thorium (Th). Their relative proportion, measured in the spectral gamma ray (SGR), and the corresponding peaks are frequently used to in the hydrocarbon industry to assess depositional environments and diagenesis (Schlumberger, 1982; Davies and Elliott, 1996; North and Boering, 1999; Ehrenberg and Svånå, 2001) as well as identification of major surfaces within the succession. Hence, SGR is one of the most reliable techniques in borehole geophysics to correlate certain types of rocks. In siliciclastic sedimentary rocks, it is also possible to determine the approximate grain size using the shale content as an indicator. However, the use of NGR measurement to estimate the "shaliness" of a formation is rather confusing. The real source of NGR is not clay or even shale, but rather corresponds to associated radioactive isotope concentrations (Ellis and Singer, 2007). These isotopes accumulate in the finer-grained fraction of the sediments. In general, the NGR can be used as an index for clay content and mean grain size of sedimentary deposits, respectively. One of the main problems in interpreting bulk gamma-ray measurements is the problem of interpretation. On the one hand, there are clays and shales with low or even no radioactivity, whereas on the other hand, "hot" dolomites occur, which exhibit relatively high radioactive decay. To overcome this problem, a SGR device was used, which measures the decay, and thus the energy levels, of K, Th, and U separately. According to these data, it is possible to recognize anomalies in formations with some unusual peaks in U, K, or Th, or a hot dolomite.

In general, most geophysical borehole investigations are executed by the use of a NGR tool that does not apply spectroscopy and produces an output of API (American Petroleum Institute) units. For reasons of correlation to borehole logs, the SGR data from measurements in outcrops were converted and plotted as API units. The relationship between the concentration of U, K, and Th and the total gamma-ray signal in API (γAPI) units is given following Ellis and Singer (2007):

$$\gamma\text{API} = 4\ \text{Th[ppm]} + 8\ \text{U[ppm]} + 16\ \text{K[\%(per weight)]}$$

The specific values of the individual spectra can be used to determine the respective type of sediment. An interesting possibility for the present study is the distinction of clay minerals based on the presence of K-radiation (kaolinite versus montmorillonite and illite).

In this study, the SGR was used to demonstrate the general trends of the logs of the individual formations in order to provide a basis for the application in wells drilled during the Wasia–Biyadh–Aruma groundwater project and to get an idea about the distribution of aquifers and aquitards in the subsurface. It is *not* intended to discuss in detail the origin of the peaks and to establish an internal detailed stratigraphy within the formations, as, for example, has been done by Ehrenberg and Svånå (2001).

Device and Measurement Methods

The portable radiation detector RS-230 BGO SuperSPEC (produced by Radiation Solutions Inc.) containing a 6.3 cu ins BGO detector was used for the field measurements. Following other outcrop analogue studies, the SGR measurements for this study were performed in selected sections with spacing of 30 cm (12 in.). The duration of the measuring time was set to 30 seconds. The detector of the device has to be pushed hard against the rock face during this period of time. Where necessary, the rock face was cleaned from interfering contaminants to avoid errors in measurements. In finer-grained successions, hand-dug trial pits were excavated to ensure accessibility to unweathered rock. The SGR log curves are attached to the lithologic logs discussed later.

Technical Problems and Possible Errors in Measurements

The basic requirement for a proper measurement is a precise stabilization with the radiation of the background (i.e., radiation of surrounding rock formations and other unknown sources). Without this stabilization, the data contains not only the radiation of the measured rock but also that of the background. During the field campaign, some technical problems occurred due to the extremely arid climate conditions in Saudi Arabia, and the lack in natural radiation background at the surface. Consequently, the obtained values may be systematically too high. The component responsible for stabilization contains a very sensitive electronics with susceptibility to high temperatures. Moreover, the relatively low background radiation led to some unclear stabilization problems. This may be due to a lack of finer-grained sediments in deserts and rare outcrops of rocks in the study area. These two factors were the reasons why the device occasionally could not be stabilized and the measurements had to be aborted and repeated.

Another possible source of error is the exposition of the measured rock face to weathering. Most of the investigated sections are composed of sedimentary rocks with high porosity and permeability. Hence, during the rare wet periods and rainfall, water-carrying impurities possibly infiltrated the rock. At some outcrops, the values of the measurements seemed to be unusual high for clean quartz arenites without any obvious traces of clay material. The inaccuracy of these data may be caused by clay, eroded from up section and infiltrated as suspension onto the face of the outcrop. To avoid this error, the rock face was scraped off if possible and the measurement was repeated. If the values remained high, the source of the radiation can be attributed reliably to the presence of heavy-mineral stringers in the sediments.

Sampling and Plugging

A number of samples were collected during the fieldwork for laboratory analyses on porosity and permeability. The samples were collected as hand specimens in the outcrop and later reprocessed by drilling and sawing to plugs of 4 × 4 cm (1.5 x 1.5 in.). Some of the friable sandstones were already destroyed during transport and others during analysis. Altogether, 168 samples of different Cretaceous formations were successfully prepared for subsequent laboratory analysis.

Porosity and Permeability Analysis

The measurements were performed in the laboratories of the Technical University of Darmstadt (TU Darmstadt). Whereas the measurement of rigid sample plugs of carbonates and well-cemented sandstones was easy to perform, the predominantly friable plugs of rather uncemented sandstones had to be handled with care. As the best aquifer properties are normally linked to the least consolidated sediments, the absence of data from these samples will generally introduce a bias toward lower values for both porosity and permeability.

Porosity Analysis

The total porosity can be calculated by the specific volumes of the sample (envelope volume, net volume). The net volume (V_{net}) describes the volume of a sample excluding pores. To determine this volume, the weight and net density of the sample are required and were measured by use of a helium pycnometer (*Accupyc 1330*, Micromeritics Company). The envelope volume (V_{en}), including the pore volume within the sample, was determined by a powder pycnometer (*Geopyc 1360*, Micromeritics Company). Finally, the porosity can be calculated by the following equation:

$$\Phi(\%) = (V_{en} - V_{net})*100V_{en}$$

Permeability Analysis

Two different procedures were used to determine the permeability of the collected samples. The permeability of sedimentary rocks often exhibits anisotropy caused by depositional and diagenetic features (e.g., bioturbation, cross-bedding, and burial). The mean horizontal (*X* and *Y* directions) and vertical (*Z* direction) permeability of the sample plugs was determined with a mini-permeameter. An apparent average porosity can be calculated by means of these values (total permeability). The mini-permeameter is a gas-based device for measuring permeability and was used under laboratory conditions.

The disadvantage of this device is the small diameter through which the gas is injected into the porous rock sample. To obtain more reliable permeability data, a gas-based column permeameter was used, which provides injection through a specimen of up to 40 mm (1.5 in.) height with a diameter of 40 mm (1.5 in.). However, it is only possible to measure the mean vertical permeability using the column permeameter. As a subsequent step, a Klinkenberg correction was performed to approach the real permeability values for fluids like ground water.

Due to high pressures occurring during the analysis process, some samples were destroyed and could not successfully be measured. Especially the measurement of friable sandstones of the Biyadh Formation and Wasia Group caused some problems. However, about 140 samples were measured successfully with both of the devices.

Thin Sections and Scanning Electron Microscopy

Besides numeric measurements to determine porosity and permeability values, further analyses were performed to obtain a more precise characterization of the pore space and its geometry. About 40 selected samples were cut into thin plates, impregnated with synthetic resin, and polished. The samples were stained by methylene blue for better visualization of the pore spaces. Additionally, the samples were chosen and prepared for analysis under the scanning electron microscope (SEM). These samples were

crushed into pieces, affixed to small object slides, and finally vaporized with a thin coat of gold dust with a Cressington sputter coater. The sputter coater uses argon gas as transmitting medium. SEM analyses were carried out using a VEGA Tescan XMU scanning electron microscope. The specimens were set on a sample stage that can be rotated in three dimensions during analysis. Nitrogen was used as flush gas in the sealed and evacuated sample chamber. A thermo-ionic tungsten wolfram filament produced an electron beam at a voltage of 20 kV and emitted electrons that are accelerated toward the sample. The electrons were bundled with apertures and lenses to a thin monochromatic beam of extremely high energy. These electrons interact with the atoms that are located at or near the surface of the sample causing the emission of secondary electrons. These backscattered electrons were collected by an Everhart–Thornley detector and transformed into an image via photomultiplier. The produced high-resolution image provides a detailed 3-D appearance of the sample's surface in high magnification (Goldstein, 2003).

GEOLOGICAL SETTING

Geologically, the Kingdom of Saudi Arabia and the Arabian Peninsula are situated on the Arabian plate. Several margins with differing characteristics surround the Arabian plate. To the south and west, the Arabian plate has two passive margins in the Gulf of Aden and the Red Sea (Figure 1). In the north and east, it is bounded by active margins in the Taurus simple fold belt of southern Turkey, the Zagros fold and thrust belt, and the Makran thrust belt in the southeast. Further southeast and in the northwest, transform margins can be found, which separate the Arabian plate from the adjacent Indian and African plates, respectively (Owen Transform, Dead Sea Transform; Al-Husseini, 2000; Konert et al., 2001).

Lithologically, the Arabian Peninsula consists of two major geological entities represented in the Kingdom of Saudi Arabia: the Arabian shield and the Arabian platform (Figure 1). The western Arabian shield mainly exposes Precambrian crystalline basement. The rock series of the basement are composed of metamorphic rocks and bodies of intrusive igneous rocks analogous to the Nubian shield (Zötl, 2006). Before the rifting that led to the opening of the Red Sea during the Miocene, the Arabian and Nubian shields together formed an even larger entity, the Arabian–Nubian shield. From the eastern foothills of the Arabian shield, the Arabian platform extends to the east and northeast until it reaches the front of the Zagros fold and thrust belt in the Arabian Gulf. The Arabian platform is founded on the basement and represents the former shelf of the Tethys Ocean. This shelf accommodated the sedimentary Phanerozoic succession that covers the giant peneplain, which developed rapidly during the latest Neoproterozoic time through the denudation of the East African orogeny. The sedimentary succession of the eastern Arabian plate is up to 12,000 m (39,000 ft) thick (Christian, 1997, 1998; Konert et al., 2001) and hosts the giant hydrocarbon reservoirs of the Arabian Gulf states. In addition, it is the almost exclusive source for groundwater hoisted in Saudi Arabia.

While most of the Paleozoic deposits are dominated by alluvial and shallow-marine sandstones and shales, the first significant accumulation of marine carbonates commenced during the latest Permian with the deposition of the Khuff Formation. The remainder of the Triassic is dominated by terrestrial and shallow-marine siliciclastic deposits, whereas the Jurassic is almost entirely composed of carbonate platform rocks. The long-term decrease in accommodation culminated with the deposition of the latest Jurassic Hith anhydrite. Together with the overlying Sulaiy–Yamama–Buwaib interval, they form a major aquiclude and the lower boundary of the Wasia–Biyadh–Aruma aquifer system. This aquifer system is a complex facies mosaic of siliciclastic sediments and carbonate platform rocks. Its upper boundary is the aquiclude of the Lina Formation of the Aruma Group.

GEOGRAPHICAL SETTING

The main study area of the Wasia–Biyadh–Aruma groundwater project is located within the Kingdom of Saudi Arabia; the study area, however, extends into adjacent countries (Figure 1). In the south and southeast, the watersheds of the Hadramaut Mountains of Yemen and the frontal thrusts of the Oman Mountains form natural boundaries. The western and northwestern limits are the outcrops bordering the Arabian shield. To the northeast, the valleys of Euphrates and Tigris form the continuation of the ultimate receiving waters of the aquifers, which coincide with the center of the Arabian Gulf and approximately with the frontal thrusts of the Zagros fold-and-thrust belt in the east. Two recent studies (MEWA, 2017a, b) describe the complex facies interrelations across the Arabian shelf and their bearing on the distribution of aquifers and aquitards.

The results presented here are from the belt of well-exposed Cretaceous strata along several

Table 1. Geographic coordinates of the sections measured and stratigraphic interval.

Section	Northing	Easting	Stratigraphic Interval
TH-1	25°27′29.40″	046°34′29.40″	Majma-Khanasir
TH-3	25°21′08.90″	046°36′14.90″	Biyadh-Majma-Khanasir
BWA-1	25°11′23.92″	046°48′43.52″	Biyadh-Majma
B-1	24°55′41.00″	046°58′37.00″	Biyadh-Majma-Khanasir
B-2	24°55′46.00"	046°58′24.00″	Biyadh
BKD-1	24°55′46.00"	046°58′24.00″	Biyadh
S-1	24°28′38.90″	047°34′22.30″	Sallah
KW-2	24°23′17.00"	047°45′09.00″	Qibah-Malihah-Khanasir
KW-3	24° 25′20.00"	047°43′25.00″	Majma-Qibah-Malihah
KW-4	24°29′49.20″	047°36′49.40″	Huraysan-Majma-Qibah-Malihah
KW-5	24°23′16.10″	047°45′59.50″	Malihah-Khanasir
KR-1	24°10′29.00″	047°44′03.00″	Majma-Qibah-Malihah-Khanasir
KR-2	24°11′16.20″	047°44′21.70″	Malihah-Khanasir
KR-3	24°09′32.20″	047°43′52.00″	Majma-Qibah
AR-1	24°23′00″	047°46′56″	Malihah-Khanasir
AR-2	24°23′09″	047°49′09″	Khanasir-Hajajah
AR-6	24°22′28″	047°53′01″	Hajajah-Lina
AR-10	24°21′39″	047°52′11″	Hajajah

escarpments, extending from the northwest of Ar Riyadh (Ath Thumamah) via the Ar Riyadh area toward Al Kharj in the southwest, where Khashm Wisi, Khushaym Radi, and the Aruma Plateau provide excellent outcrops (Figure 2). Table 1 gives the geographic coordinates of the sections measured.

TECTONO-SEDIMENTARY FRAMEWORK

During the Cretaceous, the Arabian shelf provided accommodation for terrigenous and marine sediments. The Cretaceous deposits of the Arabian plate form different groups, formations, and members that show alternations of sandstones, siliciclastic mudstones or claystones, paleosols, and carbonate rocks. Sedimentation was triggered by frequent relative changes of sea level and the beginning of major tectonic events that started to affect the margins of the Arabian plate. These interactions have been documented by Sharland et al. (2001, 2004), who established a succession of "tectonic mega sequences" (TMS) for the Arabian plate (AP). Davies et al. (2002) have interpreted the concomitant migrations of facies belts in the Cretaceous in detail.

Strata discussed in this chapter are the Thamama, Wasia, and Aruma groups. They were deposited from the Early Cretaceous Berriasian through the early Paleogene (Al-Husseini, 2008; Thomas et al., 1999). Hence, these strata correspond to TMS AP 8, TMS AP 9, and basal TMS AP 10 of the "Sharland" succession (Figure 3). The major tectono-stratigraphic events of these TMS are briefly summarized further.

TMS AP 8: Late Jurassic–Late Cretaceous (149–92 Ma) REFS

Plate-Tectonic Setting

With the rifting and the subsequent separation of India–Australia–Antarctica from Africa–Arabia yet another passive margin became established in the southeast of the plate. By this time, the present-day Arabian plate was surrounded by passive margins; to the west, however, it still was attached to Africa.

Opening of the Atlantic at ever-increasing rates submitted stresses across Africa and Arabia. The effects of this stress-induced regime included the evolution of a subduction zone outboard of Arabia in the Neo-Tethys and increasing subduction of the Tethys beneath Eurasia. The newly induced subduction was southwest directed and later affected the Arabian plate. Concomitantly, the western part of the Arabian shield was uplifted and provided

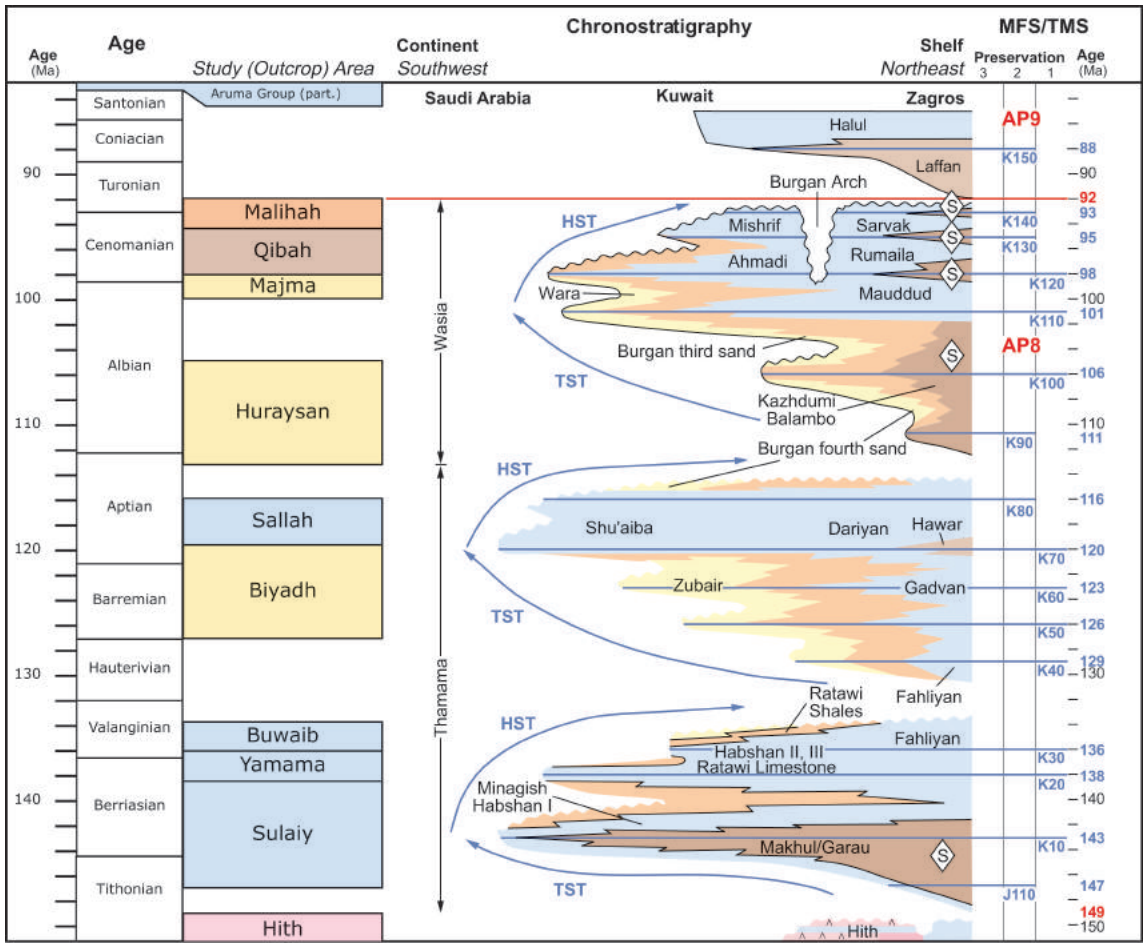

Figure 3. Stratigraphic column for the Arabian plate and subdivision in tectonic megasequences. Subdivision is from Sharland et al. (2001). The maximum flooding surfaces (e.g., K100 and K110) shown in the right column of the illustration are used for basinwide correlation.

increasing volumes of siliciclastic detritus shed in an easterly direction.

Structural Evolution

Flexural deformation dominated on the Arabian plate, no prominent tectonic features were formed during this TMS.

Sedimentary Evolution

Basically, there was a simple paleogeographic pattern across the Arabian plate: an alluvial to marginal-marine to shallow-shelf siliciclastic belt bordered the rising hinterland on the Arabian shield. This belt contains the majority of strata discussed in this chapter, the Biyadh Formation and the entire Wasia Group (Figure 3). To the north, east, and southeast, large carbonate platforms covered the Arabian platform. Two deep-marine basins evolved toward the Neo-Tethys Ocean and the Garau and Rayda basins. Their sedimentary succession shows an alternation of deep-water siliciclastic deposits and deep-water limestones (Alsharhan and Nairn, 1990; Ziegler, 2001; Navidtalab et al., 2014).

TMS AP 9: Late Cretaceous–Early Paleogene (92–63 Ma)

Plate-Tectonic Setting

During TMS AP 9, the Arabian plate was subject to both compressional and extensional stresses. The former were induced by the rapid opening of the Atlantic Ocean and the corresponding evolution of a subduction zone along the eastern margin of the Arabian plate. These compressional forces resulted in widespread obduction of oceanic crust along this margin (e.g., Semail Ophiolite in Oman) and the subsequent formation of deep foreland basins that accommodated thick successions of siliciclastic detritus.

Extension was mainly concentrated along the northern and northwestern margin of the plate. It resulted from the continuing opening of the Mediterranean Sea and is responsible for the formation of the Euphrates graben, the Sinjar trough, and associated structures.

Structural Evolution

In many parts of the plate, structural uplift and inversion were the major acting forces induced by plate conversion. Several earlier fault systems were reactivated, blocks were uplifted and became subject to erosion. Subsequently, these blocks were onlapped by the ensuing transgressions. At the same time, some of the earlier diapiric structures were reactivated so that TMS AP 9 is the time of major trap formation on the Arabian plate.

Sedimentary Evolution

Ophiolite obduction in the northeast created several foreland basins that accommodated thick successions of siliciclastic detritus. Toward the foreland, that is, the Arabian shield in the southwest, carbonate ramp systems became established that landward grade into marginal-marine and continental siliciclastic deposits. This was the time of deposition of the Aruma carbonate platform and its southwestern siliciclastic fringe as part of the Cretaceous sandstone aquifer (Figure 1).

TMS AP 10: Early Paleogene–Late Eocene (63–34 Ma)

Plate-Tectonic Setting

The Atlantic Ocean was still opening, as was the Indian Ocean. These movements were compensated for by subduction along the northern and eastern margins of the Arabian plate. These movements finally led to the closure of the Neo-Tethys Ocean and the trapping of the continental slivers of the Lut block, the Afghan, and Sanandaj–Sirjan terranes between Arabia and Eurasia. With these events, the Zagros fold belt began to evolve as the suture between Arabia and Eurasia.

Toward the close of the Eocene, the lithospheric uplift and stretching within the Arabian–Nubian shield initiated the rifting that later gave way to the formation of the Red Sea and the separation of Arabia from Africa.

Structural Evolution

TMS AP 10 is characterized by relatively few structural events outside the Zagros fold belt (minor folding in eastern Saudi Arabia). In the Arabian Gulf, halokinesis persisted from the underlying TMS AP 9. The Oman margin experienced compressional deformation associated with the emplacement of the Masirah ophiolite and the uplift of the Oman Mountains as a morphologic feature.

Sedimentary Evolution

To the southeast of the collision zone was a foredeep that accumulated thick successions of erosional detritus. With the elimination of the structural highs, sediment input decreased giving way to the deposition of deep-water fines. Toward the Arabian platform, shallow-marine carbonate platforms became established (Umm Er Radhuma Formation, Dammam Formation) that onlapped the Arabian shield. The Lina Formation as part of the Aruma Group was deposited at that time (Figure 3).

CRETACEOUS STRATIGRAPHY

The Cretaceous and Cenozoic deposits of central and northern Saudi Arabia are subdivided into a number of stratigraphic sequences (TMS) that show an alternation of sandstones, shale, and carbonate rocks. The stratigraphic column for this interval is given in Figures 3, 4 (Sharland et al., 2001; Le Nindre et al., 2008). In the following paragraph, the Cretaceous strata of the outcrop belt will be described and some correlations to the subsurface will be made. The principal stratigraphic subdivision of the Biyadh–Wasia interval in the study area (Figure 4) is based on Powers et al. (1966) with the amendments by Vaslet et al. (1991) and Le Nindre et al. (2008).

The Aruma Group is mainly a calcareous unit comprising shallow marine limestone, massive dolomites, and subordinate shales. Detailed lithostratigraphy on the Aruma was carried out by Powers et al. (1966), Powers (1968), El Asaad (1983a, 1983b, 1989), Alsharhan and Nairn (1990), Thomas et al. (1999), and Philip et al. (2002). Whereas Powers et al. (1966) studied sections in the Wadi al Atk, some 120 km (75 mi) northwest of Ar Riyadh, and subdivided the Aruma Formation into four members (Lower Atj Member, Middle Atj Member, Upper Atj Member, and Lina Member), El Asaad (1983a, 1983b, 1989) identified only three in his revision (Khanasir Member, Hajajah Member, and Lina Member). Later, Alsharhan and Nairn (1990) raised the Aruma Formation to group rank, hence the former members to formation rank. This stratigraphic subdivision will be followed in this study.

The Biyadh–Wasia Problem

Powers et al. (1966) and Powers (1968) noted that there is an apparent misfit in the stratigraphic correlation of the surface outcrops with the subsurface (Figure 4). In the subsurface, the Biyadh Sandstone is separated from the Wasia Group by the intervening Shu'aiba Formation, which is not recognized as such in the outcrop area. Paleontological work by Vaslet et al. (1991)

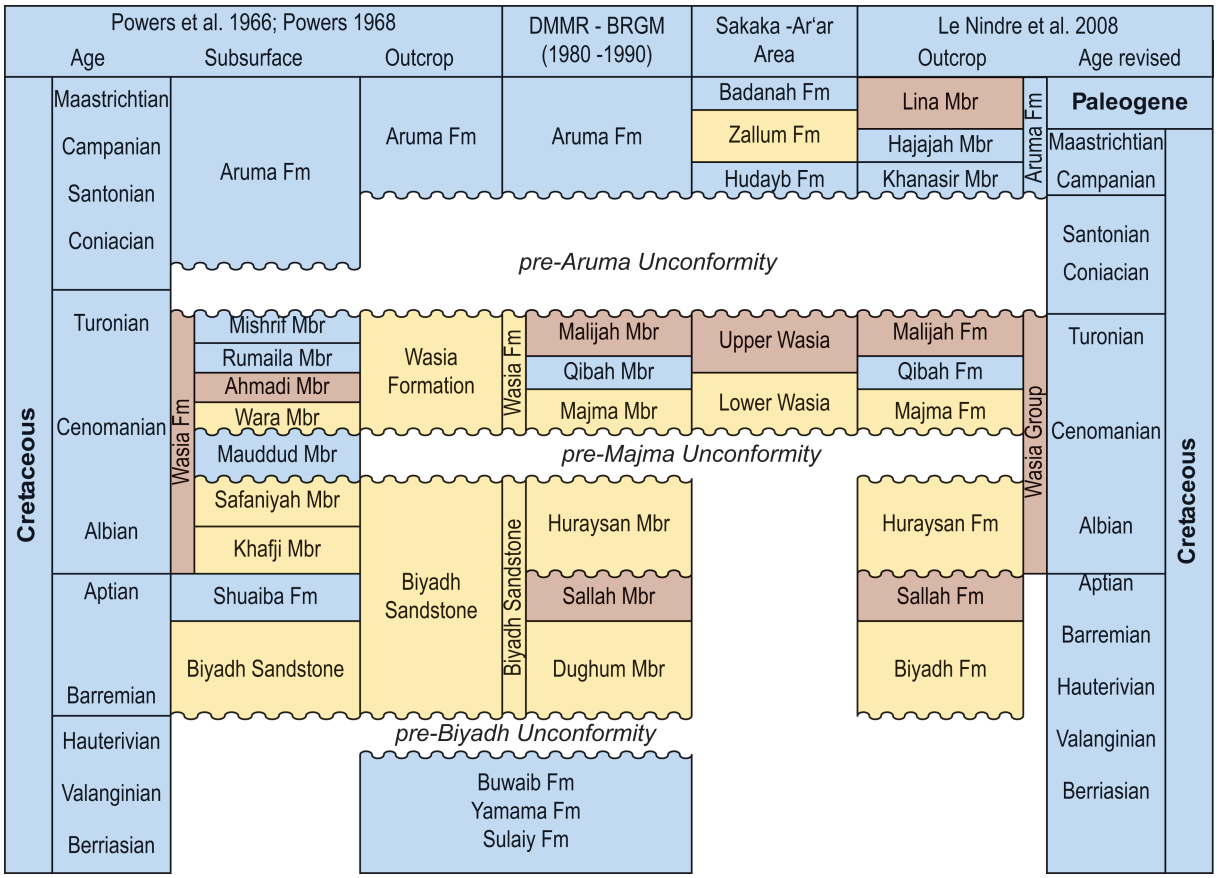

Figure 4. Different stratigraphic nomenclatures for the Cretaceous of Saudi Arabia. Le Nindre et al. (2008) subdivided the Wasia and raised it to group rank with members becoming formations. Thomas et al. (1999) and Le Nindre et al. (2008) placed the Lina Formation into the Paleogene separated from the Cretaceous through a major unconformity (pre-Umm Er Radhuma unconformity). The Aruma Formation was raised to group rank by Alsharhan and Nairn (1990).

has shown that the Sallah Member of the Biyadh Sandstone seems to be the surface equivalent of the Shu'aiba Formation. Hence, the lower part of the Biyadh Sandstone in the sense of Powers et al. (1966) of the outcrop area corresponds to the entire Biyadh Formation as known from the subsurface (Figure 4). The subsurface Shu'aiba Formation has its equivalent in the Sallah Member of the outcrop. Finally, the Huraysan Member, the upper part of Biyadh Sandstone in the sense of Powers et al. (1966), is equivalent to the Khafji, Safaniya, and Mauddud formations of the Wasia Group in the subsurface, which overly the Shu'aiba Formation (Figure 4). Consequently, the Huraysan Formation is described as part of the Wasia Group in this chapter.

The Cretaceous Sands Aquifer

South of Layla (Figure 1) and more pronouncedly from the Sulayymiyah quadrangle southward, the entire Cretaceous succession above the Buwaib carbonates and the beneath the Umm Er Radhuma Formation is one thick (locally >1000 m [3280 ft]; GTZ/Dornier, 2011; MEWA, 2017b) siliciclastic package. Although paleontologically not dated, this succession is supposed to contain stratigraphic equivalents of the Biyadh, Sallah–Shu'aiba, Wasia, and Aruma. Hydraulic data from this succession, which forms an aquifer system of its own, are scarce (MEWA, 2017b) but in general are similar to those from the Biyadh Formation and the Wasia Group. Because of the stratigraphic uncertainties, these deposits were excluded from the present study.

The Unconformities

Within the stratigraphic framework of the Cretaceous, several major unconformities are present, which not only govern sediment distribution but also exert control on the architecture of aquifers and aquicludes or aquitards. The base of the stratigraphic interval

covered in this study is the pre-Biyadh unconformity (Figure 4). It is most pronounced to the north (Qibah Quadrangle; Robelin et al., 1994) and south (Sulayyimah Quadrangle; Vaslet et al., 1985) of the study area, where the Biyadh Formation cuts down into the Triassic succession. In the outcrop area, the Biyadh cuts down "only" to the Jurassic succession. In between, and within the study area, the unconformity becomes less pronounced or is even absent. In the Ar Riyadh quadrangle, it rests on the Buwaib Formation. Whether the sharp and easily identified boundary there between both units is a conformable contact or not is still ambiguous. The age of the Biyadh Sandstone was assumed to be Barremian by Powers et al. (1966), whereas the top of the Buwaib limestones was recently dated as Valanginian (Le Nindre et al., 1990, 2008).

The significance of the "pre-Wasia" unconformity is well known since Powers et al. (1966). In ARAMCO's (1975) subdivision of the Phanerozoic succession into unconformity-bounded units, this unconformity (Figure 4) plays a major role as it cuts out successively strata from south to north down to the Devonian. In the Ar Riyadh quadrangle, it was taken as the natural boundary between the Wasia sandstone and the Biyadh sandstone. Detailed sedimentological and biostratigraphic investigations by Le Nindre et al. (2008), however, showed that not only is an outcrop equivalent of the Shu'aiba Formation present but that the actual unconformity lies *within* the Wasia Group at the base of the Majma Formation (Figure 4). Consequently, they called it the pre-Majma unconformity and it will be as such in this chapter. In the study area, the pre-Majma unconformity truncates the underlying strata increasingly from southeast toward the northwest. East of Al Kharj, the unconformity cuts down into the Huraysan Formation and then into the underlying Sallah Formation. East of Riyadh, the Sallah and Huraysan formations have completely been removed and the unconformity cuts deeply into the Biyadh sandstone (Figure 5). In the Qibah and Turabah quadrangles (Figure 1), the pre-Biyadh and the pre-Majma unconformities merge so that the Majma Formation rests on Triassic rocks. The deeply weathered, pre-Majma rocks form a bauxite deposits, mapped as the Az Zafira bauxite (Figure 1; Robelin et al., 1994, Lebret et al., 1999).

Another basinwide event of relative fall and rise is recorded in the pre-Aruma unconformity (Figures 4 and 6), which principally marks the end of major siliciclastic input onto the Arabian shelf during the Coniacian and the establishment of a vast carbonate platform. The deposits of the Aruma Group unconformably overly the Wasia Group. The pre-Aruma bauxite, several paleosols, and an erosion surface represent a nearly 20-Ma-long stratigraphic gap from the Turonian through the Coniacian, Santonian, and part of the Campanian (Le Nindre et al., 1990, 2008). The Aruma Group represents the latest Campanian with the remainder of the Cretaceous; its uppermost part (Lina Formation) already originated in the Paleogene.

Additional Remarks

As will be shown in the description of the lithologies of the individual units, the siliciclastic units of the Valanginian through Turonian were deposited in shallow-marine to terrestrial environments. Lateral shifts of facies are frequently observed within the individual units. A few paleosols associated with bauxites have been described by Vaslet et al. (1991) and Le Nindre et al. (2008) who placed emphasis on their occurrence beneath sequence boundaries that separate individual formations. This is true for the Az Zafira bauxite (Figure 1) and the pre-Aruma bauxite, although they have a regionally restricted occurrence. Fieldwork, however, has shown that paleosols, which also locally show bauxite relicts, are much more common than previously described and that they cannot be taken as a reliable marker for one distinct unit or for the proximity to a formational boundary. Although many of the soils, especially beneath the major sequence boundaries, show a red to purple stain, there are sections where the soils are gray or beige. Formation and preservation of paleosols and associated bauxites apparently depended on climatic conditions, suitable bedrock, and the intensity of ravinement during the ensuing transgression. Hence, bauxites indicating extended periods of emersion may have been entirely removed, whereas others, still preserved, may indicate only short-time emergence. Whether the soils will be recognized in wells at all and whether they indicate major unconformities will thus depend on local and regional factors.

Biyadh Formation

Lithology and Environment

Powers et al. (1966) and Le Nindre et al. (2008) gave detailed descriptions for the type section of the Biyadh Sandstone and subdivided the formation into four informal units.

The basal unit (~60 m [197 ft] thick) is composed of black weathered conglomeratic to fine-grained ferruginized sandstone showing 2-D and 3-D cross-stratification.

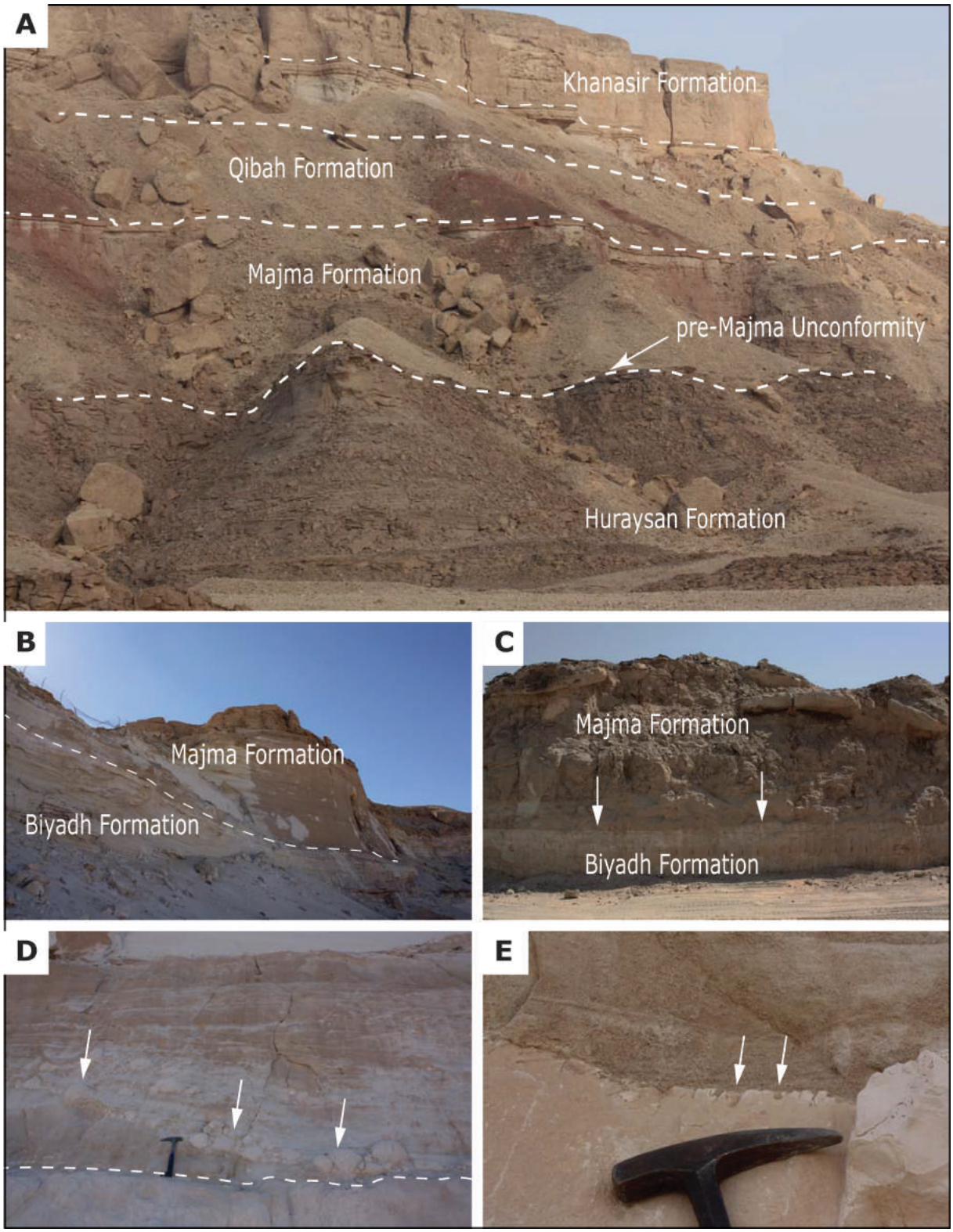

Figure 5. Aspects of the pre-Majma unconformity. (A) Stratigraphic succession at Khashm Wisi. The Majma Formation unconformably overlies the Huraysan Formation (pre-Majma unconformity). (B) Thick succession of fluvial Majma sandstones on Biyadh Formation. The Biyadh Formation is deeply truncated by the pre-Majma unconformity, also with considerable relief. Section BWA-1. (C) Fluvial siliciclastic rocks of the Majma Formation overlying a fine-grained deltaic succession of the Biyadh Formation. Uppermost bed of Biyadh Formation is strongly cemented and burrowed. (D) Fluvial deposits of the Majma Formation on tidal sandstones of the Biyadh Formation. Arrows point to clasts of kaolinitic clay and tidal sandstones that were reworked from the subjacent Biyadh. Section BWA-1. (E) Detail of C. Strongly burrowed hardground (arrows) at the contact between the Biyadh Formation and the Majma Formation. Locality Section B-1. Localities as in Figure 2.

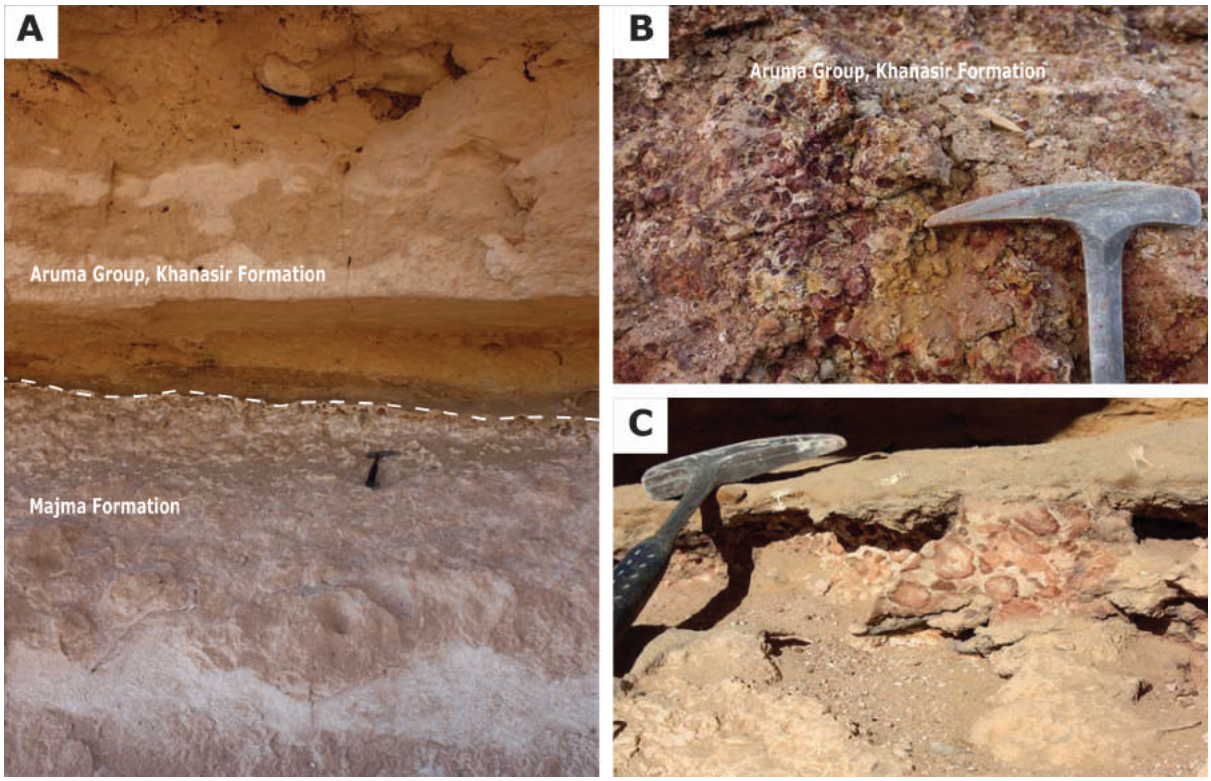

Figure 6. Aspects of the pre-Aruma unconformity. (A) The Aruma Group overlies the Majma Formation. The unconformity is often marked by the development of a thick bauxite layer in the uppermost Majma Formation. (B) Detail of the bauxite deposit. (C) Redeposition of reworked bauxite in the basal Aruma sediments is common. Section BWA-1. Locality as in Figure 2.

Quartz gravel layers and silicified wood can be found as channel lag at the bottom of troughs. Layers of silt- and claystone also occur.

The next unit (~110 m [360 ft] thick) is mainly composed of fining-upward units from fine-grained sandstone to siltstone and clayey siltstone with ferruginized and pedogenic horizons. Conglomeratic and coarse-grained sandstones are found at the base of these fining upward cycles.

The third unit is a coarser-grained assemblage composed of brown conglomeratic sandstone, gray to white coarse- to fine-grained sandstone. Cross-bedding, secondary ferruginization, and strong silicification is common throughout the sandstone. In the upper part of these fining-upward sequences, varicolored siltstone and clayey siltstone can be found. The unit is about 56 m (185 ft) thick.

The uppermost 54 m (177 ft) of the Biyadh Formation are composed of varicolored pedogenic silt- and claystones. Channels filled with coarse- to fine-grained sandstone with ferruginization cut into this assemblage.

Moshrif (1979, 1980) was among the first who gave a comprehensive interpretation of the Biyadh Formation as being of fluvial origin. He documented that dominantly the successions were formed in a meandering system with dunes in the channel thalwegs. Locally, he recognized tidal influence as is common in streams near the shore. He interpreted many of the sedimentary structures as indicating high stream velocities and high sediment load. Figure 7A through F documents the tidal influence on the system, Figure 7G, H show details of the meandering successions.

The repetitive motif in the lower part of the Biyadh Formation are fining-upward facies successions (Figure 8; Section TH-3), from sandstones with an erosional base to siltstones and terrigenous mudstones. The latter often show pedogenic fabrics. These units represent fluvial meandering channel fills (Moshrif, 1983). Some of the coarse channels cutting through these deposits formed as cut-off channels (Reineck and Singh, 1980; Miall, 1996).

Higher up in the succession, 2-D cross-beds prevail and fining-upward cycles are less apparent (units 2 and 3 of Le Nindre et al., 2008). According to their interpretation, these sandstones represent a deltaic environment. Sections B-1 and B-2 (Figure 9; Section B-1) provide good examples of these

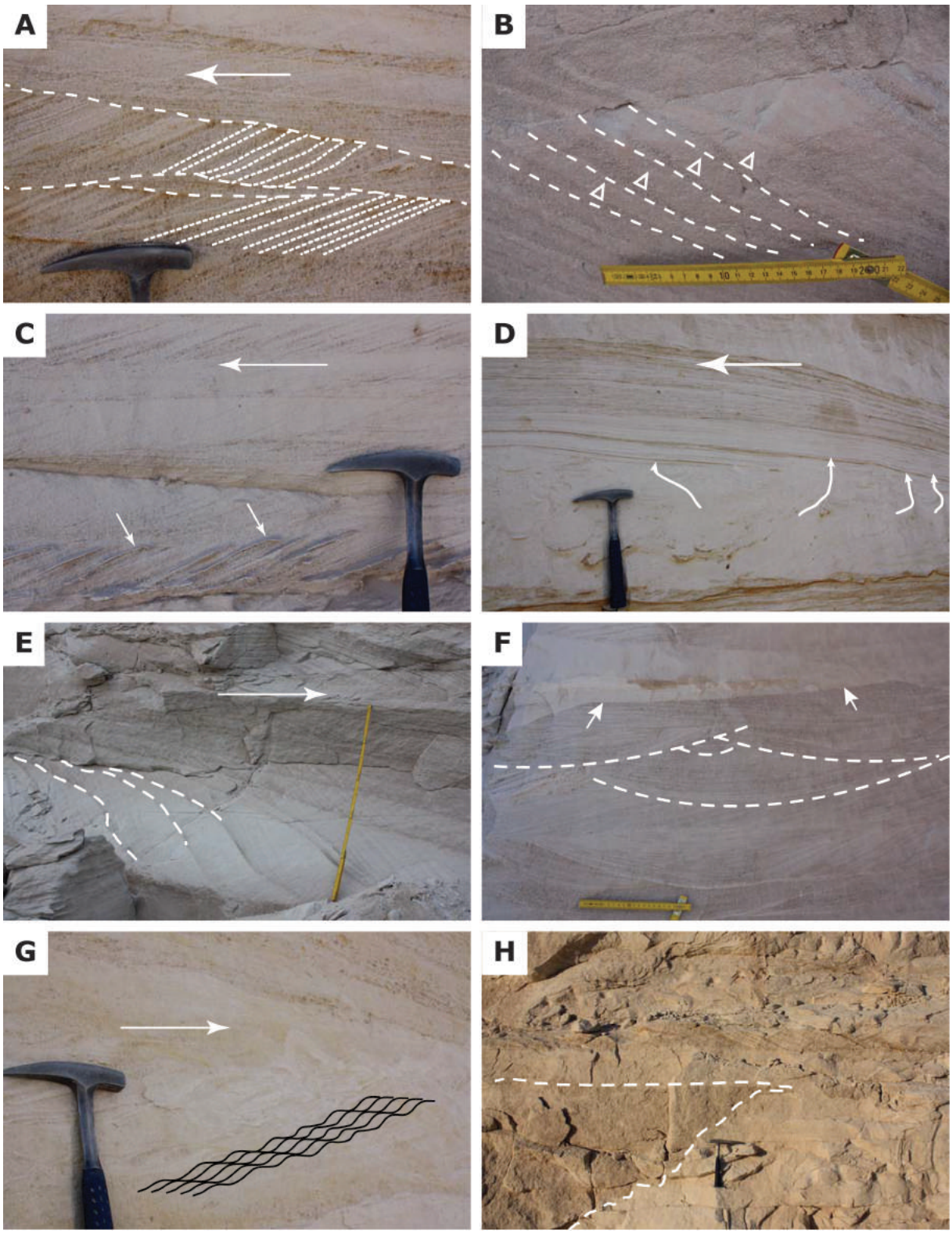

Figure 7. Bedforms of the Biyadh Formation. (A) Planar cross-bedding in medium-grained sandstone. Note irregular reactivation surfaces (white lines). Flow direction indicated by arrow. (B) Close up of foresets found in planar cross-bed set. Each foreset is graded from coarse- or medium-grained sand grains toward fine sand (triangles). Direction of flow was toward right. (C) Planar cross-bedding with reactivation surfaces and mud drapes on top of foresets (arrows). Mud drapes indicate influence by tidal currents inverse to mean flow direction (arrow). (D) Dewatering structures in fine-grained sandstone (arrows) destroy the previous horizontal lamination. (E) Thick set of sigmoidal-shaped cross-beds indicate tidal bundles. Mean flow was toward right. (F) Trough cross-bedding in medium- to fine-grained sandstones. Flow was into direction of view. (G) Climbing ripples in fine-grained sandstone are a typical current deposit in fluvial environments. Both lateral (migration) and vertical (aggradation) of the bedform are recorded. Mean flow is toward right. (H) Scour-and-fill structure in fine-grained sandstone. Sediment was repeatedly eroded and filled by coarser grained sediments. Section B-1 and B-2. Locality as in Figure 2.

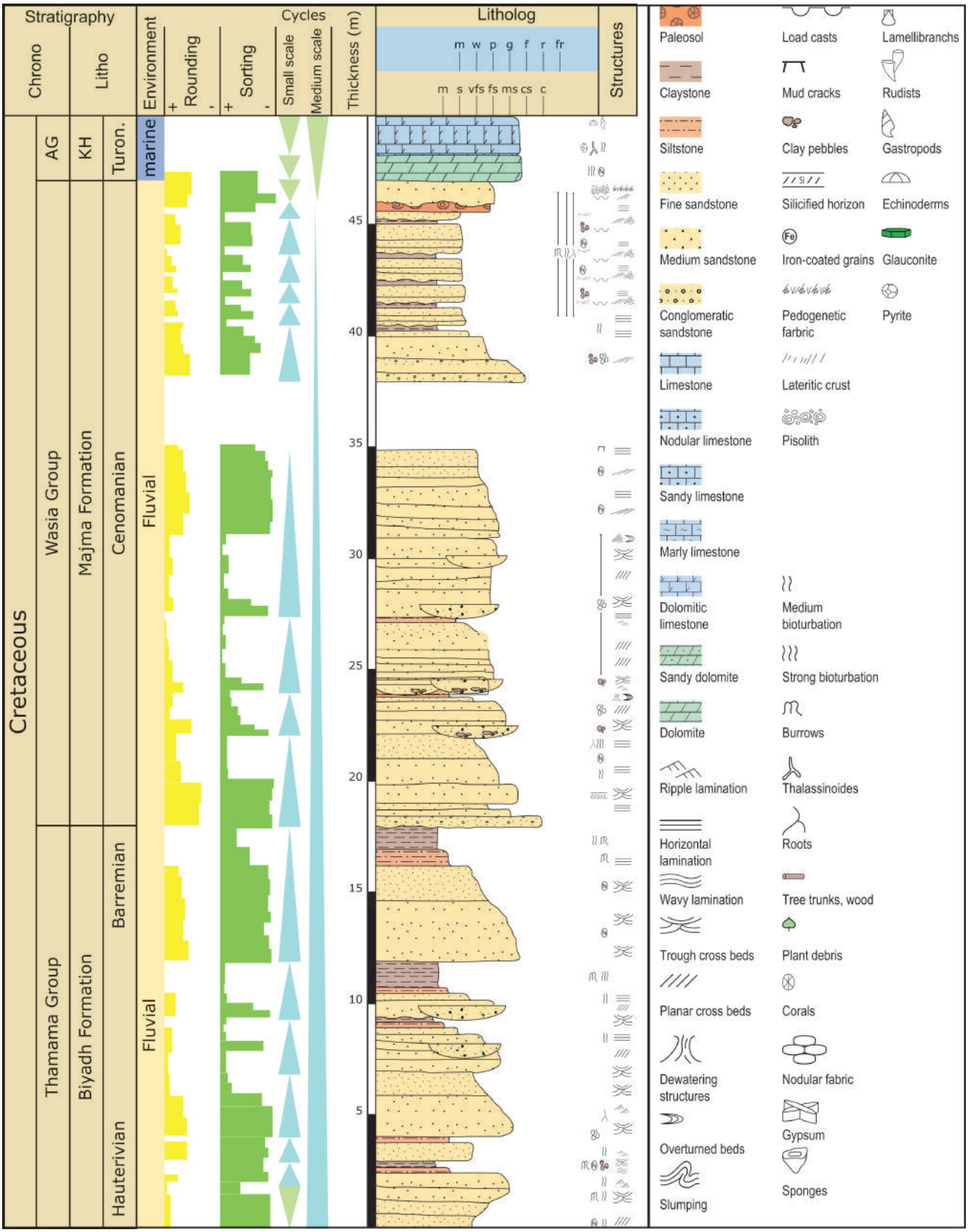

Figure 8. Litholog of Section TH-3 and legend to all sections. AG = Aruma Group; KH = Khanasir Formation. Locality as in Figure 2.

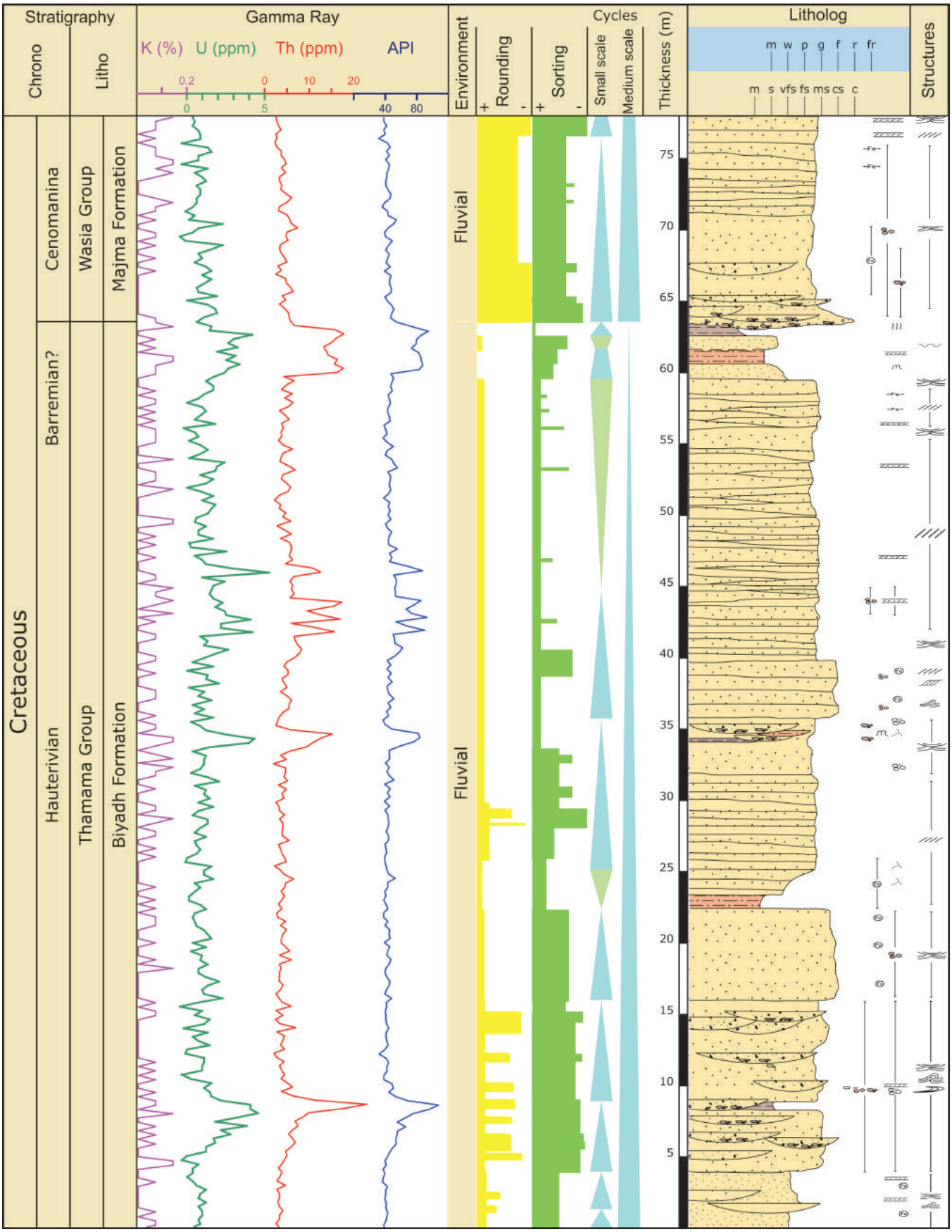

Figure 9. Litholog and SGR log of Section B-1. Locality as in Figure 2. Legend as in Figure 8.

deposits. Figure 10 is a detailed sketch of one quarry wall demonstrating the lateral shifts of facies through channel migration within the delta environment. Mud drapes on ripples, rare herringbone cross-stratification, abundant reactivation surfaces, and sigmoidal megaripples are evidence that the delta was at least influenced by tides.

The uppermost unit is dominantly fine grained with siltstones and terrigenous mudstones and occasional carbonate interbeds with a restricted marine fauna (lamellibranchs, gastropods; Figure 11, Section BKD-1). This succession is here interpreted to represent a coastal plain or delta environment (Reineck and Singh, 1980), interfingering with a nearby tidal flat complex. This is evidenced by abundant fine-grained material, intercalated sheet-like sandstones, abundant organic material locally forming thin peat layers, and the restricted-marine carbonates.

SGR Characteristics

The fluvial siliciclastic sediments of the Biyadh Formation (Figures 10, 12) show very low levels of gamma radiation typical of clean sandstones (Ellis and Singer, 2007). Significant increases in U and Th in section B-1 are observed at levels that correspond to terrigenous mudstones at the top of meandering-river shallowing-upward cycles. Pedogenic fabrics and locally plant remains indicate the presence of organic matter, which is known to absorb preferentially U (Ellis and Singer, 2007), whereas Th is associated with the clay minerals. Similarly, the unconformable contact to the Majma Formation in both sections shows the same patterns, although the interval of increased SGR readings is considerably higher, reflecting the higher thickness of the preserved weathered surface. In the southeast, Section BKD-1 (Figure 11) overall shows slightly higher values, which apparently coincide with the finer-grained material in this area.

Sallah Formation

Lithology and Environment

Following Le Nindre et al. (2008), the basal 10 m (33 ft) are composed of an alternation of variegated

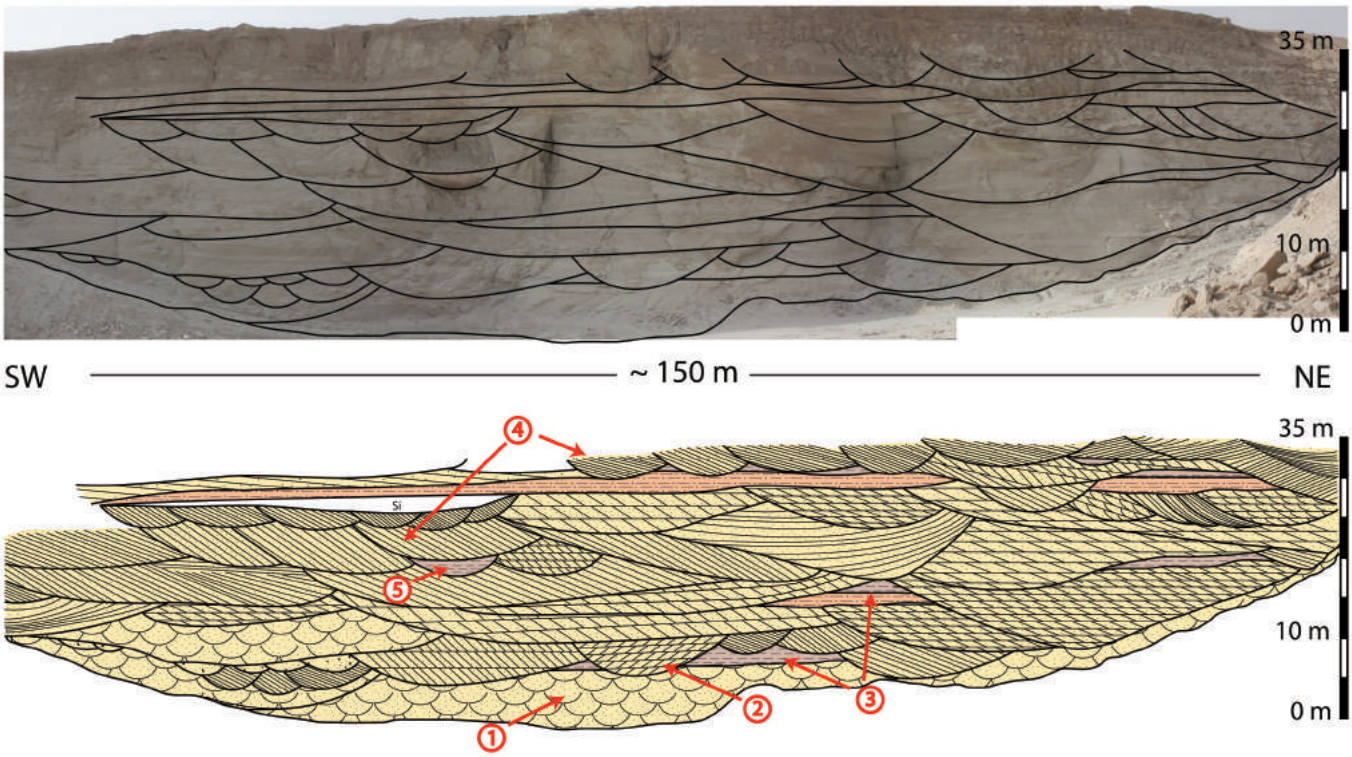

Figure 10. System of amalgamated fluvio-deltaic channels in the Biyadh Formation. The succession is mainly composed of channels containing medium- to fine-grained sandstones with (1) trough cross-bedding and (2) planar cross-bedding. These channels are "feeding" the delta with siliciclastic material and incise into the delta plain represented by (3) burrowed and rooted fine-grained siliciclastic deposits (clay, silt) of the delta plain. (4) Large channels with inclined bedding indicate lateral migration. (5) Abandoned channels (oxbow lake) were filled with fine-grained material. Section B-1. Locality as in Figure 2, legend as in Figure 8.

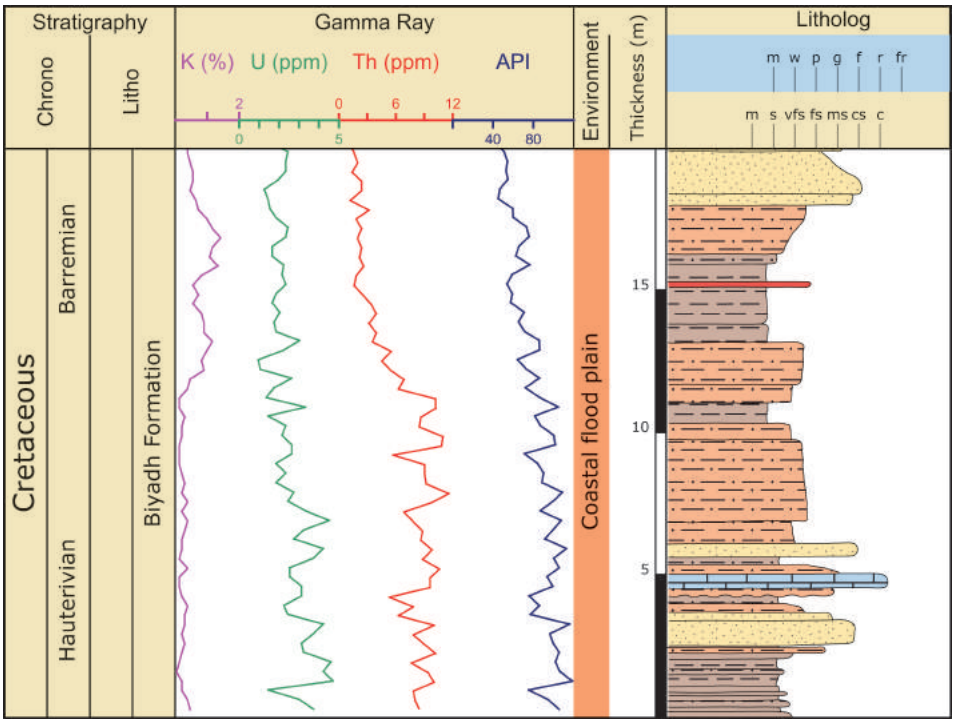

Figure 11. Litholog and SGR log of Section BKD-1. Locality as in Figure 2. Legend as in Figure 8.

gypsiferous claystone with medium to coarse-grained ferruginous sandstone (Figure 13a). The following interval (11 m [36 ft]) consists of calcareous claystone, pelletoidal limestone with a marine fauna capped by bioclastic, and fossiliferous limestone (Figure 13B, C) with secondary dolomitization. The upper 9 m (29.5 ft) are gray to green calcareous claystone intersected by black iron crusts.

During fieldwork, these observations were easily verified (Figure 14). Additionally, in some wells just northeast of Riyadh, a few meters of organic-rich black shales have been observed (Forestier, personal communication, 2012).

The partially dolomitized, sandy, and pelletoidal limestones of the Sallah Formation are interpreted to be of lagoonal and tidal origin (Le Nindre et al., 2008). The coeval Shu'aiba carbonate platform was deposited during a relative rise in sea level (Sharland et al., 2001; Davies et al., 2002) with a maximum flooding surface (K-70) during the early Aptian (Figure 3). The Sallah deposits are probably the most cratonward deposits and reflect the culmination of the preceding sea level rise. Hence, it is logical to assume that these sediments represent a widespread, mixed siliciclastic-carbonate tidal flat environment. Only fine-grained material was delivered from the craton and mixed up with marine calcareous sediment. Local ponds in the underlying Biyadh topography may have triggered the production of black shale.

SGR Characteristics

The Sallah Formation is an alternation of shallow-marine carbonates and siliciclastic coastal flood-plain deposits. As is to be expected, SGR values are low in the marine carbonates and the few sandstones (Figure 14). In contrast to the other formations, U (5 ppm) and Th (12 ppm) do not show high values. This may result from the rather low contents of plant material preserved in the sediments and continental-derived siliciclastic sediment. As the Sallah Formation (as an equivalent to the subsurface Shu'aiba Formation, Figure 4) was deposited during the major Aptian sea-level rise and probably contains the maximum flooding surface (Sharland et al., 2001; Le Nindre et al., 2008), this is a viable interpretation.

Huraysan Formation, Wasia Group

Lithology and Environment

Outcrops of the Huraysan Formation are located east to southeast of Riyadh in the Khashm Wisi area (Figure 3). Toward the northern part of the study area, the Huraysan Formation is progressively truncated by the pre-Majma unconformity until it totally disappears east of Riyadh. Due to its very friable character and the masking through piedmont deposits of the eastern Aruma escarpment, it was not possible to log an entire section of the Huraysan Formation.

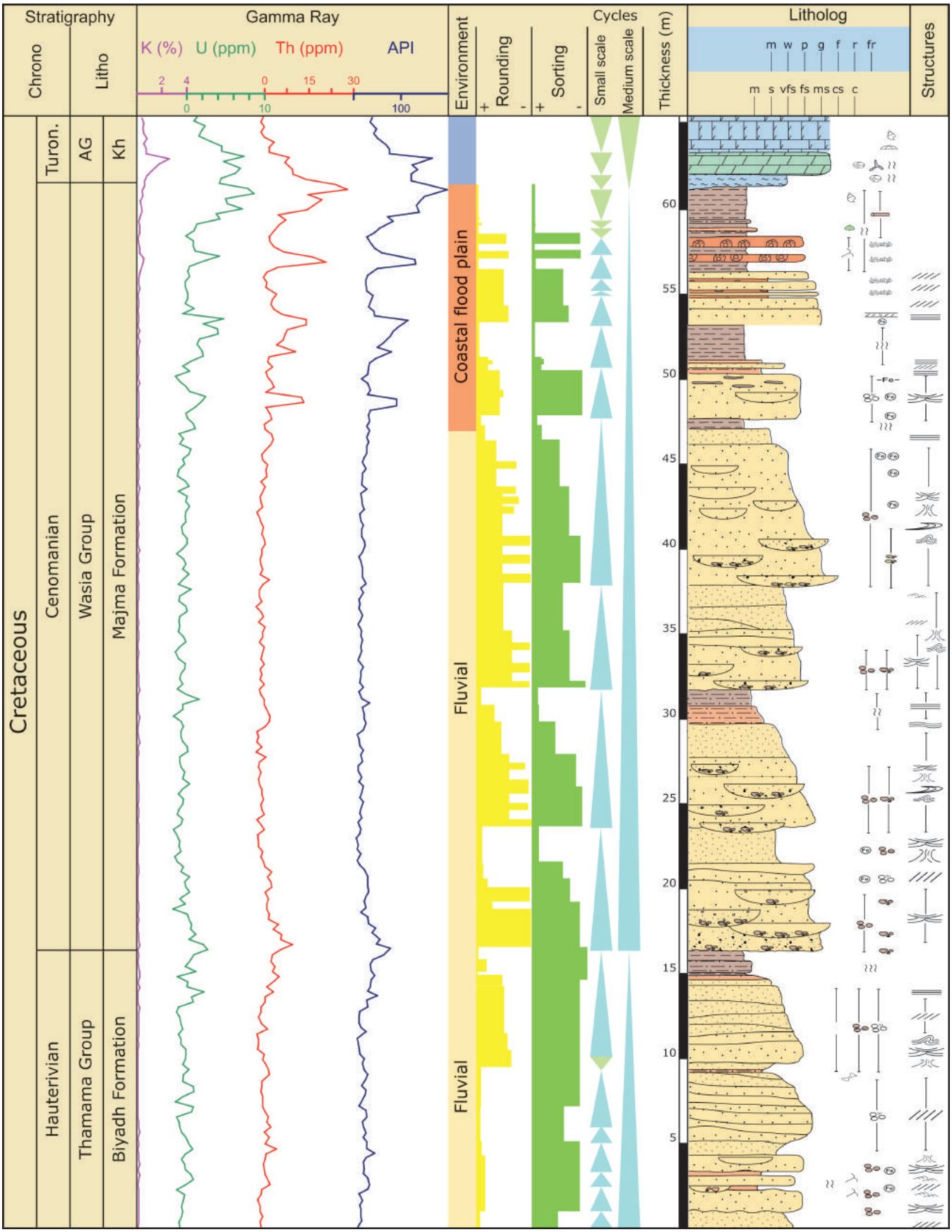

Figure 12. Litholog and SGR log of Section BWA-1. Locality as in Figure 2. Legend as in Figure 8.

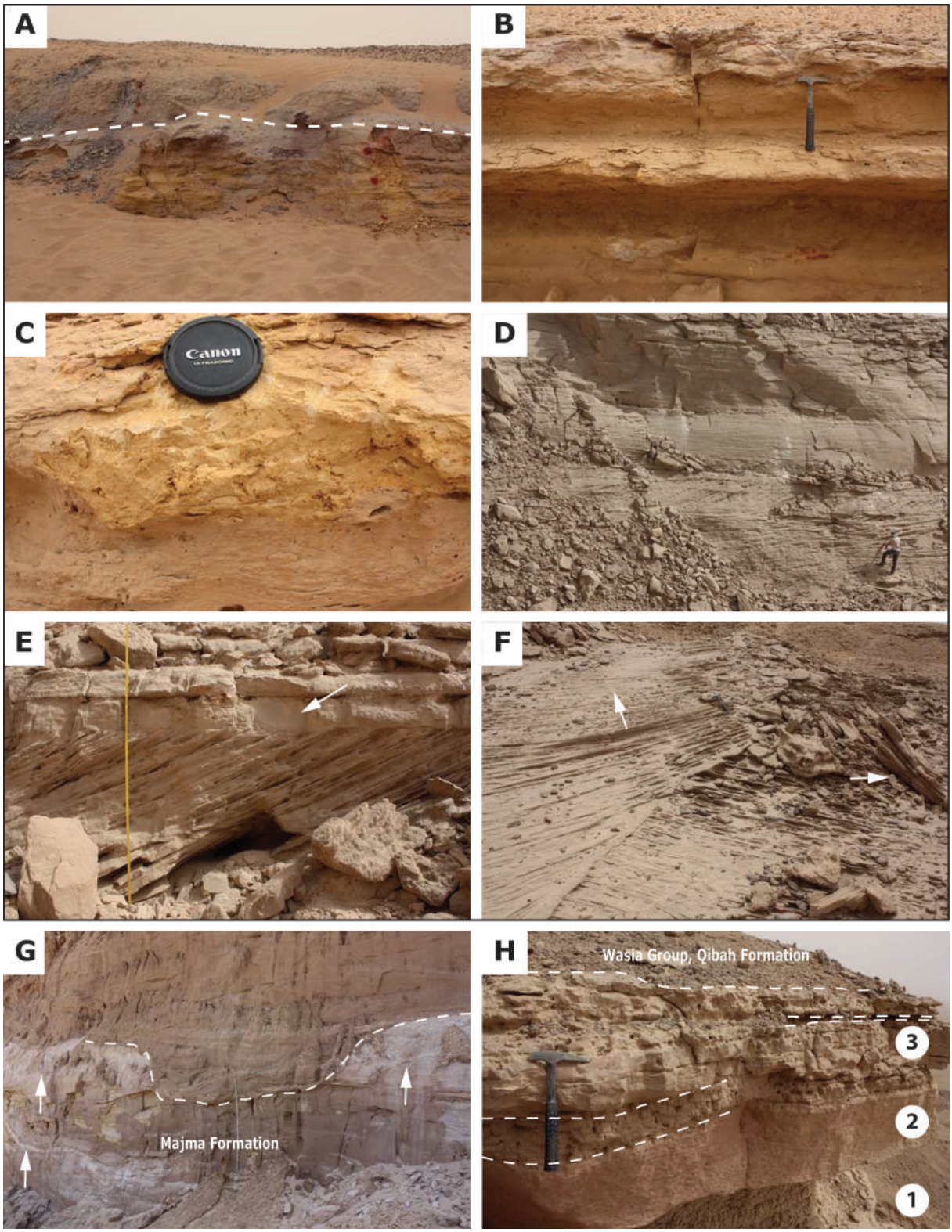

Figure 13. Depositional features of the Sallah (A–C), Huraysan (D–F), and Majma (G–H) formations. (A) Lower part of Sallah Formation. Beige ferruginous siltstones grade into bluish gypsiferous shales. (B) Middle part of the formation showing carbonates of marine origin. Hammer rests between bioclastic and fossiliferous limestones with secondary dolomitization. (C) Dolomitic claystone is intercalated between carbonate beds. Section S-1. (D) Gray and beige coarse- and medium-grained sandstones of the Huraysan Formation arranged in a succession of stacked fluvial cycles. (E) Close up of one fluvial cycle showing big set of planar cross-beds capped by ripple cross-laminated fine-grained sandstone (arrow). (F) Bedding plane view of stacked planar cross-bed sets. The foresets show different dip indicating changes of flow directions due to channel migration (arrows). Hammer in middle of photograph is approximately 30 cm (12 in.) high. Section KW-4. (G) Thick kaolinite horizon (arrows) in the upper part of the Majma Formation. Note deep fluvial channel cutting into the kaolinite. Section BWA-1. Localities as in Figure 2.

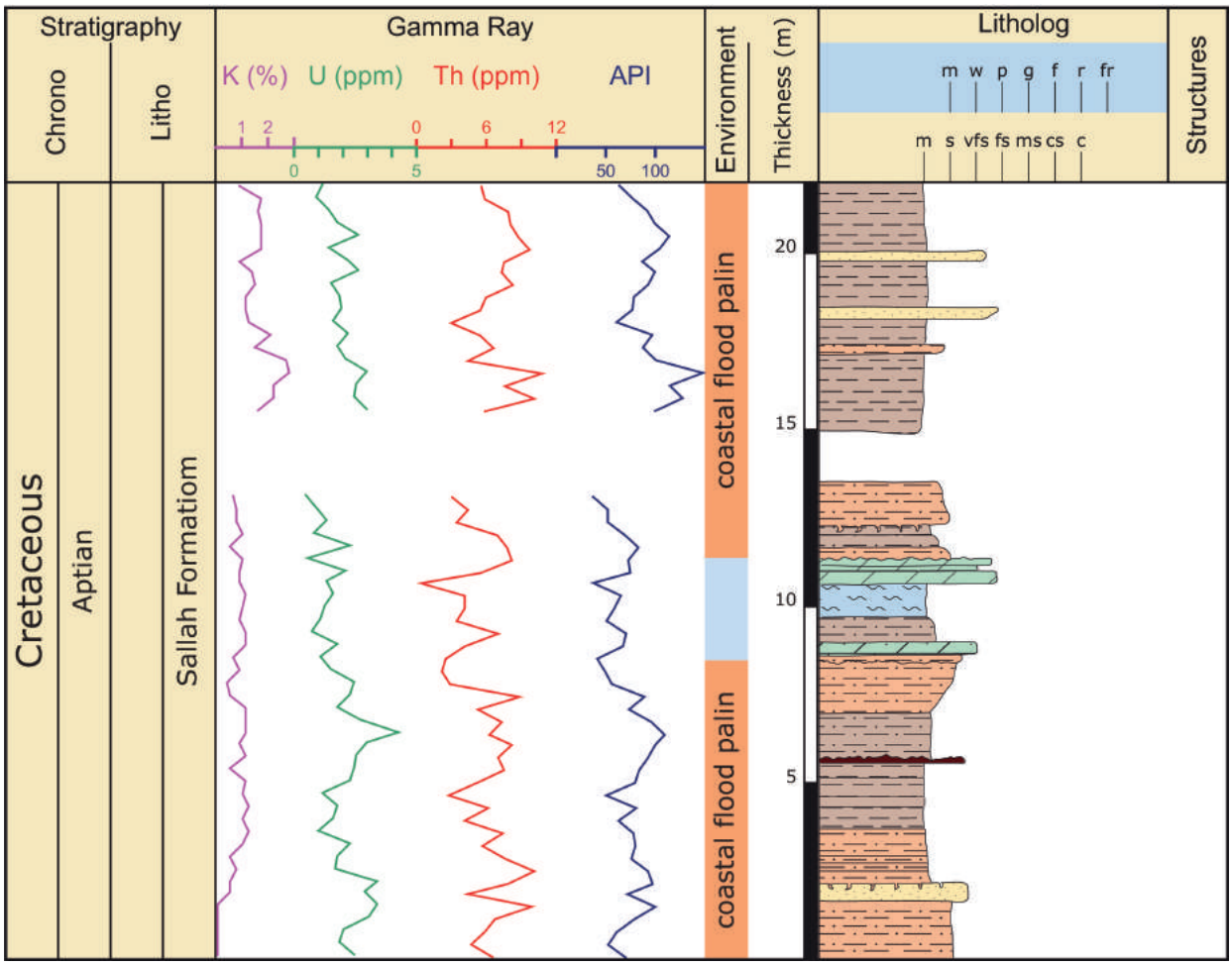

Figure 14. Litholog and SGR log of Section S-1. Locality as in Figure 2. Legend as in Figure 8.

Le Nindre et al. (2008) subdivided the formation into three informal parts.

The basal 10 m [33 ft] are composed of white quartz-pebble conglomerate and coarse-grained sandstone with cross-stratification. Locally, silicified tree trunks can be found in the deposits.

The following 70 m [230 ft] are light-colored medium- to fine-grained sandstones with cross-stratification, locally with conglomeratic horizons or siltstones (Figure 13D).

The top of the formation consists of a fine-grained, varicolored paleosol, which contains abundant roots. This part is about 7 m (23 ft) thick, capped by ferruginized and rooted fine-grained sandstone.

Section KW-4 (Figure 15) shows a succession of fining-upward cycles. The lowermost is capped by terrestrial mudstones with pedogenic texture. Thickness of the cycles varies strongly. In the basal part of unit 2, cycles tend to be thinner but more "complete," that is, they fine up into terrestrial mudstones.

The restricted outcrops of the Huraysan Formation hamper a proper interpretation of the depositional environment. Vaslet et al. (1991) and Le Nindre et al. (2008) envisaged a fluvio-deltaic setting with the finer-grained succession in the southeast resembling a broad fluvial braided fan. At least the basal part of unit 2 shows sedimentary patterns that are more compatible with meandering river systems. The large-scale cross-beds and troughs of the higher part (Figure 13E, F), in contrast, may well resemble migrating braided fluvial deposits. Indicators of a deltaic component as described by Le Nindre et al. (2008) have not been observed.

SGR Characteristics

Similar to the Biyadh Formation, the Khuraysan Formation is a fluvial succession dominated by clean sandstones. Hence, the SGR log (Figure 15) and its interpretation are directly correlatable to those of the Biyadh Formation: Clean sandstone show very

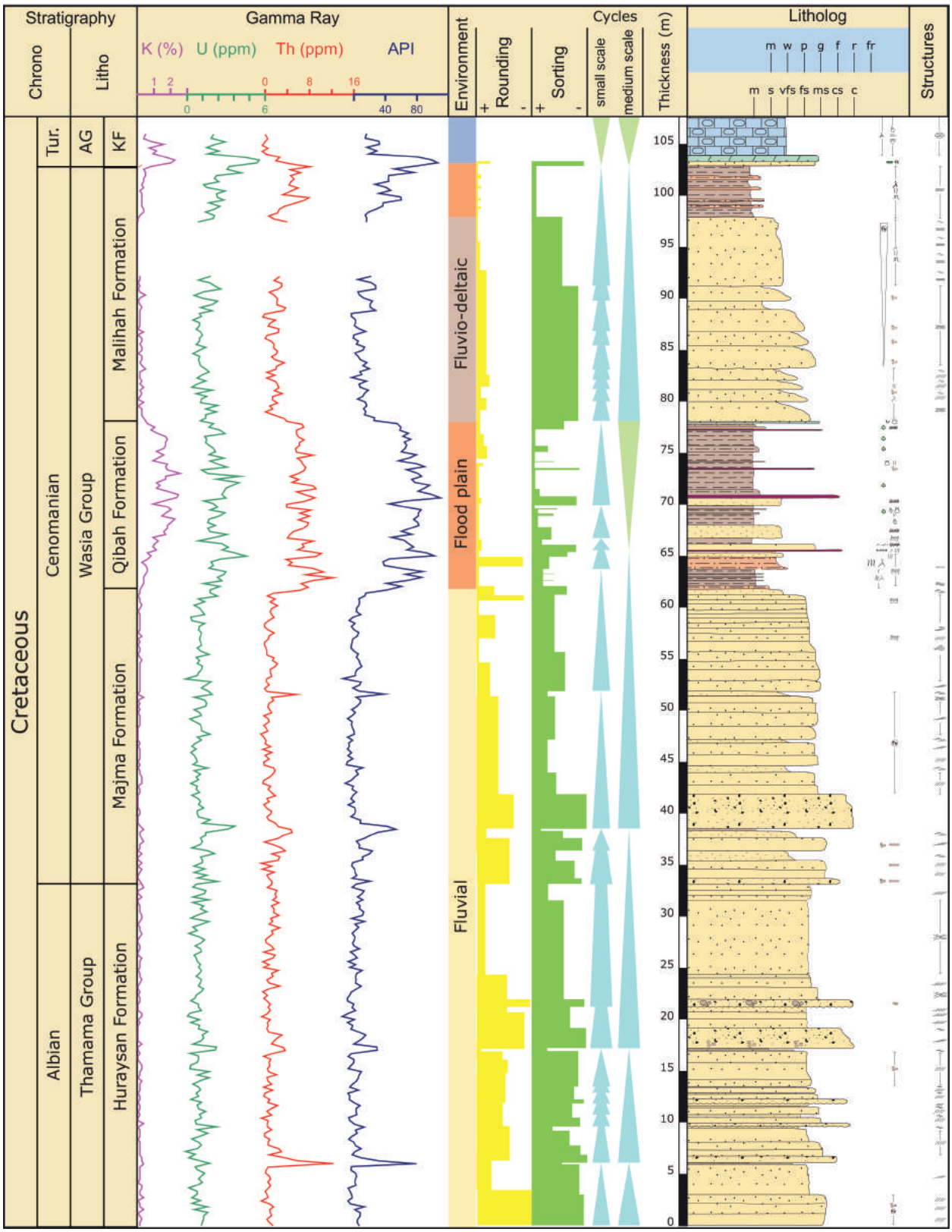

Figure 15. Litholog and SGR log of Section KW-4. TUR = Turonian; AG = Aruma Group; KF = Khanasir Formation. Locality as in Figure 2. Legend as in Figure 8.

low emissions, and mudstones with plant debris are clearly recognized in all individual element peaks.

Majma Formation

Lithology and Environment

In the Ath Thumama area, a lower unit (~24 m [80 ft] thick; Figure 16) consists of conglomeratic channel sandstone including pebbles/cobbles of white kaolinite (Figure 5D) and often white kaolinitic sand as a basal channel lag. Up section, light-colored fine- to medium-grained sandstones with cross-bedding are present. They are intersected by coarse-grained channels with kaolinitic pebbles as lag deposits, followed by white to beige fine-grained sandstone with planar bedding. The upper unit (thickness ~15 m [50 ft]; Figure 16) is composed of medium grained, cross-bedded sandstones with rare clay pebbles. Next follows white massive kaolinite (Figure 13G) and then medium-grained friable sandstone. Above a second white massive kaolinite, the top consists of variegated kaolinitic claystone with bauxitic pisoids and fragments of wood.

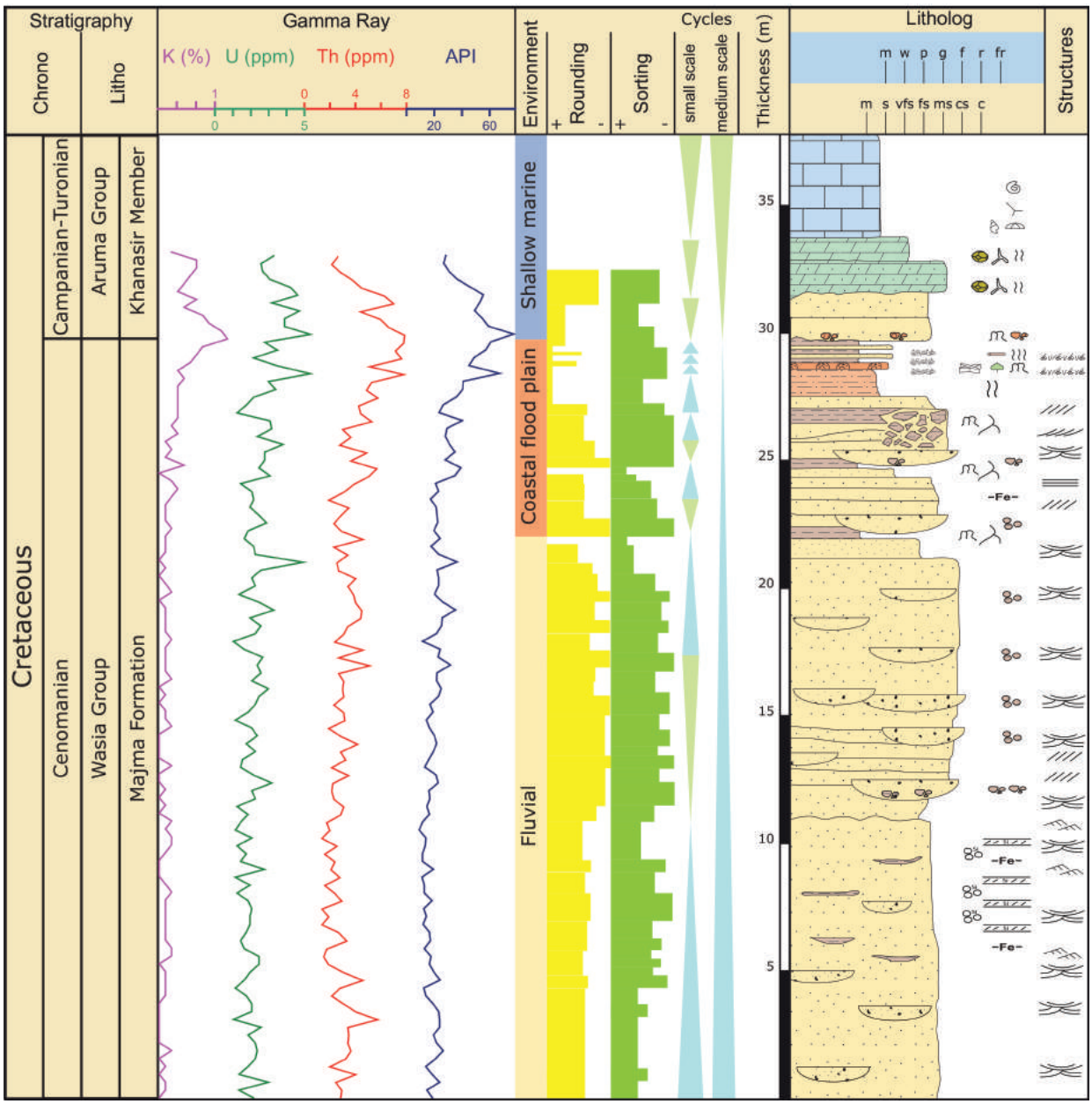

Figure 16. Litholog and SGR log of Section TH-1. Locality as in Figure 2. Legend as in Figure 8.

Around Khushaym Radi, the basal 14.5 m (47.5 ft) are composed of claystone, fine- to coarse-grained sandstone, clay- and siltstone, claystone with limonitic nodules, and ferruginous crust with concretions around gastropods. Red and brown colors dominate. The upper unit (Figures 17, 18) of 17.5 m starts with variegated gypsiferous claystone and yellow sandstone. Upsection, the sediments are strongly ferruginized. Siltstones to medium-grained sandstones prevail. Some of them contain plant remains, others are of pedogenic origin. Some limonitic crusts with evaporite nodules are also present as are calcareous mudstones with rare foraminifera. The top is formed by a hardground with bioturbation (Figure 13H).

Prior to the deposition of the Majma Formation, a major reorganization affected the Arabian shelf during the Albian (Figure 3; Ziegler, 2001; Sharland et al., 2001). Hercynian structures were reactivated and caused segmentation of the shelf. The sediments of the Majma Formation were deposited across this topography. The Ath Thumama area (Figure 2) remained continental with a well-developed fluvial system. Cycles of meandering rivers with point bar development are present; however, not all of the cycles are completely preserved due to frequent channel migration (Moshrif, 1980, 1983).

Toward the southeast, this system passed into coastal flood plains dominated by finer-grained sediments and the frequent occurrence of paleosols. Rare foraminifera in the intercalated calcareous mudstones indicate proximity to the marine environment. As distinct environmental indicators in the corresponding deposits are missing, their presence may indicate high-frequency small-amplitude sea-level variations or, storm events that transported them onshore, or flood tidal currents entering the river mouth.

SGR Characteristics

The lower, fluvial succession of the Majma Formation starts with very low SGR readings (Figures 9, 12) typical of clean sandstones (Ellis and Singer, 2007). Paleosol horizons of mudstones with plant debris are recognized through the increase in the U and K curves. The upper part of the formation with its coastal flood-plain deposits and abundant paleosols shows a strong increase in these values (Figures 17, 18), whereas the intercalated sandstones are recognized through an abrupt drop. K is negligible throughout the formation. The macroscopic observation of kaolinite as distinct layers and as pebbles and boulders indicates that the clay mineralogy is responsible for the almost complete absence of K in the logs. In the BWA-1 section (Figure 12), the Majma Formation is unconformably overlain by the Khanasir Formation of the Aruma Group. This unconformity shows the highest Th and U peaks observed in all sections and all formations. It is interpreted to result from the intensive weathering prior to the deposition of the Aruma Group, which led to widespread formation of laterite and bauxite on top of the older formations (Figure 6; Le Nindre et al., 2008). It coincides with the boundary between AP 9 and 10 (Sharland et al., 2001).

Qibah Formation

Lithology and Environment

The sediments of the Qibah Formation are mainly composed of variegated claystone, siltstone, and sandstone, locally containing calcareous deposits. Le Nindre et al. (2008) described three different successions. At Khushaym Radi, the brown to green succession starts with basal calcified sandstones, claystone, and clayey sandstone. Nodular dolomite containing abundant calcite-filled vugs is found on top of this succession (Figure 19B, C). At this locality, the Qibah Formation is about 8 m (26 ft) thick (Figures 17, 18).

In the area around Khashm Wisi, the formation is also about 8 m (26 ft) thick (Figure 15), but is composed of a lower gray to reddish claystone, and an upper reddish brown bioclastic dolomite (Figure 19A, E). The dolomite is up to 4 m (13 ft) thick and contains an abundant marine fauna.

At some localities of the Khashm Wisi area, this calcareous unit is much thinner or even completely absent and replaced by sandstones channeling down from the overlying Malihah Formation (Figure 19F, G).

In the type section in the Qibah Quadrangle, two limestone beds are present (Robelin et al., 1994; Le Nindre et al., 2008). The dolomitic Rotalina Limestone and the calcareous Nezzazata Limestone were named after their dominant marine fauna (*Rotalina sp.* or *Trocholina [Nezzazata] cf. simplex*). These limestone beds possibly correlate to the calcified sandstone at the base and the nodular dolomite bed on top of the section near Khushaym Radi (Le Nindre et al., 2008).

The thin and laterally discontinuous succession hampers an environmental interpretation. As it overlies the Majma Formation, on top of which a well-developed paleosol is present, and as it contains (restricted) marine faunas, it is likely that the Qibah Formation was deposited during an initial renewed sea-level rise. Clay and silt were delivered to the nearshore environment, where they mixed up with the products of the newly established carbonate factory. Most likely is a nearshore part of a carbonate ramp or a tidal flat complex.

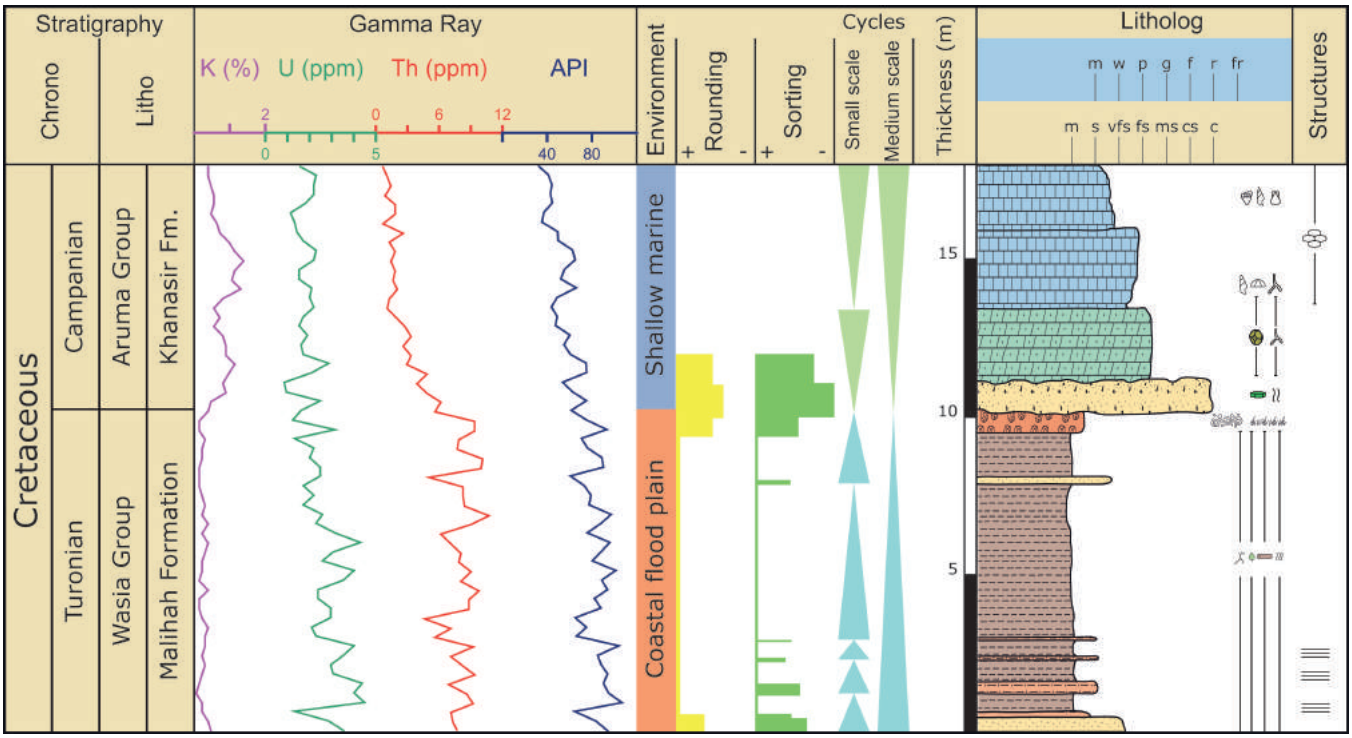

Figure 17. Litholog and SGR log of Section KR-2. Locality as in Figure 2. Legend as in Figure 8.

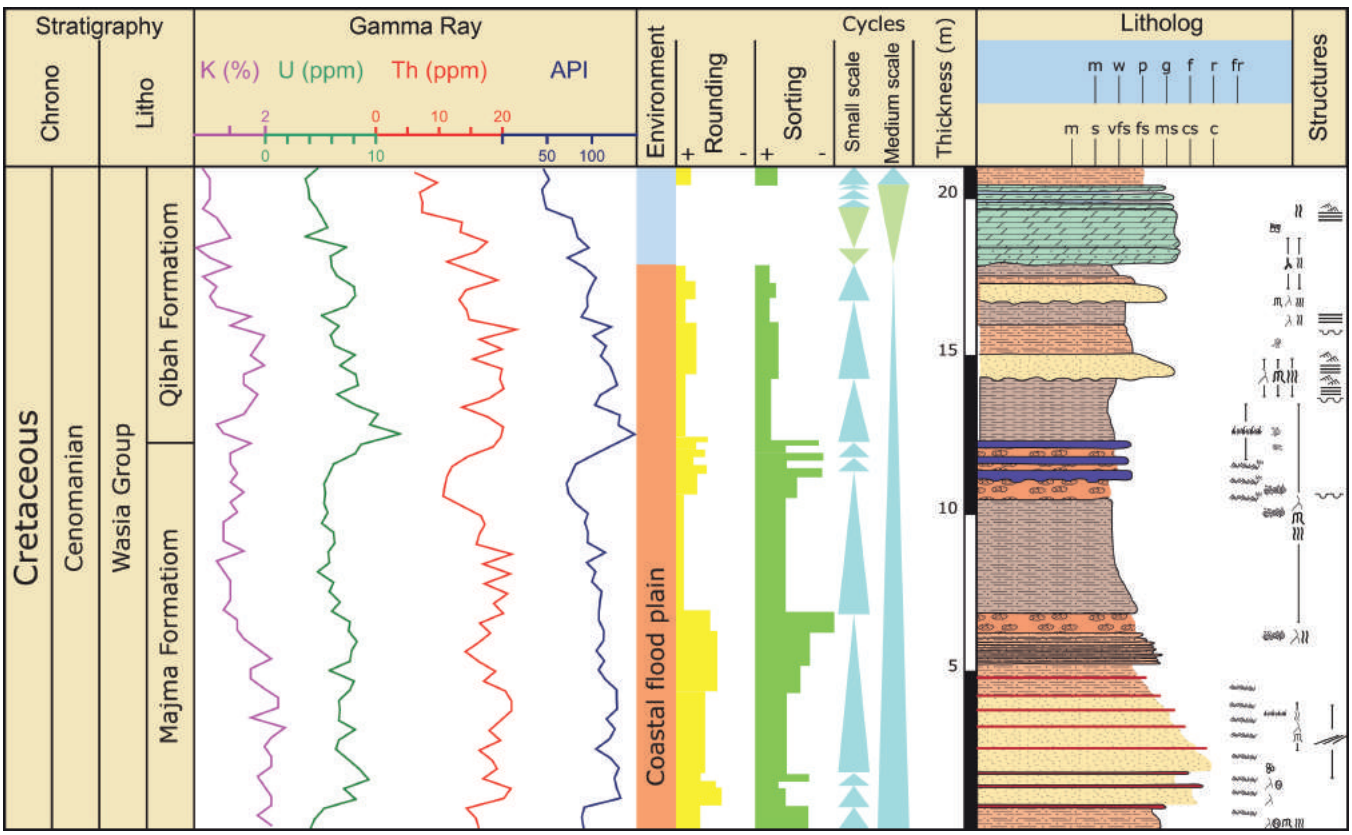

Figure 18. Litholog and SGR log of Section KR-3. Locality as in Figure 2. Legend as in Figure 8.

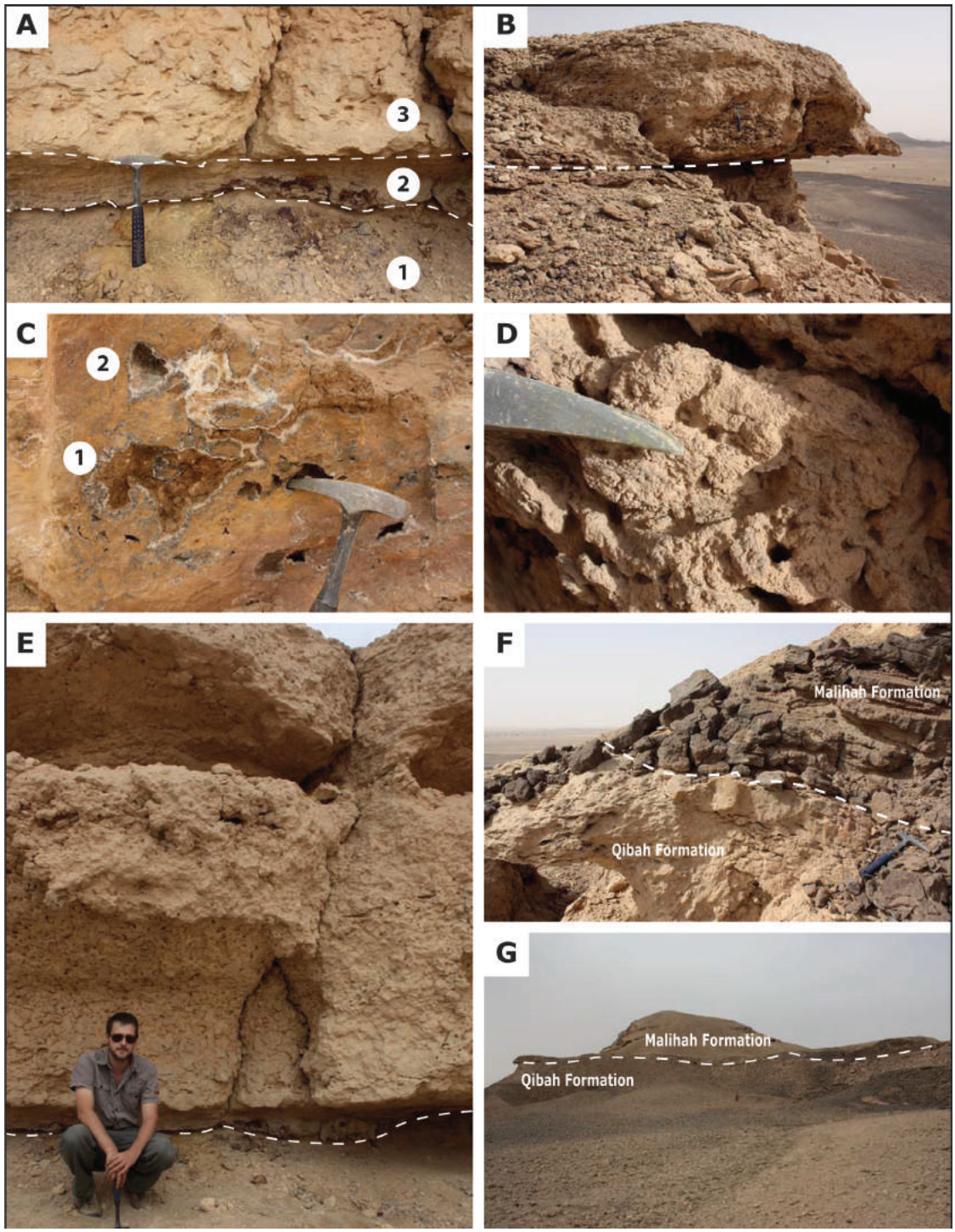

Figure 19. Aspects of the Qibah Formation. (A) (3) Bioclastic limestone overlies the (1) basal clayey succession of the Qibah Formation. (2) Decimeter-thick limonitic crust is developed at the contact. Khashm Wisi. (B) Upper nodular, dolomitic limestone containing an abundant marine fauna of sponges and solitary corals. The bed overlies a succession of tidal siltstones of the lower Qibah Formation. Khashm Wisi. (C) Dolomite containing abundant vugs. (1) The vugs are mainly filled with calcite; (2) some are filled with brownish to reddish fine-grained sand, the insoluble residue of karstification. Khushaym Radi. (D) Solitary coral found in fossiliferous limestone of the Qibah Formation. Khashm Wisi. (E) Thick (~4 m [13 ft]) bioclastic limestone overlying the clayey deposits of the lower Qibah Formation. Khashm Wisi. (F) Coarse-grained ferruginized sandstones of the Malihah Formation truncating limestone of the Qibah Formation. The sandstones represent channel-fill deposits and show cross-bedding. Very coarse and angular grains indicate proximity to the source area. Khashm Wisi. (G) At some locations, the limestone is completely absent and replaced by deep-channeling sandstone bodies of the Malihah Formation. Khashm Wisi. Localities as in Figure 2.

SGR Characteristics

In section KW-4 (Figure 15), where the underlying Majma Formation is dominantly fluvial, the conformable contact to the Qibah Formation is recognized through a significant increase in the SGR log. All individual element values remain high throughout the formation; however, the sandstone intercalations are marked by negative peaks.

Around Khushaym Radi, the upper Majma Formation is of coastal flood plain origin with yet elevated SGR values. Here (Section KR-3; Figure 18), these high values are also present in the Qibah Formation. With the onset of marine carbonate deposition, all logs show a gradual decrease in gamma radiation. This decrease is also visible in the prominent limestone package of section KW-2 (Figure 20). The transition into the Malihah Formation coincides with a further decrease in all values in the fluvial sandstone (sections KW-4, KW-2; Figures 15, 20).

Malihah Formation

Lithology and Environment

Following Le Nindre et al. (2008), the Malihah Formation is about 12 m (40 ft) thick around Khushaym Radi (Figures 17, 21) and consists of gray claystone, followed by fine-grained bioclastic sand with clay pebbles, which in turn is overlain by gray mudstone. Up section, brown coarse-grained sandstone and variegated mudstones are observed. (Figure 23A, E).

In the Khashm Wisi area, the succession is about 20 m (66 ft) thick and composed of basal varicolored

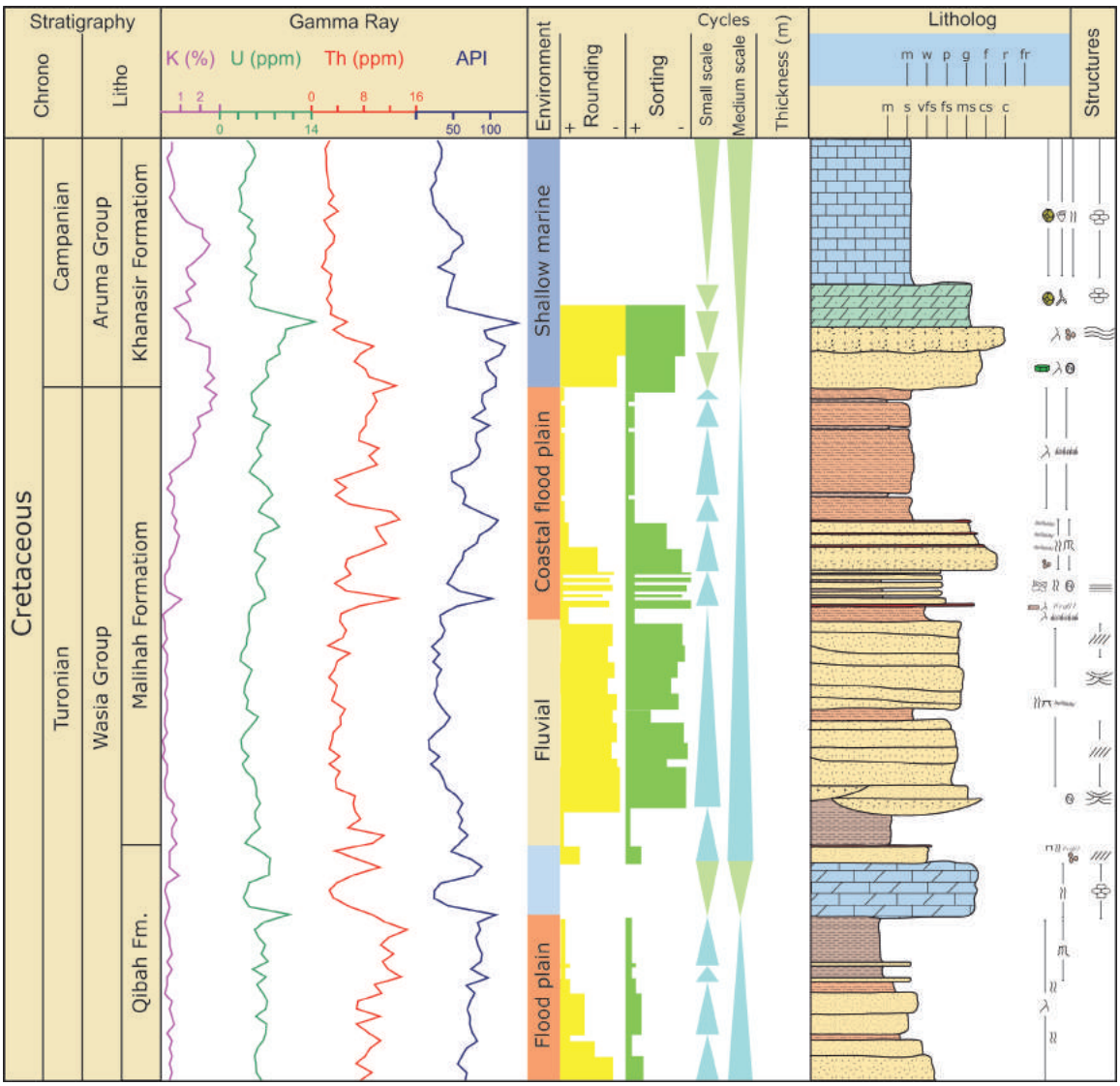

Figure 20. Litholog and SGR log of Section KW-2. Locality as in Figure 2. Legend as in Figure 8.

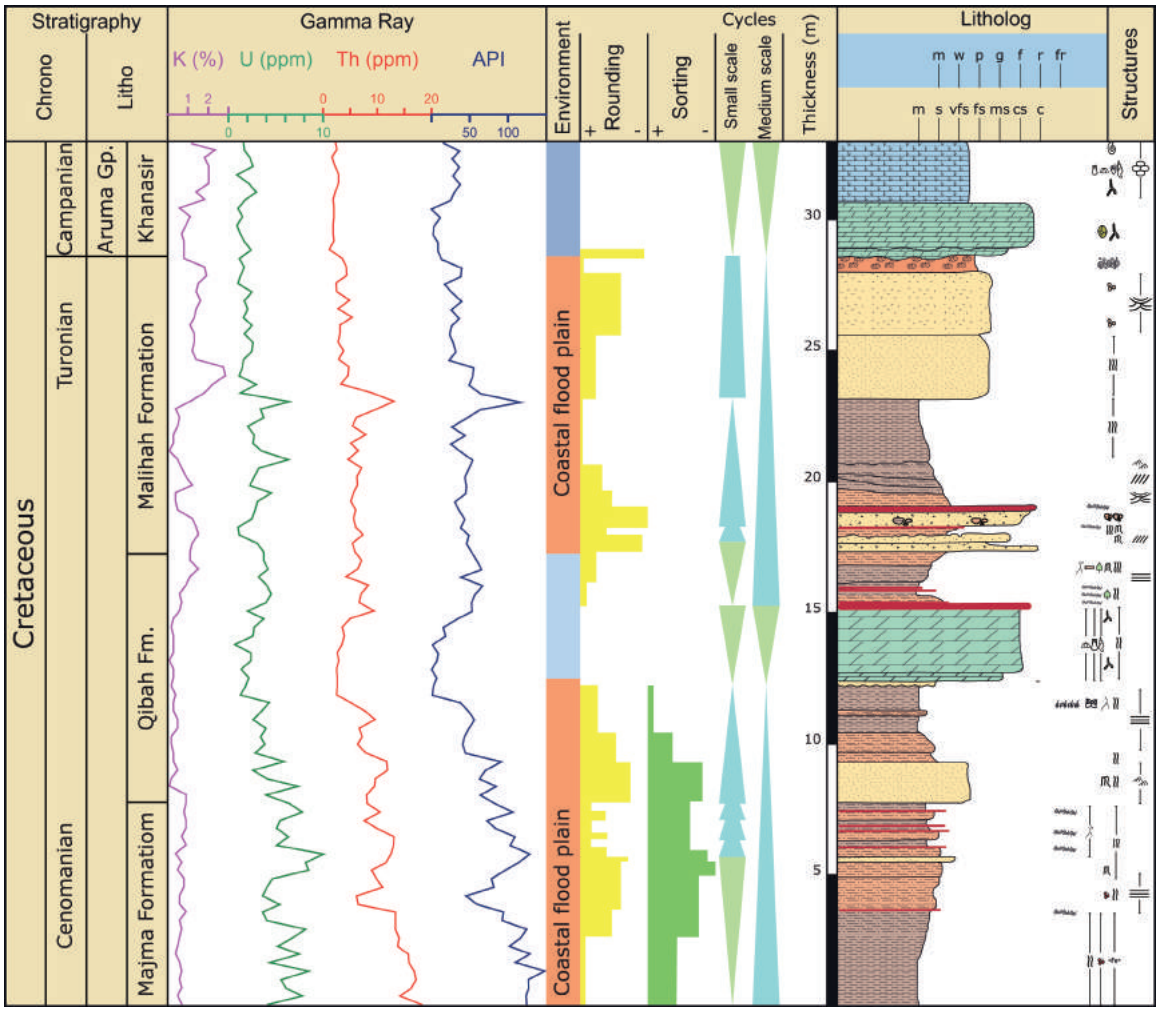

Figure 21. Litholog and SGR log of Section KR-1. Locality as in Figure 2. Legend as in Figure 8.

mudstones followed by a prominent coarse-grained to conglomeratic sandstone with wood remains (Figures 20, 22). The upper part of the section is an alternation of mudstones and sandstones.

During fieldwork for this study, lateral changes in lithology along the outcrop belt were observed. The southernmost sections at Khushaym Radi exhibit overall finer-grained sediments than the sections in the area of Khashm Wisi. In those sections, conglomerates are locally developed. Variations in thickness are common. They are caused by the presence of locally developed channels and the truncation beneath the pre-Aruma unconformity. Noteworthy is a section of thin- to medium-bedded, fine- to medium-grained sandstones overlain by siltstones containing a very prominent horizon of roots and tree trunks in life position (Figure 23C, D). This horizon is laterally represented by paleosols, rooted siliciclastic rocks, swamp deposits, or truncated by fluvial channels. The upper part of the unit there is dominated by thick rooted paleosols and locally minor channels.

At Khushaym Radi, the uppermost deposits contain an exploitable bauxite (pre-Aruma Bauxite), which is only preserved as reworked pisoids in sandstones of the Khashm Wisi sections.

Genetically, the Malihah Formation represents the upper regressive limb of the transgressive regressive cycle initiated with the Qibah Formation (Figure 3). The transition from dolomites of the Qibah Formation to siliciclastic deposits of the Malihah Formation marks the turning point within this cycle. The influences of tidal currents point to a littoral environment in the basal part of the unit. The tidally generated ripples in silt- and fine-grained sandstones together with tidal channels (Figure 39B), locally intruding the tidal flat, were particularly observed in the vicinity of Khushaym Radi. Hence, this succession was deposited under similar conditions as the Qibah Formation. Paleocurrents of the

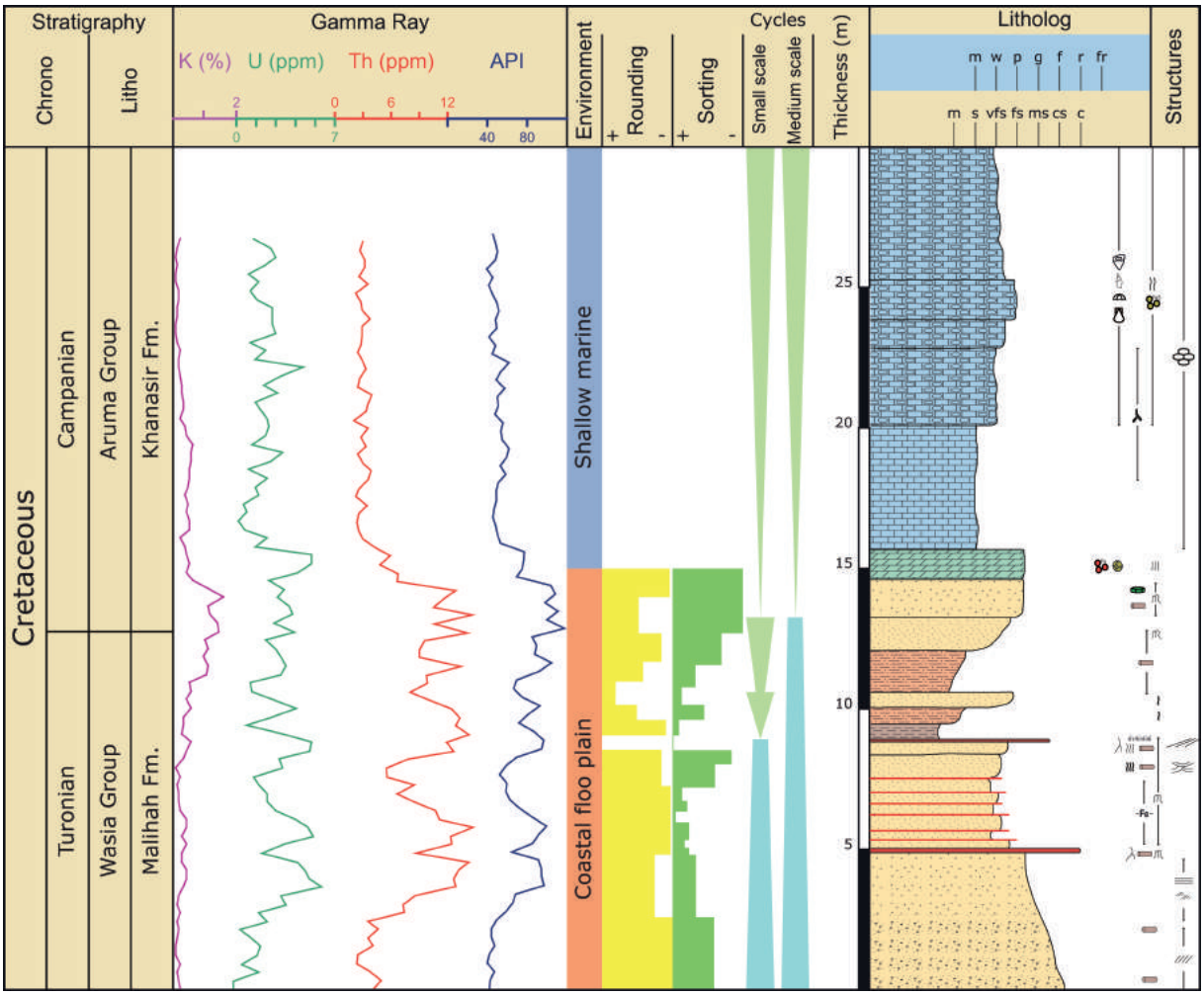

Figure 22. Litholog and SGR log of Section KW-5. Locality as in Figure 2. Legend as in Figure 8.

tidal channels show a flow direction toward the south, contrary to the direction of the fluvial system, which is also present in the Malihah Formation (Figure 39D). These currents likely represent flood-tidal currents that can travel far up the coastal backwater zone.

The tidal succession is followed by a fluvial environment reflected by trough cross-bedded sandstones, coarse-grained channels containing lag deposits with wood and various paleosols (Figure 23E). At Khashm Wisi, the fluvial environment is better developed (Figures 15, 20). The deposits in this area represent a broad, relatively distal fluvial system with coarse-grained channel sandstones and flood-plain fines. Several paleosols, including an abundant content of flora in situ, are preserved here.

The formation of bauxite at the top of the Malihah Formation is an indication of a major regional hiatus, which occurred throughout the Arabian peninsula. This stratigraphic gap was caused by uplift and exposure of the central Arabian area and marks the pre-Aruma unconformity.

SGR Characteristics

The Malihah Formation is composed of a lower, sand-dominated unit and an upper unit, in which siltstones and mudstones with paleosols dominate. The resulting SGR logs (e.g., Figures 15, 17) correspondingly show very low values in the lower succession and an increase to medium and high readings in the upper part. Especially the ferruginous horizons and limonitic crusts show high values.

Khanasir Formation

Lithology and Environment

The lowermost deposits (~4 m [13 ft] thick; Figures 22, 24) are composed of medium- to coarse-grained sandstone (Figure 25A, B) showing reworked clasts and pebbles of Wasia sediments. The sandstones commonly contain iron-coated grains and glauconite. Locally,

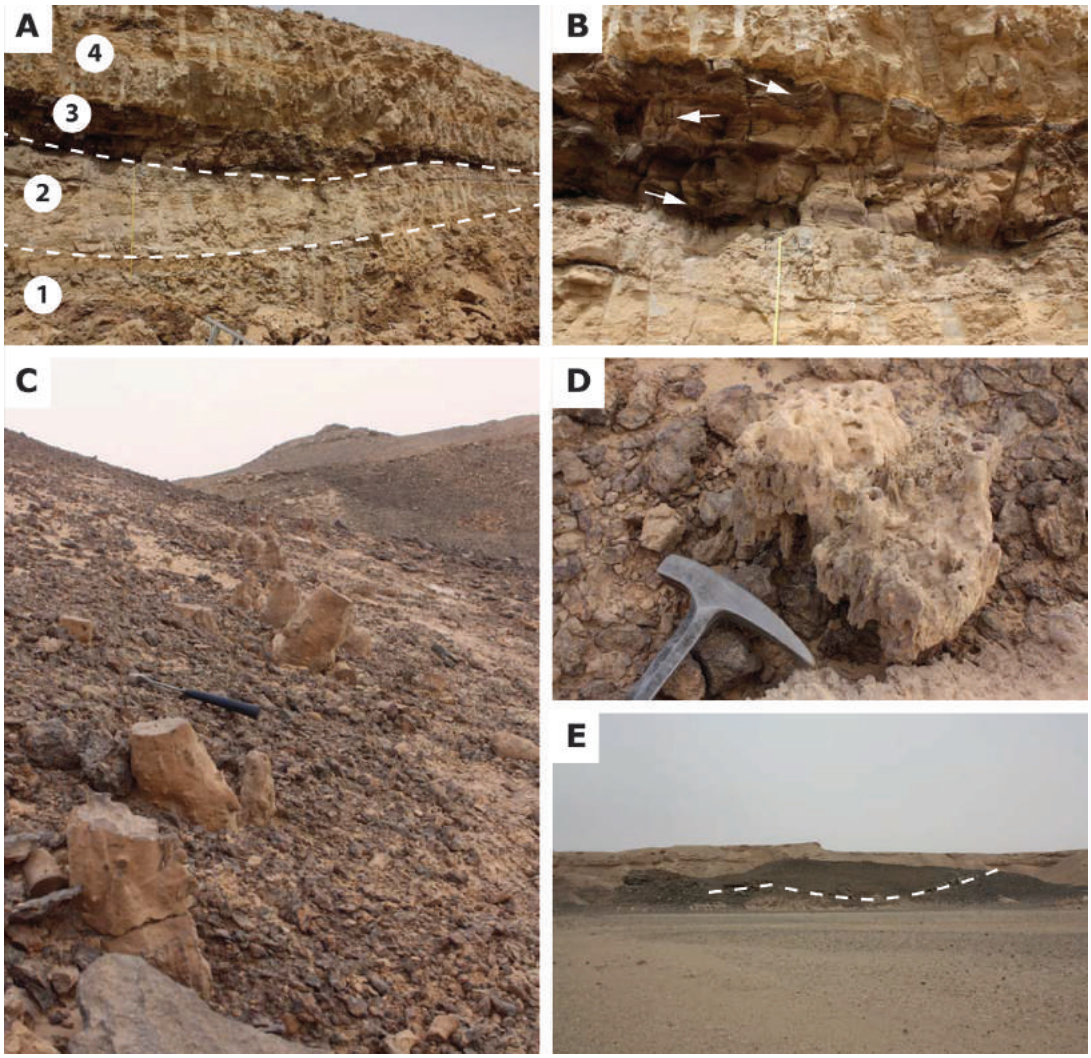

Figure 23. Aspects of the Malihah Formation. (A) Burrowed and bioturbated clay- and sandstones, showing tidal micro-ripples (1) of the tidal flat are locally incised by tidal channels (2). Ferruginized relicts of probably plant, wood, or peat remains (3) are common in thin sheets of sandstones and laterally correlate to horizons that contain abundant roots and tree trunks in life position (see C). Section KR-2. (B) Close up of tidal channel with herringbone cross-bedding. (C) Prominent horizon of roots in life position. The roots probably stem from an ancient palm family and are well preserved due to precipitation of iron minerals. The straight cut surface at the top of the roots possibly indicates the ancient water table. Section KW-2. (D) Roots intruding tidal siltstones. Same location as (C). (E) Large fluvial channel of coarse-grained sandstones incising subjacent, tidal deposits of the Malihah Formation. Localitiy Khushaym Radi.

this sandstone unit is dolomitized or replaced by a finer-grained assemblage. Next comes orange-brown dolomite (Figure 25A, B) with abundant vugs, which are partially filled by calcite. Quartz grains are common in the basal part of the dolomite, but disappear upward.

The next 25 m (82 ft) consist of nodular bioclastic wackestones with an abundant macrofauna in the lower part (ammonites, echinoderms, gastropods, sponges, bivalves, and inoceramids). The limestones are often intensively bioturbated (*Thalassinoides*) and in patches contain efflorescences of pyrite. The unit contains several thick mudstone intervals (Figure 24).

The following unit of about 20 m (66 ft) is represented by chalky wackestones, showing moderate bioturbation and abundant fragments of dasycladacean algae. The upper 25 m (82 ft) of the formation comprise some 10 m (33 ft) of dolomitic shales, overlain by cherty dasycladacean rich wackestones. This unit is in turn overlain by shales, which upward pass into nodular bioclastic wackestones. The limestone yielded an abundant fauna including gastropods, foraminifera, echinoderms, and solitary corals. The shales are only present at some of the locations and pass laterally into limestones of shallow marine origin.

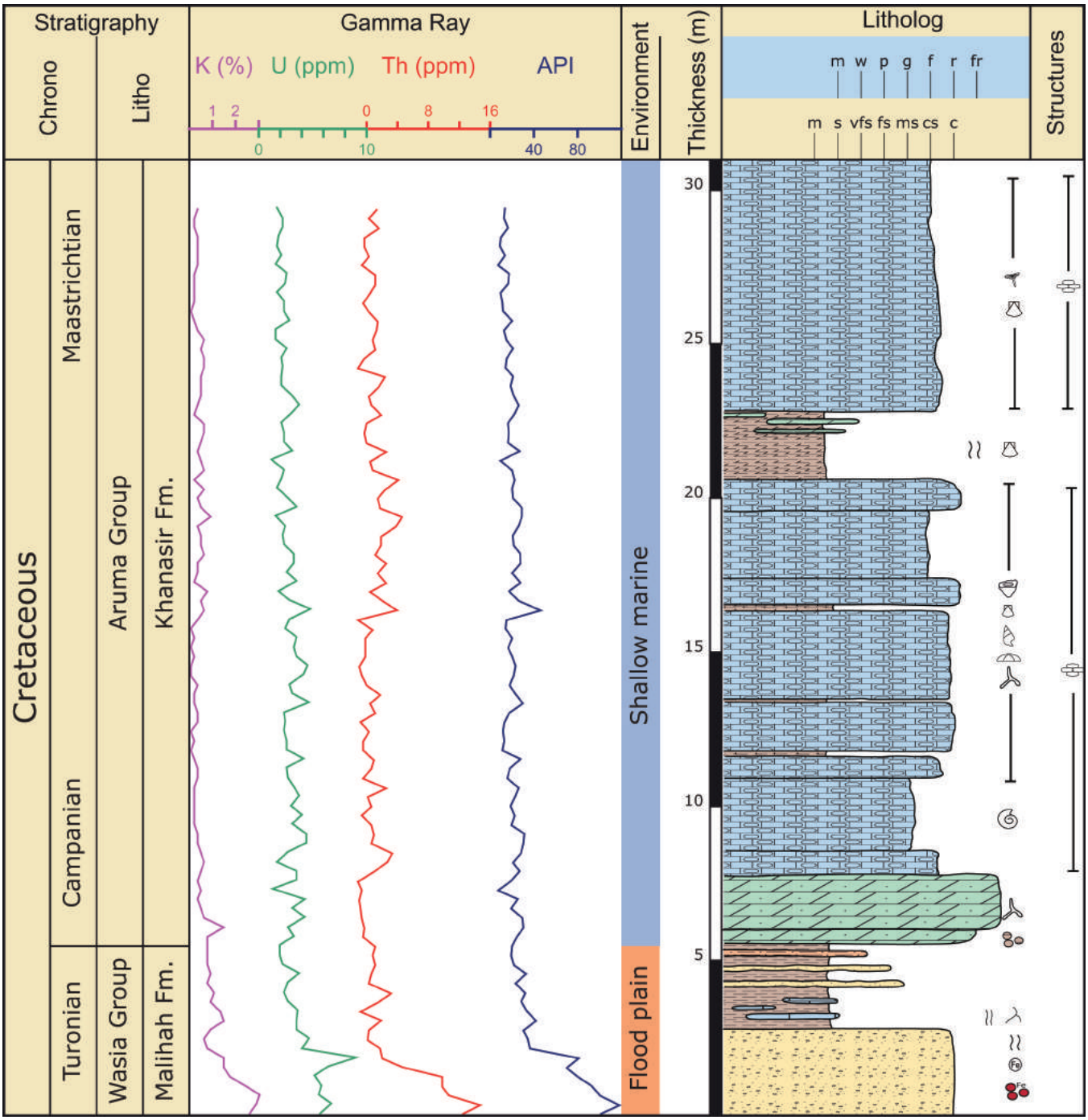

Figure 24. Litholog and SGR log of Section AR-1. Locality as in Figure 2. Legend as in Figure 8.

The lithology and sedimentary succession of the Khanasir Formation observed during the fieldwork only differs in details from that reported by Vaslet et al. (1991) and Philip et al. (2002). It mainly concerns lateral variations in thickness of specific units.

The Aruma Group originated during a transgressive–regressive cycle (Figure 3; Sharland et al., 2001), with the Khanasir Formation as its lowermost unit reflecting the transgressive stage. The obduction of ophiolites along the eastern and southeastern Neo-Tethys margin resulted in crustal loading and, as a consequence, the regional eastward tilting of the Arabian plate (Alsharhan and Nairn, 1990). In contrast, the western Arabian Peninsula was uplifted and exposed. The ensuing transgression reached its maximum extent as it flooded Jordan, central Saudi Arabia, and Yemen, where it led to deposition of shoreline siliciclastic and continental deposits. In southwestern

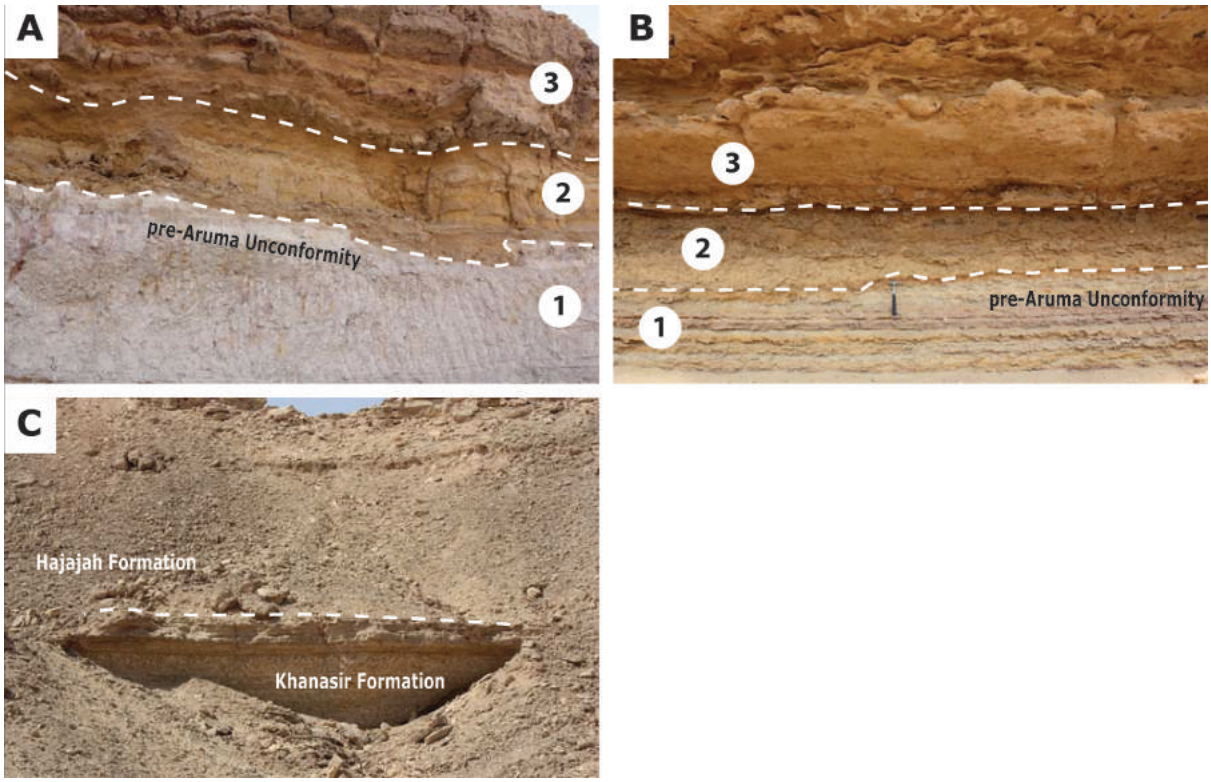

Figure 25. Outcrops and depositional features of the Khanasir Formation. (A) Erosional base of the Khanasir Formation (pre-Aruma unconformity). (1) The surface truncates the fine-grained deposits of the Malihah Formation. (2) Dolomitic sand and sandstones of the Khanasir Formation are abruptly overlain by (3) dense dolomite. Section KR-1. (B) (1) Unconformable contact with the Majma Formation. (2) The basal sediments form a transgressive lag deposit with reworked clasts of subjacent deposits. (3) Here, too, a dense crystalline dolomite is developed above these deposits. Section TH-1. (C) Boundary between the Khanasir Formation and the overlying Hajajah Formation. Nodular wackestones of the Khanasir top are capped by a hardground. The hardground is conformably overlain by mudstones of the Hajajah Formation. Section AR-3.

Saudi Arabia, the Aruma siliciclastic deposits, not considered in this study, are part of these fringing sands as part of the Cretaceous sands aquifer (Figure 1).

The middle and upper units of the Khanasir Formation are a shallowing-upward succession developed under highstand conditions. It is composed of bioclastic, nodular, and partially dolomitic limestones, as well as shales. It probably originated in a relatively protected, low-energy carbonate platform environment, which is suitable for the development of green algae associations (Philip et al., 2002). This succession in turn is capped by a conspicuous hardground.

SGR Characteristics

The Khanasir Formation is an overall calcareous unit. Correspondingly, the SGR logs all show very low values (Figures 22, 24). In the basal part, however, it is constituted by a thick package of coarse sandstones that rest on the underlying Malihah Formation. Conventionally (Le Nindre et al., 2008), the pre-Aruma unconformity was drawn at the base of this thick sandstone package. In sections KW-2, KW-4, and KW-5 (Figures 15, 20, 22), the SGR values in these sandstones are very high and in fact represent the culmination of the general rise observed in the underlying Malihah Formation. A sharp decrease marks the transition to the normal values for limestones in the Aruma Group.

In the Khushaym Radi area, the basal sandstones are absent (Figure 17) and the base of the Khanasir Formation is marked by a decrease in comparison to the underlying Malihah sediments. In the subsurface, a correlation would certainly be made in all sections at the base of the drop of the values and this would be taken as the base of the Khanasir Formation.

Hajajah Formation

Lithology and Environment

The lithology of the Hajajah Formation is rather uniform throughout central Arabia (Figures 26, 27; Vaslet et al., 1991). Philip et al. (2002) gave a detailed description for the sections at Khushaym Radi (Figure 27):

The base is composed of variegated shales, marls, and thin-bedded limestones. The shales contain plant

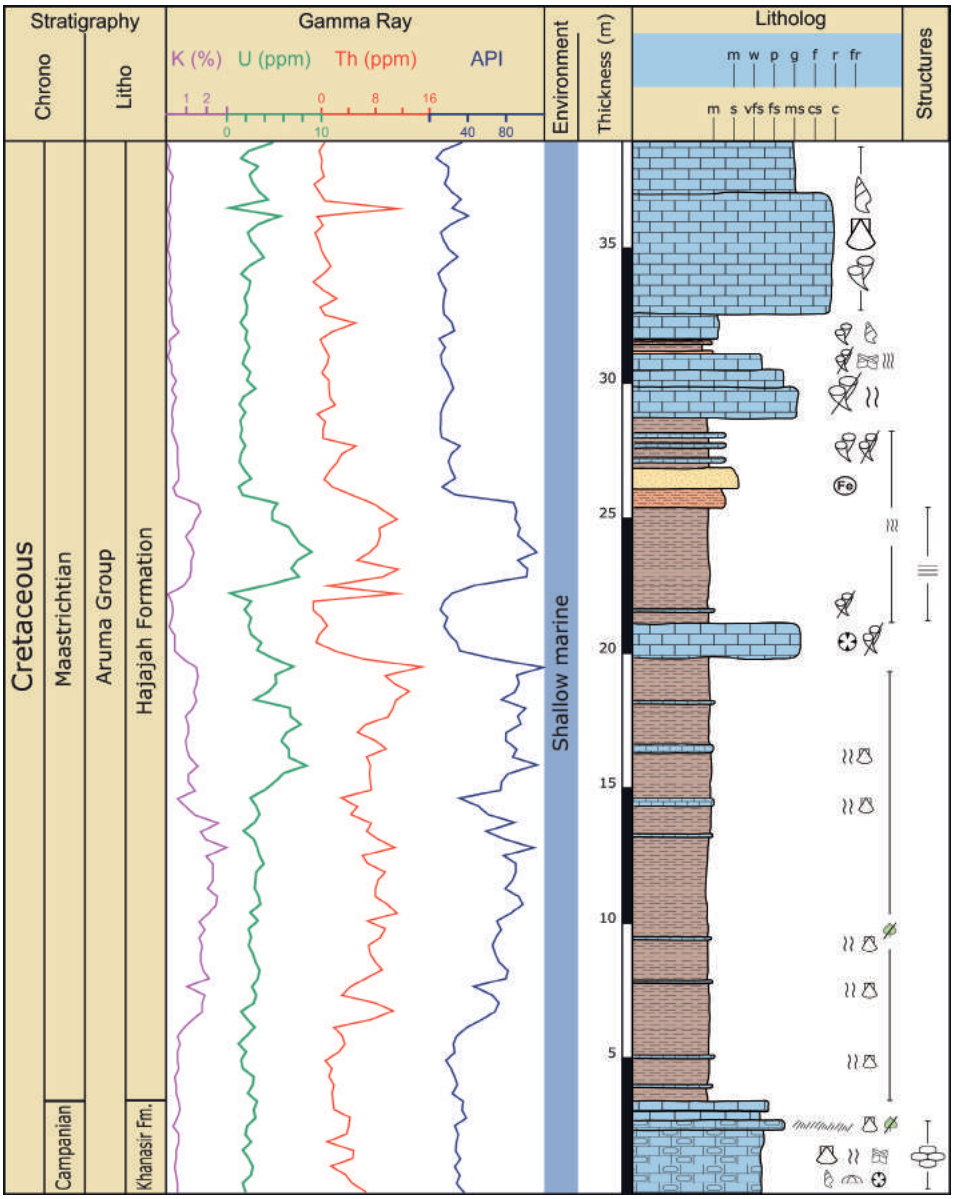

Figure 26. Litholog and SGR log of Section AR-3. Locality as in Figure2. Legend as in Figure 8.

fragments and fish bones and display a laterally varying thickness from 1 or 2 m (3–6 ft) to about 20 m (66 ft), depending on the erosional incision prior to deposition. The limestones yielded an abundant fauna of rudists, corals, and larger foraminifera.

This succession grades upward into 7 m (23 ft) of shales with plant fragments, passing into fine ocherous silt and siliciclastic sands. Locally, these siliciclastic rocks are replaced by pedogenic mudstones or a floatstone–framestone unit composed of biostromal rudist, corals, and chaetetid sponges (Figure 28A). This unit is capped by a hardground including features like teepees, fossil debris, and encrusting fauna (Figure 28C). The top of this succession is locally truncated by channel-like bodies of about 6 m (20 ft) thickness formed by cross-bedded packstone–grainstones containing fragments of rudists and corals.

Next come about 5 m (15 ft) of green shales, locally with plant fragments and iron oxide nodules. An up to 2-m (6-ft)-thick biostromal body formed of massive and branched corals follows the shaly succession. Toward the top, small *Biradiolites* and gastropods were observed in bioturbated layers, followed by another hardground.

The following 6 m (20 ft) are composed of olive green or ochre shales that grade upward into silty shales and siltstones and locally calcareous mudstones containing small *Biradiolites sp.* The upper part of this succession locally shows intense bioturbation (Figure 28D, E) and is overlain by lenticular dolomitic

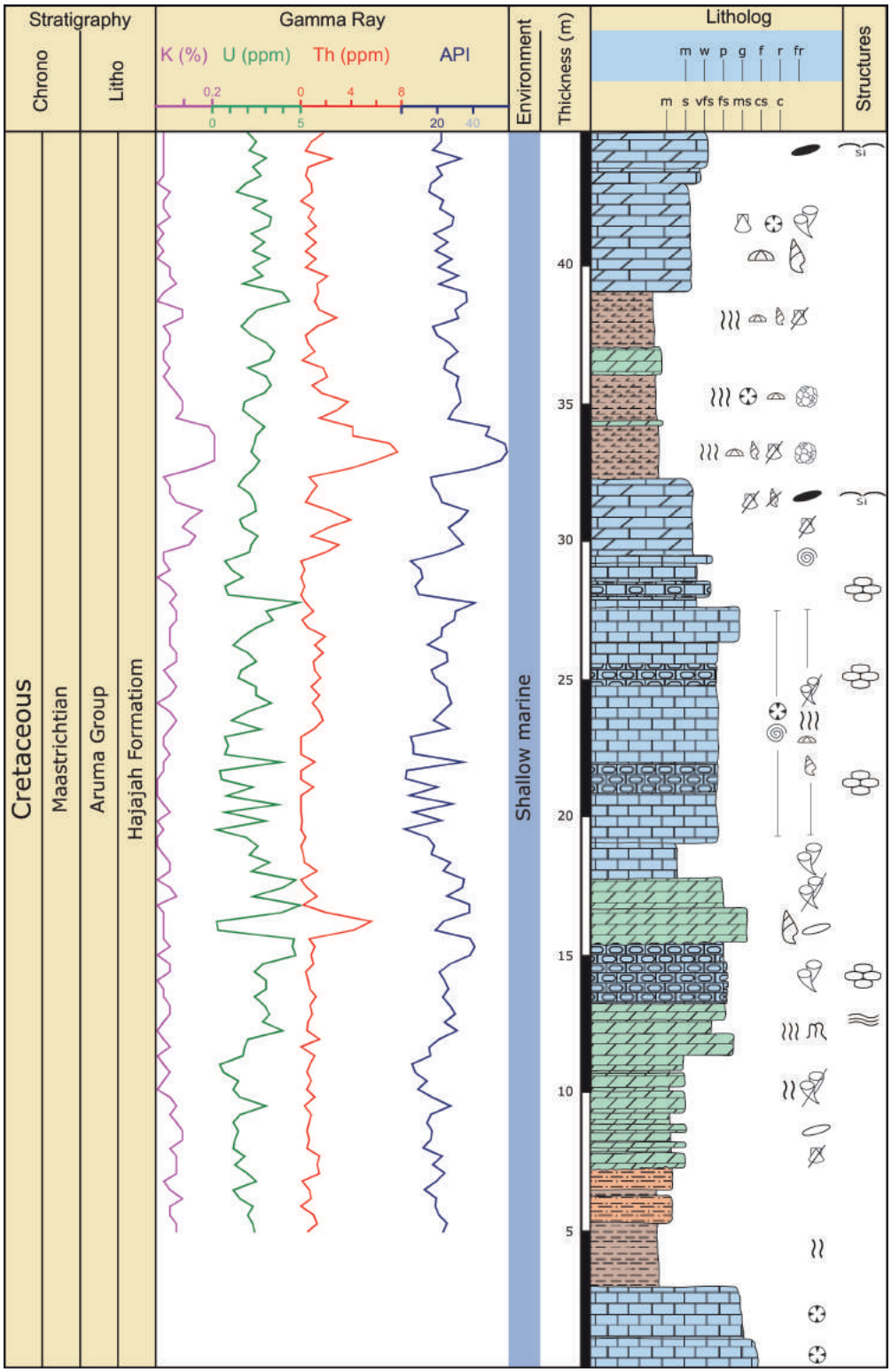

Figure 27. Litholog and SGR log of Section AR-10. Locality as in Figure 2. Legend as in Figure 8.

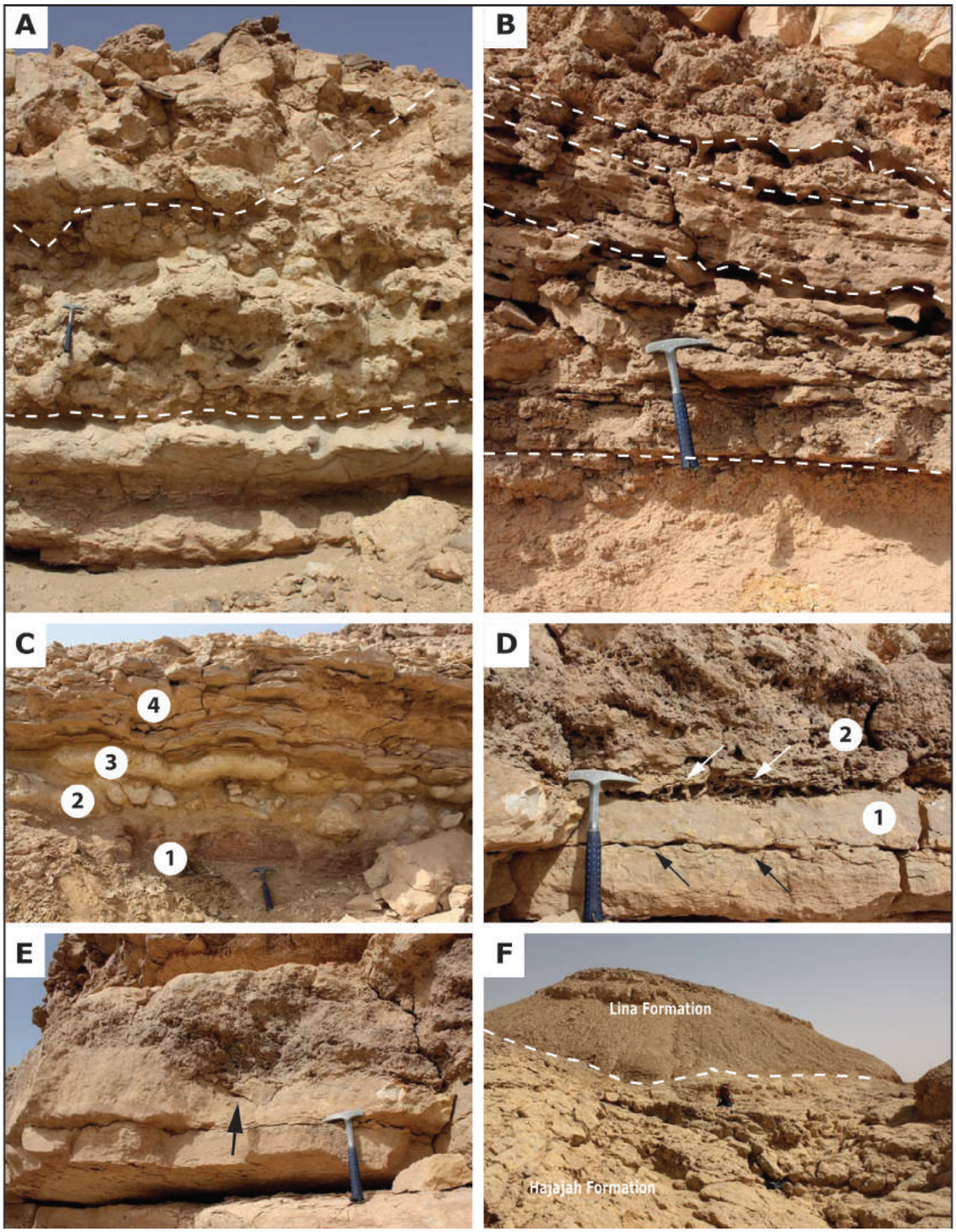

Figure 28. Outcrops and depositional Features of the Hajajah Formation. (A) Top deposits of the Khanasir Formation composed of bioclastic wackestones overlain by a rudist-rich biostrome (dashed lines). Section AR-4. (B) Siltstones erosionally overlain by cross-bedded grainstones-rudstones. The latter are probably the product of major storm events. Section AR-4. (C) Boundary between the Khanasir and Hajajah formations: (1) reddish shales of a paleosol are overlain by (2) a conglomeratic layer of reworked limestone nodules followed by (3) 20 cm thick, wavy wackestone. The upper part of the Khanasir Formation is represented by (4) thin-bedded, wavy and laminated dense limestones. Section AR-1. (D) (1) Thick-bedded, calcareous siltstones are overlain by (2) extremely bioturbated limestone. The siltstone shows loading structures at the base of beds (arrows). The top of the siltstones is affected by intense bioturbation that destroyed the primary structure of the siliciclastic bed. Section Ar-2. (E) Same horizon as (D) with bioturbation penetrating down into the siltstone. Locally the entire bed has been destroyed. (F) Unconformable boundary (pre-Umm Er Radhuma unconformity) between the Hajajah and Lina formations (dashed line). Dolomitic floatstones are overlain by basal gypsiferous shales of the Lina Formation that grade into clayey and fossiliferous limestone.

grainstones packstones with cross-bedding, incising into the subjacent layers (Figure 28B), which in turn are capped by rudist-rich floatstones. Laterally, they merge with small rudist biostromes. This coarser-grained unit laterally varies in thickness between 4 and 10 m (13–33 ft).

The next subunit is about 10 m (33 ft) thick and mainly composed of rudist-bearing grainstones and bioturbated packstones. Very prominent large gastropods and rudists can be observed in these limestones. Laterally, the grainstone–packstones pass into biostromes and banks composed of rudists (Figure 28E). The basal part of this unit is a lag deposit containing fragments of rudists eroded from the underlying unit. Locally, a rudstone is developed interfingering with biostromal bodies (Figure 28D).

Bioturbated packstones wackestones grade upward into bioclastic, medium-bedded grainstones. This section is about 8 m (26 ft) thick and contains abundant larger foraminifera (*Omphalocyclus*, *Orbitoides*, and *Lepiorbitoides*) as well as abundant fragments of other fossils.

The upper middle part of the Hajajah Formation is composed of about 8 m (26 ft) of mudstones and wackestones bearing brachiopods, solitary corals, echinoderms, and rare rudists. Locally, the mudstones and wackestones are dolomitized with only few faunal remains of echinoderms. In the middle part of the deposits, siliceous incrustation was observed, and the top is capped by a prominent silicified surface. In these areas of silicification, chert nodules can be found, which are blackened by iron oxides where exposed to the surface. Beige, slightly dolomitized wackestones with fossil fragments directly overlie the silicified surface and grade upward into platy shales and marls. The shales are dolomitized, bioturbated, and contain many fragments and imprints of fossils (bivalves, gastropods, solitary corals, and echinoderms). Clayey mud- and wackestones with an abundant fauna overlie the shales. Besides solitary corals, echinoderms, brachiopods, and foraminifers, some very large gastropods and rare rudists were found in these deposits. The top of this succession is silicified and blackened due to weathering. Throughout this section, abundant silicified nodules and rose like nodules were observed. This subunit is about 8 m (26 ft) thick.

The top deposits of the Hajajah Formation comprise bioturbated mud- and wackestones with solitary corals and gastropods in its lower part. The upper part is composed of bioturbated, nodular mud- and wackestones rich in nautiloids, and a benthic fauna of rudists, corals, bivalves, and abundant gastropods. Dolomitized floatstones with abundant corals, rudists, and fragments of other fossils represent the top of the Hajajah Formation. This unit strongly varies laterally in thickness beneath the pre-Lina unconformity documented by Thomas et al. (1999).

The Hajajah Formation contains the highstand deposits of the sea-level rise that started with the Khanasir Formation (Figure 3). The formation is composed of medium- to small-scale cycles and can be grouped into two sequences (possibly third-order) and several parasequences (Philip et al., 2002). The deposition of the formation took place in a broad shallow-marine shelf, probably a nearshore ramp with tidal-flat environments.

The basal deposits reflect a medium-scale transgression represented by paleosols, tidal channels, and biostromes. These biostromes are mainly composed of rudists and chaetetid sponges that originated in warm shallow water conditions of onshore and shoreface environments. According to Philip et al. (2002), tidal flat indicators are a scarce fauna and tidal channels that cut through underlying sediments. Biostromes of corals and rudists, as well as rudist banks, progressively evolved, until a rudist carbonate platform developed in the upper part of the sequence (Philip et al., 2002). A major erosional event affected this platform during a major sea-level fall and a channel like erosional pattern developed.

Although a coastal floodplain with a transition into adjacent tidal flats is a viable scenario for the depositional environment, the presence of grainstones–rudstones on floodplain siltstones (Figure 28B) is hard to explain through tidal currents. It seems more likely that these coarse deposits are the results of major onshore storms, which destroyed the biostromes and transported the debris shoreward.

The second sequence within the Hajajah Formation represents a renewed sea-level rise and the evolution from an initially high-energy carbonate platform toward low-energy offshore environments (Philip et al., 2002). The base of the sequence is a transgressive lag deposit containing fragments of rudists and demonstrates reworking of the underlying rudist carbonate platform. Upsection, a high-energy system developed. Cross-bedded grainstones and bioturbated rudist packstones and rudist banks evolved during this period. The subsequent mud- and wackestones yielded an abundant marine fauna and represent an environment of lower energy. The occurrence of nektonic faunas (nautiloids) represents the maximum flooding surface in the upper third of the sequence (Philip et al., 2002).

SGR Characteristics

The Hajajah Formation is dominantly a calcareous unit; only in its lower part and its upper part (Figures 27, 29), there are two prominent intercalations

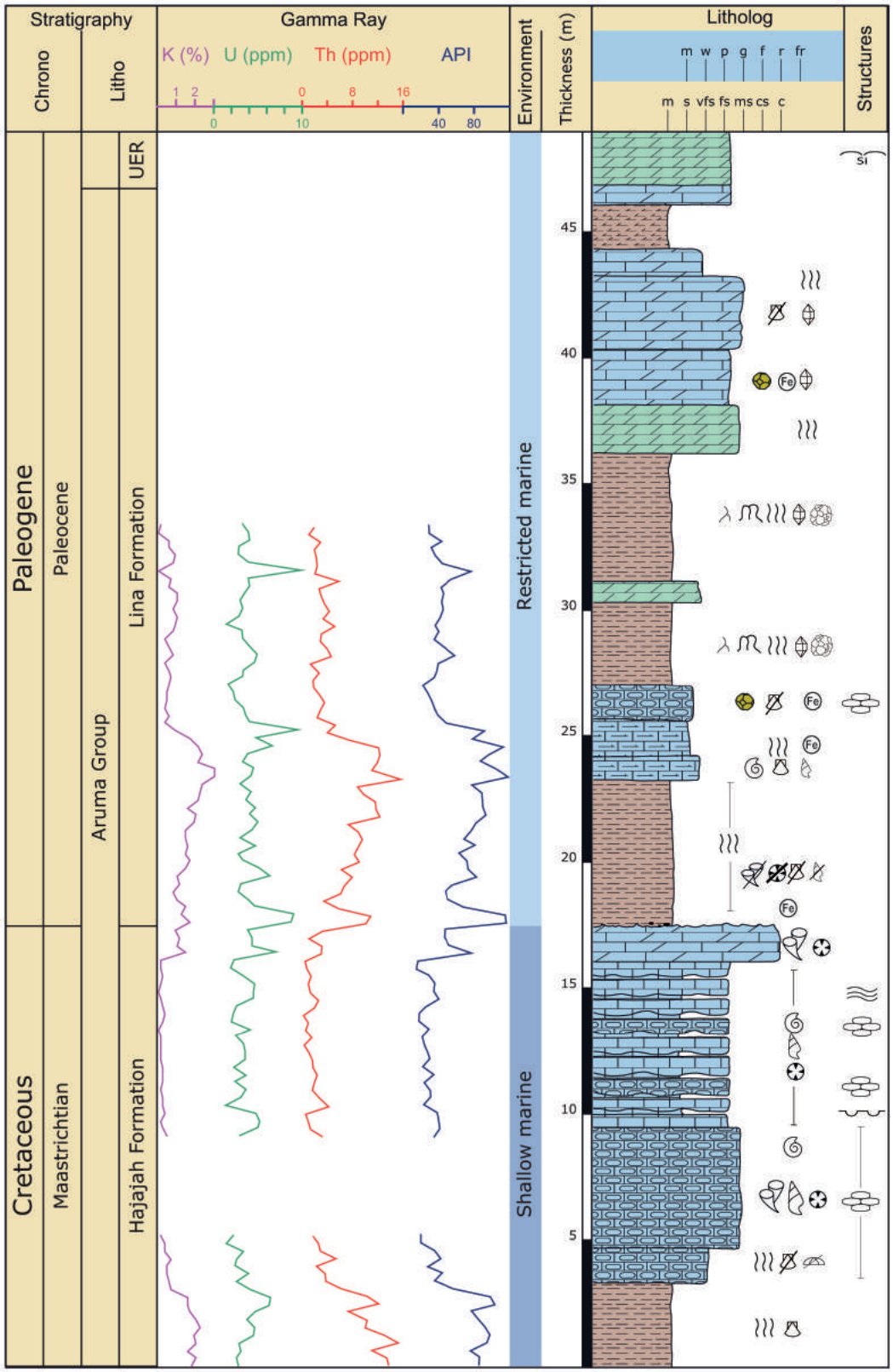

Figure 29. Litholog and SGR log of Section AR-6. UER = Umm Er Radhuma Formation. Locality as in Figure 2. Legend as in Figure 8.

of terrigenous siliciclastic deposits. These rocks are characterized by somewhat elevated values; however, in comparison to similar intercalations in other formations, the values are still at a low level.

Lina Formation

Lithology and Environment

Vaslet et al. (1991) and Thomas et al. (1999) observed about 25–30 m (82–98 ft) of sediments of the Lina Formation in the Khashm Wisi area (Figure 29).

Basal beige to red, pyritic, and gypsiferous shales (~2–5 m [6.5–16 ft]), containing abundant iron oxide nodules. Bioturbation, silica nodules, and pyritic fossils (solitary corals, bivalves, and gastropods) are common in these deposits.

Next come clayey and fossiliferous limestone (~7 m [23 ft]) and nodular biosparite. The limestones are bioturbated and vugs filled with calcite are common. The fossils are partially pyritic and include gastropods, bivalves, and rare echinoderms.

Up section, there is an alternation of varicolored pedogenic claystone and silty shales, with bioturbated, thin-bedded dolomitized limestones (~10 m [33 ft]). Ferruginized remains of roots were found in this interval. Evaporite nodules of former sulfates, now replaced by quartz, as well as pyritic nodules are abundant.

Sparry dolomitized limestone of about 4 m (13 ft) containing quartz nodules and bipyramidal quartz crystals overlies the subjacent unit. Some fragments of fossils (bivalves and gastropods) are visible in the limestone.

The top of the Lina Formation is composed of 2 m (6.5 ft) of ochre, pedogenic dolomitic shale beneath carbonate mudstones of the Umm Er Radhuma Formation.

Although stratigraphically (still) part of the Aruma Group, genetically it is independent from the underlying deposits. In contrast, the Lina Formation has to be regarded as part of the Umm Er Rhaduma depositional system. With its sparsely rooted horizons, evaporitic nodules, and their cyclic alternation with thin dolomitic beds, it indicates the initial interplay between terrestrial and restricted marine environments at the beginning of the ensuing transgression above the sequence boundary separating TMS 9 and TMS 10 (Sharland et al., 2001).

SGR Characteristics

Only the basal part of the section of this unit could be logged (Figure 29). Its base is marked by a sharp increase in values compared to the underlying Hajajah Formation. Above this is a package of terrigenous mudstones that pass into carbonates. Contrary to the expected, the K and Th values increase into the basal carbonates. The reasons for this are not clear. Up section, and within the carbonates, there is a drop to normal values for carbonates. At about 31 m in this section, there is a dolomite horizon overlain by terrigenous mudstones. Both Th and U values increase in the mudstones; in contrast, K remains just above the detection value. This interval is interpreted to reflect the clay mineralogy, the dominant mineral being kaolinite.

CRETACEOUS AQUIFERS

A reservoir is defined as a layer or layered sequence of rock or sediment that contains a fluid (water, crude-oil, and natural gas) and that is able to release or transport significant quantities of this fluid under an ordinary hydraulic gradient (Hiscock, 2005). Aquifers are special reservoirs that contain significant and abstractable amounts of water. In contrast, aquitards (and aquicludes) have a tight fabric that does not provide significant hydraulic conductivity; hence, they act as seals and give way to the confinement of the aquifers.

The primary rock fabric (including the early diagenetic phenomena) is one of the main critical factors that determine the quality of an aquifer. A suitable aquifer should have a high storage capacity and additionally substantial transport paths for the medium that is desirable to be produced. Consequently, the prevailing rock type should rather have a porous fabric than a tight and fine matrix to provide enough pathways for the medium. According to Pettijohn (1983), in a first approximation, the permeability is proportional to the porosity and inversely proportional to the specific surface (cm^3/cm^2). Hence, permeability is directly related to the specific surface, and thus to the grain size. Consequently, the coarser the grains of a deposit are, the smaller the specific surface and the larger the permeability would be.

The Cretaceous succession discussed here forms one of the most important aquifer systems in Saudi Arabia. The system is composed of several aquifers separated by low-permeable aquitards or impermeable aquicludes. It comprises two principal aquifers (Biyadh Formation and Wasia Group), a secondary aquifer (Aruma Group), and several semipermeable or impermeable formations or parts of them (e.g., Buwaib aquitard, Sallah–Shu'aiba aquitard, and Upper Wasia–Lower Aruma aquitard). A third aquifer system, the Cretaceous sands aquifer (Figure 1), is not part of this study.

Biyadh Aquifer

The Biyadh aquifer is a principal aquifer composed of an alternation of medium- to coarse-grained, poorly cemented sandstones with interbedded siltstones and shales. The Biyadh Formation directly overlies the rather impermeable limestones (aquitard) of the Buwaib Formation and in turn is overlain by the Sallah aquitard.

In central Saudi Arabia, near Al Kharj (Figure 4), the Biyadh aquifer constitutes a single porous sandstone aquifer bound by impermeable layers and hence exhibits confined conditions. Further northwest, near Ar Riyadh, the Biyadh Formation is unconformably overlain by sandstones of the Wasia Group without intervening aquitards. Together, these deposits form a single principal aquifer system on the Northern Interior Homocline (Edgell, 1997). Toward the south of Al Kharj, where the Aruma Formation is developed in sandy facies, the Biyadh aquifer, Wasia aquifer, and the Aruma aquifer together form the multistorey Cretaceous sands aquifer.

Diagenesis

Representative samples were taken from four sections and studied with respect to petrography and diagenesis. The samples together cover the entire spectrum of depositional environments of the Biyadh aquifer in outcrop.

Coarse quartz sandstones are mainly formed by a very porous and high-permeable fabric, which is locally intensively cemented by multicycle silica overgrowth. Thin sections show very well-developed inclusion-rich cement seams surrounding the detrital quartz grains (Figure 30A). A second generation of silica overgrowth that reflects incomplete overgrowth and well-developed crystal outlines was observed under the SEM (Figure 30B). In the northern sections, this feature is present in several levels of the Biyadh Formation and mostly shows an extent throughout the entire outcrop. The cementation by silica seems to be horizontal and bound to distinct layers. This probably indicates precipitation from oversaturated waters according to an ancient groundwater table and favorable conditions of the degree of acidity (high pH). However, the exact origin of this silicification is unclear and further analysis should be performed if it was formed during compaction, hydrothermal precipitation or even as organic silica cement. Because of this intensive cementation, the sandstone exhibits very low porosity (3%) and permeability (<1 mD) and might locally act as regional aquiclude where this cementation is laterally persistent. Furthermore, concave–convex structures are visible at points of contact between the detrital grains. The grains are cracked by sediment overload that caused high pressure onto the grain fabric and led to compaction. The compaction in turn led to a decrease in size of the pores and therefore a reduction of the intergranular porosity of the sandstone.

Very porous quartz siltstone to fine-grained sandstones show very poor sorting and consist of angular to subangular grains. In the thin section and SEM photography (Figure 30C, D), the high porosity (36%) is clearly visible and is caused by numerous intergranular pores and probably additional secondary porosity due to dissolution of primary cements and etching of grains. Because only thin relicts of silica overgrowth are preserved, the pore throats remained open and permeability is relatively high (2200 mD).

Mudstone samples show a very tight fabric of clay-sized material with floating grains of quartz inside. The blue staining of the sample's thin section (Figure 30E, F) shows a poorly visible porosity (15%) due to the dense fabric built by the fine-grained clay material. The presence of clay also decreases the permeability to a minimum (0.5 mD) caused by plugging of pore throats.

Figure 30G, H shows a sample of fine- to medium-grained, very porous sandstone and represents the most common rock type occurring in these parts of the Biyadh Formation. The sandstone mainly shows well sorted and subrounded to well-rounded quartz grains that were affected by compaction and dissolution processes. These events led to the development of secondary porosity and, together with the absence of unfavorable cements, result in very high porosity (35%) and permeability (3760 mD).

The upper part of the Biyadh Formation is characterized by silty marls and clayey siltstones with intercalated poorly sorted, porous quartz sandstones. These sandstones are negatively influenced by the presence of clayey material that intruded from neighboring deposits and that plugs pores and pore throats (Figure 31A, B). The pores and grains are mainly covered by clay and pore throats are closed or narrowed by clay cement that developed in meniscus position. Though the porosity remained on a relatively high level (21%), the permeability is lowered by the presence of these cements (165 mD).

Porosity and Permeability

Samples of the Biyadh Formation were taken in an active quarry (section B-1 and B-2; Figure 2). The Biyadh Formation is predominantly composed of medium-grained, uncemented quartz sandstone. Twenty-five samples were successfully taken and prepared for the subsequent measurement of porosity and permeability.

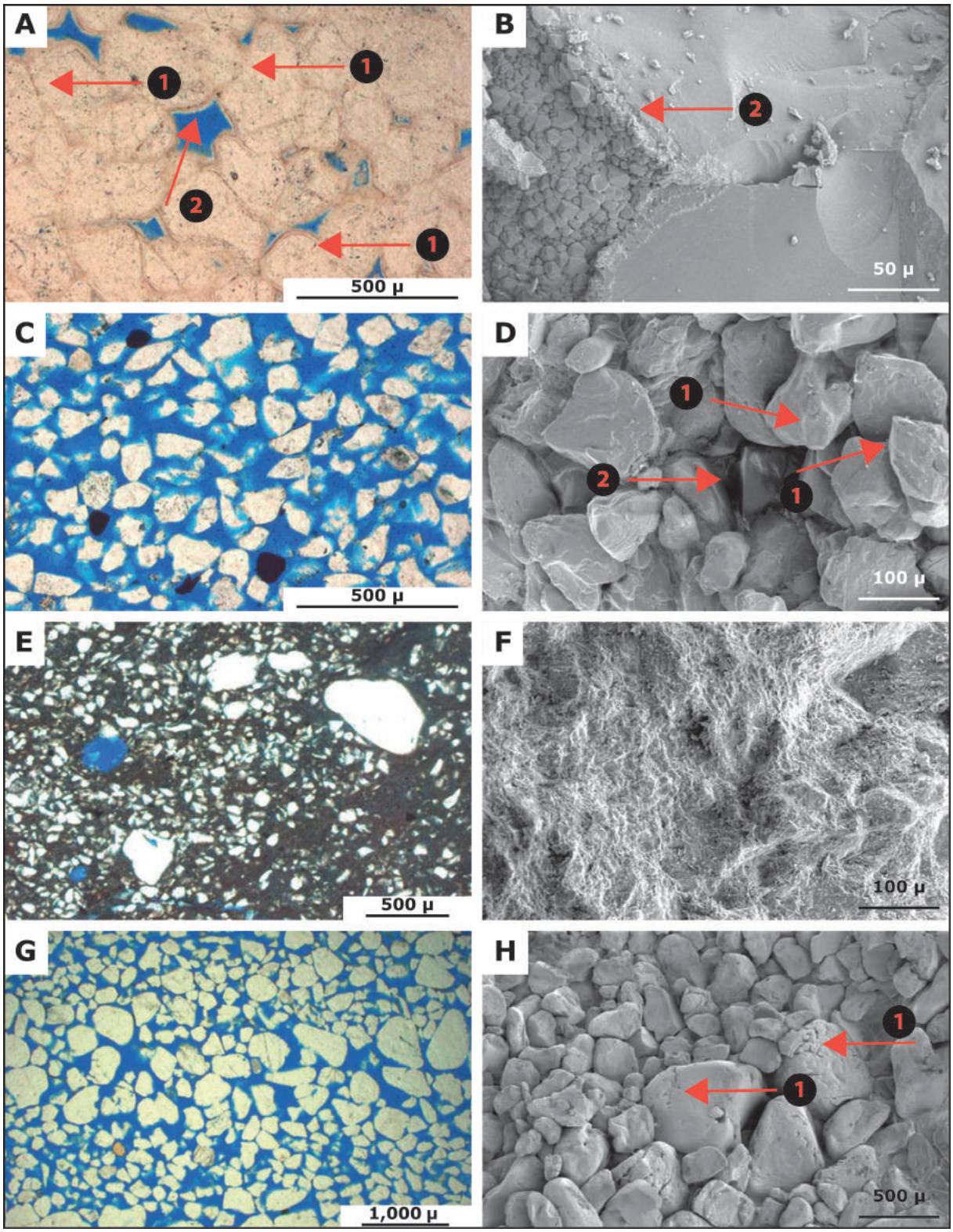

Figure 30. Diagenesis of the Biyadh Formation. (A, B) (1) Quartz sandstone (sample 215) with quartz grains completely covered by silica overgrowths. (2) A second event of silica cementation is represented by small quartz crystals. (C, D) Quartz siltstone to fine sandstone (sample 212). Angular quartz grains indicate secondary porosity due to dissolution and etching. (1) Only traces of thin relics of silica overgrowth are inherited, leading to (2) open pores and high porosity. (E, F) Subrounded quartz grains are floating in a dense matrix of clay. The porosity and permeability are very low due to plugged pore space. Sample 208. (G, H) Quartz sandstone with very angular quartz grains indicating secondary porosity due to dissolution and etching. Only traces of thin relics of silica overgrowth are inherited, leading to open pores and high porosity. Note large open pore in the middle of photograph. Sample 206.

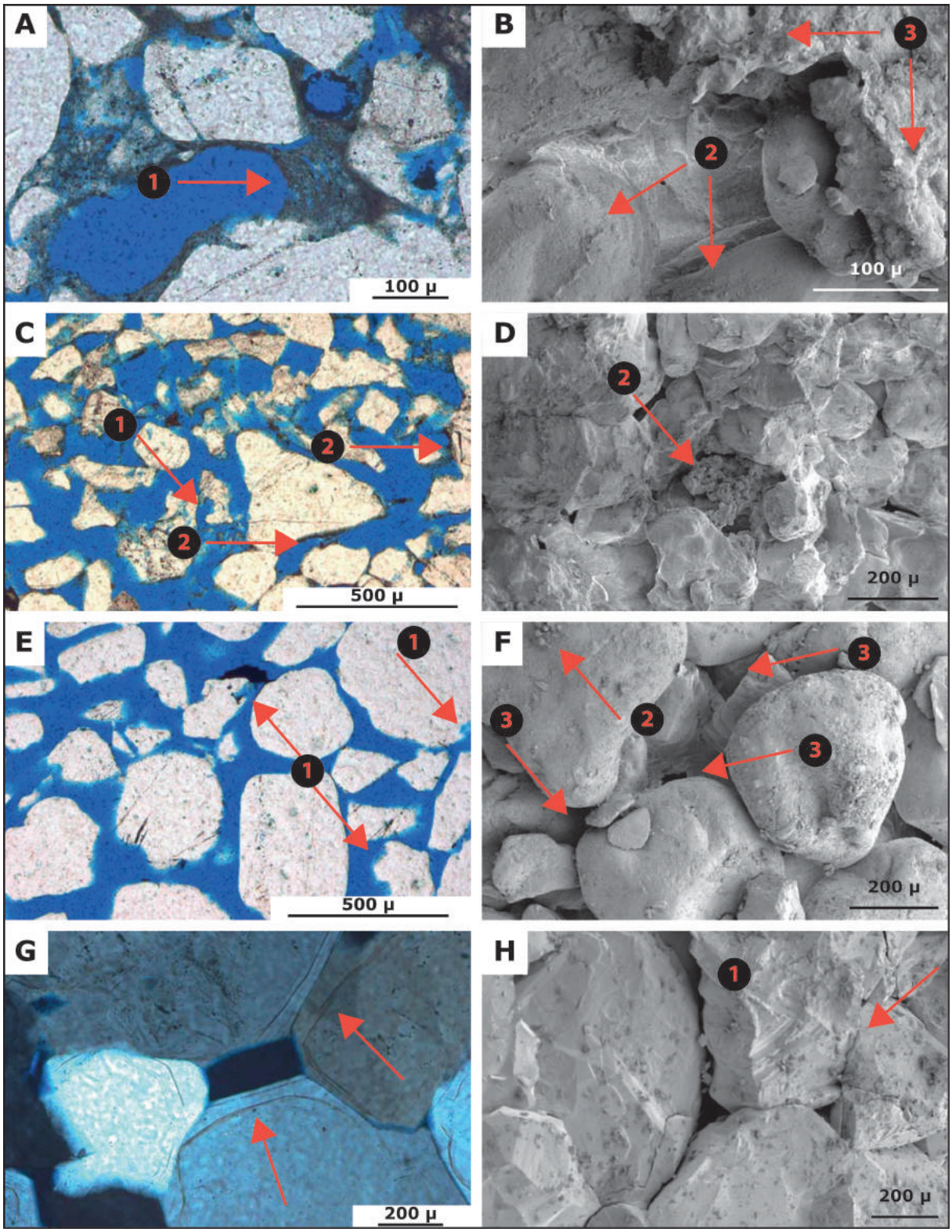

Figure 31. Diagenesis of the Biyadh, Khuraysan and Majma formations. (A, B) Quartz sandstone of the Biyadh Formation. (2) Pore throats and surfaces of quartz grains are covered by (3) abundant clay matrix that commonly occurs in (1) meniscus position. (3) Larger patches of clay possibly originated due to infiltration. Sample 163. (C, D) Moderately sorted quartz sandstone of the Khuraysan Formation. Sandstone is very porous due to (1) intergranular and secondary porosity probably caused by etching of grains. (2) Locally, patches and seams of hematite occur in meniscus position. Sample 142. (E, F) Poorly sorted quartz sandstone of the Majma Formation. (1) Angular grains indicate secondary porosity due to etching and of grains. Sandstone is very porous due to absence of cement. (2) Only relicts of silica overgrowth are inherited. (3) Large open pores lead to high permeability. Sample 167. (G, H) Intensively silicified quartz arenite of the Majma Formation. Sandstone is very tight due to multicycled silica overgrowths (arrows) connecting the detrital quartz grains. Porosity and permeability are relatively low because of missing intergranular porosity. Sample 170.

Table 2. Porosity and permeability data for the Biyadh Formation.

Sample ID	Sample Name	Lithology	Z [mD]	X/Y -Average [mD]	Total Perm. [mD]	Intrinsic Perm. [mD]	Porosity %
161	1	Qtz-Sdst.	296.29	205.55	235.8	188.54	28.14%
162	2	clay. Silt	86.71	*n.m.*	86.71	*n.m.*	21.01%
163	3	Qtz-Sdst.	42.52	87.005	72.18	165.71	21.29%
164	4	clay. Silt	0.17	0.3	0.26	0.02	26.24%
172	13	Qtz-Sdst.	47.12	140.34	109.26	90.192	25.82%
197	B-1	Qtz-Sdst.	3894.26	3039.04	3324.11	*n.m.*	28.81%
198	B-2	Qtz-Sdst.	0.07	0.145	*n.m.*	21.503	7.00%
199	B-2/1	Qtz-Sdst.	0.83	6.54	4.64	9.673	1.12%
200	B-3	Qtz-Sdst.	4199.43	3957.435	4038.1	*n.m.*	*n.m.*
201	B-3/1	Qtz-Sdst.	11727.15	13154.74	12678.87	6520	32.78%
202	B-4	Qtz-Sdst.	2647.88	3182.655	3004.4	368.6	30.42%
203	B-4/1	Qtz-Sdst.	38.79	49.875	46.18	3436	31.13%
204	B-5	Qtz-Sdst.	0.89	3.69	2.76	0.107	20.35%
205	B-5/1	Qtz-Silt/Sdst.	0.21	0.85	0.64	0.07	16.60%
206	B-6	Qtz-Sdst.	3434.4	3936.775	3769.32	*n.m.*	34.91%
207	B-7	Qtz-Sdst.	2639.22	2429.73	2499.56	*n.m.*	27.80%
208	B-8	Silty Clay	0.21	0.595	0.47	0.024	15.45%
209	B-8/1	Silty Clay	4	14.635	11.09	0.051	20.53%
210	B-9	Qtz-Sdst.	2867.36	3163.235	3064.61	400.3	32.78%
211	B-9/1	Qtz-Sdst.	10193.07	6566.29	7775.22	1211.33	31.48%
212	B-10	Qtz-Silt/Sdst.	2160.75	2312.185	2261.71	*n.m.*	36.02%
213	B-10/1	Sandy Silt	3439.07	1575.92	2196.97	3274.2	35.64%
214	B-11	Qtz-Sdst.	0.11	0.37	0.28	0.002	2.61%
215	B-11/1	Qtz-Sdst.	0.9	1.29	1.16	0.002	3.32%
216	B-12	Qtz-Sdst.	4133.85	3940.925	4005.23	*n.m.*	28.72%

The dataset is partially incomplete because some of the samples were destroyed during the measurements. The data for the samples are listed in Table 2.

The sandstones provide good porosity values due to the preserved primary intergranular porosity that is only slightly influenced by clay minerals, which usually plug the pore space. The average porosity of the sandstones is about 34% and thus indicates perfect storage conditions as well as high permeability on the order of 1000–10,000 mD. Some intercalations of silt- and claystone are also present and some beds of sandstones9 experienced intensive cementation by siliceous material. The silicified areas are arranged in layers of up to 2 m (6.5 ft) thickness and laterally continue over more than 200 m (656 ft). The pore space of the silicified sandstones is almost completely plugged by silica cement and their porosity is reduced to a minimum that does not exceed 5% (Figure 32). Hence, the permeability is also low and ranges from 0.002 mD to 1.3 mD. Intercalations of silt- and claystone also cause a drastic decrease in permeability, whereas the porosity is less reduced than in the silicified horizons. The siltstones are predominantly well sorted and provide the same intergranular pore space as the sandstones; however, fine clay material plugs the pores and reduces the porosity to about 20% with permeability ranging from 0.1 mD to a few 100 mD (Figure 32).

Permeability was measured separately for horizontal and vertical directions. It does not show high anisotropy in the sandstones of the Biyadh Formation (Figure 33). Only minor variations of the horizontal permeability are visible in the cross plot, which most likely were caused by tabular cross-beds that are abundant within the sandstones.

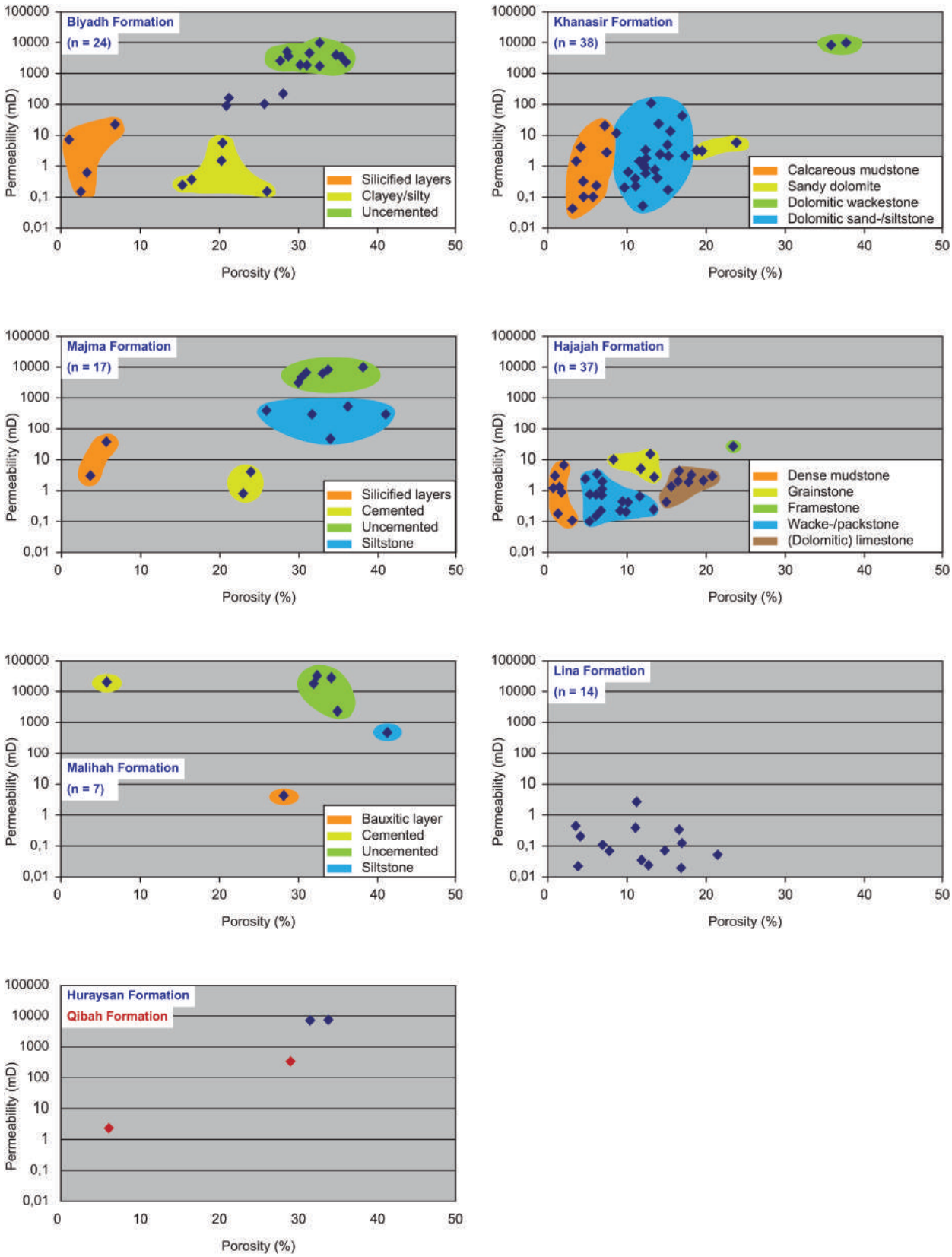

Figure 32. Cross plot of porosity versus permeability for all formations studied. See text for details.

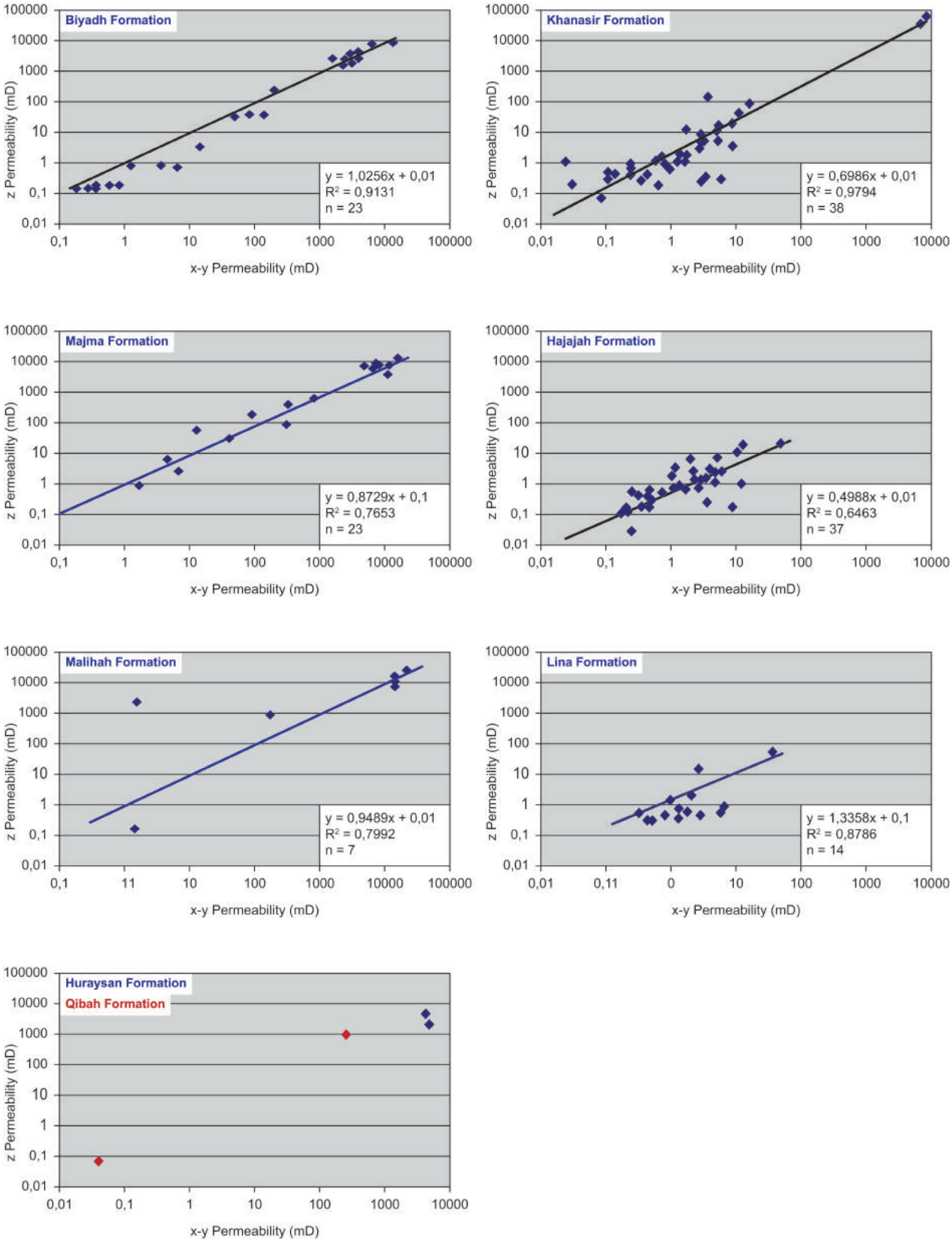

Figure 33. Cross plot horizontal versus vertical permeability for all formations studied. See text for details.

Table 3. Compilation of hydraulic properties of the Biyadh aquifer.

Hydraulic Property	Author	Value range	Average value
Transmissivity, T	*BRGM (1976)*	$1.7 \cdot 10^{-3}$–$9.0 \cdot 10^{-2}$ m^2/s	$3.3 \cdot 10^{-2}$ m^2/s
	Bazuhair (1989)	$1.26 \cdot 10^{-3}$–$7{\cdot}0\ 10^{-2}$ m^2/s	$3.6 \cdot 10^{-2}$ m^2/s
	Edgell (1997)	$1.5\ .\ 10^{-2}$–$9.7 \cdot 10^{-2}$ m^2/s	n/a
Hydraulic conductivity, K	*BRGM (1976)*	$2.5 \cdot 10^{-4}$–$4.5 \cdot 10^{-4}$ m/s	$3.0 \cdot 10^{-4}$ m/s
	Bazuhair (1989)	$3.3 \cdot 10^{-5}$–$3.0\ 10^{-4}$ m/s	$19 \cdot 10^{-4}$ m/s
Storage coefficient, S	*BRGM (1976)*	$2.3 \cdot 10^{-4}$–$9.0 \cdot 10^{-4}$	$4.9 \cdot 10^{-4}$
	Bazuhair (1989)	n/a	$3.2 \cdot 10^{-2}$
	Edgell (1997)	n/a	$2.0 \cdot 10^{-4}$
Specific yield, S_y	*BRGM (1976)*	---	5 –15 % (estimated)
Porosity, Φ	*This study*	1.1–36 %	23.30%
	BRGM (1976)	19–40 %	31%
	Aramco (1960)	7–37 %	30%
Permeability, k	*This Study*	0.2–12678 mD	1698 mD
	BRGM (1967)	240–11100 mD	2500 mD
	Aramco (1960)	2000–27000 mD	4500 mD

Aquifer Properties

Table 3 is a compilation of data on different properties of the aquifer. From these data and the present results, the Biyadh aquifer is a confined porous sandstone aquifer with a permeability varying on a high level, depending on the sedimentary facies. The cementation within the deposits is relatively poor and the primary intergranular porosity is largely conserved. Secondary porosity caused by fracturing and bedding planes is of minor importance. The aquifer contains large amounts of groundwater of generally good quality (TDS ~900–10,000 ppm). Applying different criteria and including different stratigraphic units (Biyadh, Wasia, Sakaka, Cretaceous sands), the estimated storage of the Wasia–Biyadh aquifer system is 390 billion m^3 (13,778 billion ft^3; MoEP, 2010) to 590 billion m^3 (20,836 billion ft^3; Al-Alawi and Abdul Razzak, 1994). Toward the east of the Arabian peninsula, the sandstones of the Biyadh Formation grade into an increasingly shaly facies where the formation can be considered an aquitard rather than an aquifer (GTZ/Dornier, 2011).

Wasia Aquifer

The Wasia aquifer is developed in the basal formations of the Wasia Group (Huraysan Formation in outcrop; Khafji and Safaniya Members in the subsurface) and is dominantly composed of sandstones. The lower and upper boundaries of the Wasia aquifer are the aquitard of the Sallah Formation and the Upper Wasia– Lower Aruma Shale, respectively. However, the Shu'aiba Formation as the subsurface equivalent of the Sallah Formation cannot be treated as an effective seal, as the hydraulic effectiveness remains doubtful and significant vertical leakage through this aquitard can be assumed (GTZ/Dornier, 2011). Farther east, the Shu'aiba formation even forms one of the best hydrocarbon reservoirs of the Arabian Peninsula. In the outcrop area and the adjacent subsurface, the Wasia and Biyadh aquifers are hydraulically connected and together form the Wasia–Biyadh aquifer, which is considered a principal aquifer in Saudi Arabia.

Diagenesis

Samples of moderately sorted, fine- to medium-grained quartz sandstone from the Huraysan Formation show that they are predominantly composed of angular, detrital quartz grains (Figure 31C, D). The visible intergranular porosity is relatively high (~30%) and possibly increased by secondary porosity (intragranular). Locally occurring patches of hematite covering grains and hematite cement in meniscus position might lower the permeability. However, the actual measured permeability (4348 mD) is relatively high.

In section B-1 (Figure 9), the Majma Formation overlies the Biyadh Formation unconformably and is represented by medium- to coarse-grained sandstones. Figure 31E reflects the typical lithology as it predominantly occurs in this area. The sandstones are of fluvial origin, composed of mainly angular

to subrounded, medium- to coarse-grained quartz grains, and are poorly to moderately sorted. In both the thin section and under the SEM (Figure 31E, F), visible high-intergranular porosity was observed (30%). Angular grains and etching casts indicate secondary porosity due to dissolution of earlier carbonate cement. Only thin relicts of silica overgrowth covering the detrital grains were observed sporadically; hence, the pore throats remained open, leading to very high permeability (6268 mD).

Fluvial medium-grained and moderately sorted quartz sandstone shows subangular to subrounded quartz grains, which display concave–convex contacts indicating compaction caused by sediment overload. Similar to the Biyadh Formation, this sandstone from the Majma Formation is cemented intensively by silica (Figure 31G, H). However, the cement generation observed in this sample differs markedly from the silica cements found in the sample of the Biyadh Formation and might be of different origin. Due to its silica cement, the sandstone is very tight and both porosity (3.3%) and permeability (5.6 mD) are strongly reduced.

Poorly to moderately sorted quartz sandstone with angular to subrounded grains represents the typical lithology for the lower part of the Majma Formation in the Khashm Wisi area (Figure 34A, B). The sandstone is very porous (34%) due to intergranular and secondary porosity that is probably caused by etching of grains. In the absence of cementation, permeability is also on a very high level (up to 1500 mD). Only thin relicts of silica overgrowth and small patches of hematite occur in meniscus position and the pore throats remain open. The presence of thin inherited silica overgrowth on some grains probably indicates reworking of earlier silica-cemented sandstone.

In the Majma Formation, medium- to coarse-grained quartz sandstone, poorly sorted and with very angular to sub-rounded grains, is regularly highly porous (41%) due to intergranular and secondary porosity (Figure 34C, D). The secondary porosity is caused by dissolution of earlier carbonate cement. Besides locally occurring patches of hematite and hematite in meniscus position, the sandstone is free of cements that would plug throats of pores and therefore remains very permeable (6900 mD).

In the upper part of the Majma Formation, a transition to finer-grained deposits was observed, where moderately sorted, fine-grained quartz siltstones with angular to subrounded grains are present. The siltstone is very porous (32%) due to secondary porosity and intergranular porosity (Figure 34E, F). However, the presence of abundant hematite and clay cement lowers the permeability (342 mD) considerably through plugging of pore throats.

In the Malihah Formation, moderately sorted, coarse to very coarse-grained sandstones with subangular to subrounded grains (Figure 34G, H) are common. The sandstone is very porous (26%) due to intergranular and secondary porosity (intragranular) that is caused by dissolution of former carbonate cement, which corroded surface of the grains. The permeability is also on a high level (12,000 mD) because only patches and seams of hematite occur in meniscus position and the pore throats remain open.

Fine- to medium-grained sandstones are moderately sorted. They are highly porous (39%) with intergranular and secondary porosity (Figure 35A, B). The secondary porosity resulted from the dissolution of earlier carbonate cement and corrosion of grains by etching. Only some patches of hematite cement occur in this sample, resulting in unplugged pore throats and high permeability (5865 mD).

Porosity and Permeability

Forty-three samples of the Wasia Group were taken and measured in regard to their porosity and permeability (Table 4). Most of the samples come from sections located in the areas of Khashm Wisi and Khushaym Radi, except some samples of the Majma Formation taken in a quarry northeast of Ar Riyadh.

The Wasia aquifer principally is formed by the Huraysan and Majma formations (and corresponding formations of the subsurface), which are composed of predominantly medium-grained sandstones and subordinate siltstone. The sandstones are mainly uncemented and provide good porosity (primary intergranular porosity) and permeability, whereas cementation of the siltstones is common and rather reduces the hydraulic properties. The results of 31 samples are shown in Table 5 for the Huraysan and Table 6 for the Majma Formation. In recent studies (GTZ/Dornier, 2009; MEWA, 2017b), the subsurface equivalents of the outcropping Qibah and Malihah Formations were considered to act as confining and impermeable layers capping the Wasia aquifer. However, observations during this study probably indicate good aquifer qualities for parts of these successions. The Qibah Formation is mainly composed of silt, clay, and some sandstone with a transition into marine carbonates, whereas the Malihah Formation comprises continental siliciclastic deposits ranging from coarse-grained sandstones to thick successions of fine-grained paleosols. Even though the correlative formations of the subsurface exhibit a facies with higher amounts of fine-grained sediments implicating very low values in permeability, the transition to the coarser-grained facies and its lateral extent into the subsurface should be considered with regard to its aquifer properties.

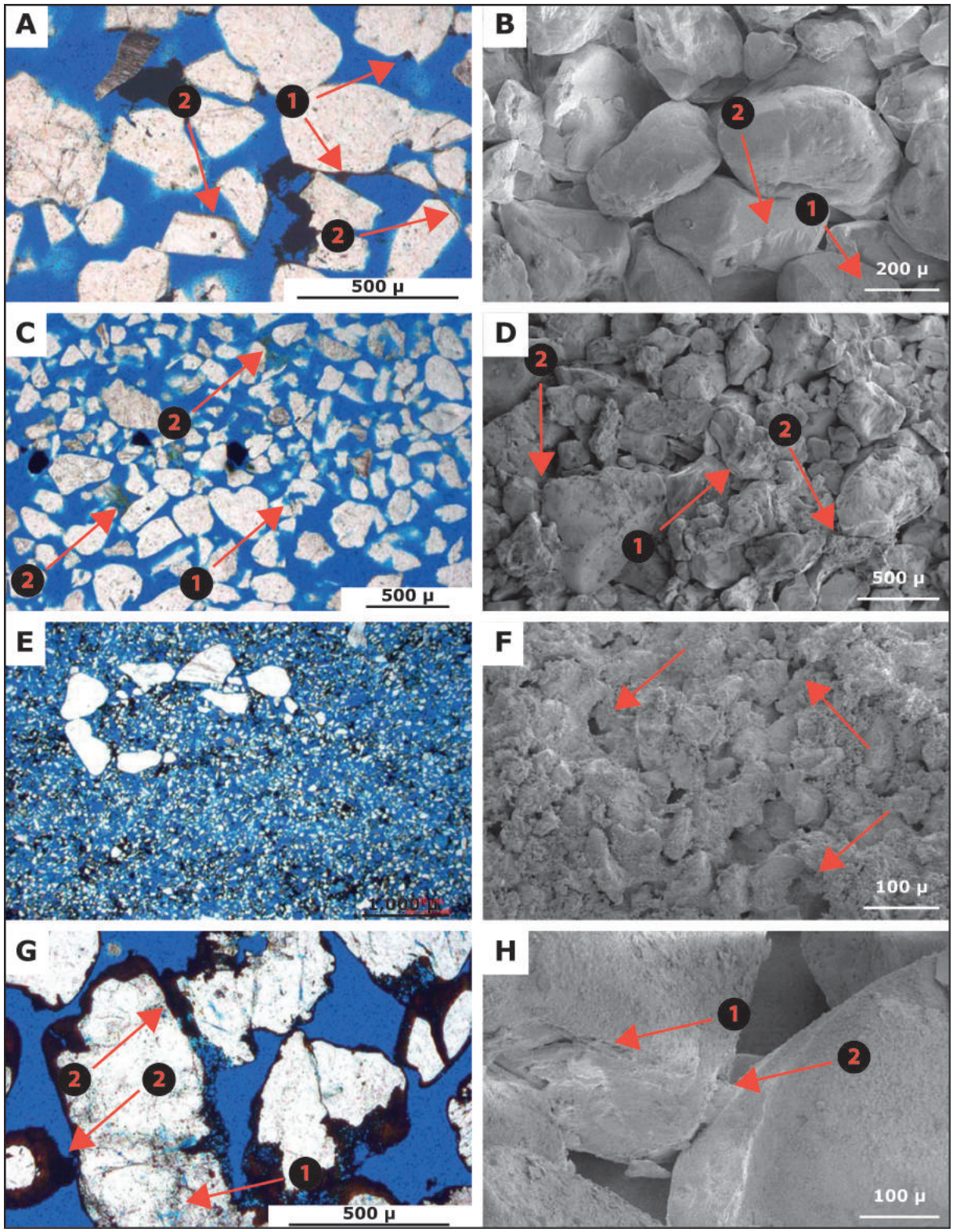

Figure 34. Diagenesis of the Majma and Malihah formations. (A, B) Poorly sorted quartz sandstone with angular to subrounded grains. (1) Sandstone is very porous due to intergranular and secondary porosity probably caused by etching of grains. (2) Locally, patches and seams of hematite occur in meniscus position. Sample 151. (C, D) Bimodal quartz sandstone with grain-size dependency on rounding. Small grains are angular, large grains subrounded to rounded. Sandstone is very porous due to (2) intergranular and secondary porosity probably caused by carbonate dissolution. (1) Locally, patches and seams of hematite occur in meniscus position. Sample 157. (E, F) Quartz siltstone. The quartz siltstone is well sorted except some large quartz grains. The quartz grains are mostly completely covered by hematite and clay cements that also plug the pore throats and reduce permeability. Arrows point to large pores that remained open. Sample 158. (G, H) Sandstone of the Malihah Formation. The sandstone is very porous due to (1) intergranular and intragranular porosity (secondary porosity) caused by dissolution of former carbonate cement that eroded the surfaces of detrital quartz grains. (2) Patches and seams of hematite cement are common and often located in meniscus position. Sample 180.

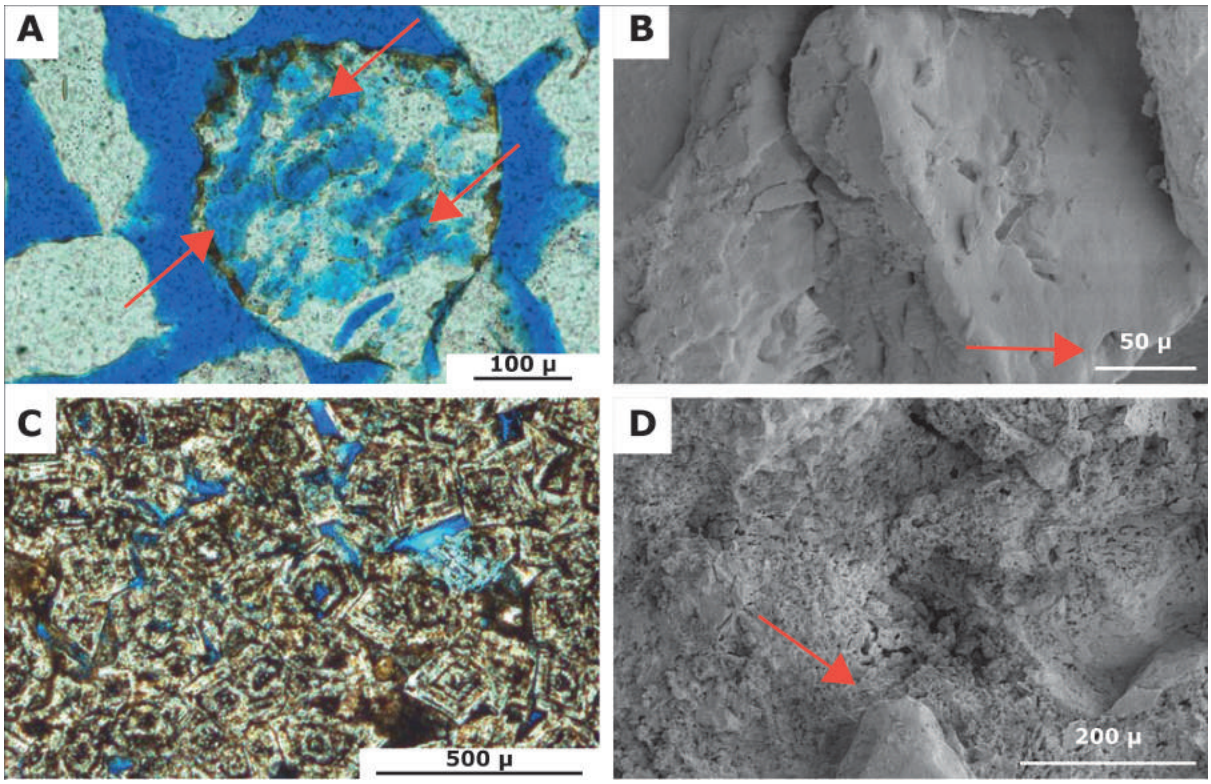

Figure 35. Diagenesis of the Malihah and Khanasir formations. (A, B) Quartz sandstone of the Malihah Formation. The sandstone is very porous due to intergranular and intragranular (secondary) porosity (arrows) caused by dissolution of former carbonate cement that etched the surfaces of detrital quartz grains. Sample 185. (C, D) Quartz-bearing dolosparite. The dolomite rhombohedra, visible in (D), reveal multicyclic formation as documented by various zones of intracrystalline secondary porosity. Floating sand grains (arrow) within the dolomite indicate very early diagenesis. Sample 187.

Table 4. Compilation of hydraulic properties of the Wasia aquifer.

Hydraulic Property	Author	Value range	Average value
Transmissivity, T	*BRGM (1976)*	$1.7 \cdot 10^{-3}$–$9.0 \cdot 10^{-2}$ m^2/s	$3.3 \cdot 10^{-2}$ m^2/s
	Bazuhair (1989)	n/a	$3.2 \cdot 10^{-2}$ m^2/s
	Edgell (1997)	$1.5 \cdot 10^{-2}$–$9.7 \cdot 10^{-2}$ m^2/s	n/a
Hydraulic conductivity, K	*BRGM (1976)*	$2.5 \cdot 10^{-4}$–$4.5 \cdot 10^{-4}$ m/s	$3.0 \cdot 10^{-4}$ m/s
	Bazuhair (1989)	$1.5 \cdot 10^{-4}$–$4.9\ 10^{-4}$ m/s	$3.2 \cdot 10^{-4}$ m/s
Storage coefficient, S	*BRGM (1976)*	$2.3 \cdot 10^{-4}$–$9.0 \cdot 10^{-4}$	$4.9 \cdot 10^{-4}$
	Bazuhair (1989)	n/a	$2.3 \cdot 10^{-7}$
	Edgell (1997)	n/a	$2.0 \cdot 10^{-4}$
Specific yield, S_y	*BRGM (1976)*	—	5–15 % (estimated)
Porosity, Φ	*This study*	3.3–41.3 %	29.46%
	BRGM (1976)	19–40 %	31%
	Aramco (1960)	7–37 %	30%
Permeability, k	*This Study*	0.7–15388 mD	2994 mD
	BRGM (1967)	240–11100 mD	2500 mD
	Aramco (1960)	2000–27000 mD	4500 mD

Table 5. Porosity and permeability data for the Huraysan Formation.

Sample ID	Sample Name	Lithology	Z [mD]	X/Y -Average [mD]	Total Perm. [mD]	Intrinsic Perm. [mD]	Porosity %
142	BH-1	Qtz Sdst.	*n.m.*	*n.m.*	*n.m.*	*n.m.*	*n.m.*
143	BH-2	Qtz Sdst.	4583.7	4230.71	4348.37	*n.m.*	33.58%
144	BH-3	Qtz Sdst.	*n.m.*	*n.m.*	*n.m.*	*n.m.*	*n.m.*
145	BH-4	Qtz Sdst.	*n.m.*	*n.m.*	*n.m.*	*n.m.*	32.00%
146	BH-5	Qtz Sdst.	2065.43	4823.17	3903.92	4366.5	31.32%
147	BH-6	Qtz Sdst.	*n.m.*	*n.m.*	*n.m.*	*n.m.*	31.99%
148	BH-7	Qtz Sdst.	*n.m.*	*n.m.*	*n.m.*	*n.m.*	30.18%
149	BH-8	Qtz Sdst.	*n.m.*	*n.m.*	*n.m.*	*n.m.*	23.84%

Hence, 12 samples of the Qibah (Table 7) and Malihah (Table 8) formations also were studied to consider their quality as subordinate aquifer or aquitard, respectively.

Most of the results for the Huraysan and Majma formations show high values in porosity and permeability (Figure 32). The porosity ranges between 30 and 38% for most of the samples with exception of a few samples, which exhibit cementation by silica, clay minerals, or iron oxides (3–25%). The permeability of both formations is relatively high in uncemented sandstones (2000–10,000 mD), whereas in cemented sandstones, the pores are partly clogged and permeability

Table 6. Porosity and permeability data for the Majma Formation.

Sample ID	Sample Name	Lithology	Z [mD]	X/Y -Average [mD]	Total Perm. [mD]	Intrinsic Perm. [mD]	Porosity %
150	BH-9	Qtz Sdst.	14140.2	16012.38	*n.m.*	*n.m.*	32.94%
151	BH-10	Qtz Sdst.	8007.82	11842.47	15388.32	412.96	33.86%
152	BH-11	Qtz Sdst.	*n.m.*	*n.m.*	10564.26	8785.8	38.31%
153	BH-12	Qtz Sdst.	*n.m.*	*n.m.*	*n.m.*	*n.m.*	30.47%
154	BH-13	Qtz Sdst.	5005.41	11133.75	*n.m.*	*n.m.*	29.00%
155	BH-15	Qtz Sdst.	*n.m.*	*n.m.*	9090.97	3511.5	33.44%
156	BH-16	Qtz Sdst.	6781.65	6960.33	*n.m.*	*n.m.*	30.57%
157	BH-17	Qtz Sdst.	102.93	315.73	6900.77	*n.m.*	32.87%
158	BH-18	Qtz Siltsone	*n.m.*	*n.m.*	244.79	342.64	41.27%
159	BH-19	Qtz Sdst.	*n.m.*	*n.m.*	*n.m.*	*n.m.*	*n.m.*
160	BH-19/1	Qtz Sdst.	475.34	326.45	*n.m.*	*n.m.*	34.97%
165	5	Qtz Sdst.	0.88	1.69	376.08	431.6	25.99%
166	6	Clayey Qtz Sdst.	9135.89	4835.01	1.42	0.043	22.63%
167	7	Qtz Sdst.	11862.08	7119.54	6268.63	6001.16	30.09%
168	8	Qtz Sdst.	8004.62	7924.94	8700.39	32.335	30.43%
169	9	Qtz Sdst.	2.87	6.955	7951.5	2979.5	30.85%
170	10	Qtz Sdst.	67.35	12.81	5.59	0.0025	3.32%
171	11	Qtz Sdst.	30.62	40.9	30.99	35.99	5.33%
191	MaKr-2	Siltstone	620.07	820.66	37.47	52.28	34.01%
193	MaKr-4	Siltstone	*n.m.*	*n.m.*	753.79	329.59	36.34%
194	MaKr-5	Qtz Sdst.	227.18	90.63	*n.m.*	*n.m.*	33.33%
195	MaKr-6	Qtz Sdst.	6.57	4.605	136.14	481.51	31.87%
217	MaKr-1	Sandy Siltst.	*n.m.*	*n.m.*	5.26	2.003	24.10%

Table 7. Porosity and permeability data for the Qibah Formation.

Sample ID	Sample Name	Lithology	Z [mD]	X/Y -Average [mD]	Total Perm. [mD]	Intrinsic Perm. [mD]	Porosity %
196	QKR-4	Qtz Sdst.	964.25	245.51	458.09	246.91	29.01%
218	QKR-2	Sandy dolomite	1.98	0.04	0.05	3.91	6.05%

is drastically reduced (<60 mD). The siltstones are well sorted and very porous (26–41%) with local patches of hematite cement that slightly reduces the permeability (70–800 mD). Porosity values close to the maximum porosity of clean unconsolidated sand are rather unusual in sedimentary rocks and might point to systematic errors during measurement. However, it is well known by drilling companies (e.g., R. Salvi, personal communication, 2012) that the Wasia sediments indeed are almost unconsolidated sands even at drilling depths of several hundreds of meters, posing major problems for drilling, well efficiency, and long-term well operation.

The porosity and permeability for deposits of the Qibah Formation are primarily relatively low due to the high content of clay and dolomite (Figure 32). However, intercalations of fine-grained sandstones show practicable values, especially in vertical permeability (Figure 33) caused by vertical burrows. Very low permeability and porosity was measured for a dolomite sample of the upper part of the formation (Figure 32). However, these dolomites are laterally not persistent (only up to 300 m [984 ft] wide), and moldic porosity is very abundant in this succession so that connected molds possibly provide good pathways for fluids.

Compared to the Qibah Formation, the Malihah Formation is composed of mainly coarse to medium-grained sand bodies with intercalations of siltstones and locally occurring bauxitic paleosols overlying the formation. Due to the irregularity of sedimentary characteristics like bedding or bioturbation and regional distinctions of cementation, the porosity and permeability values are slightly varying (Figure 32). Except for the fine-grained paleosols and intercalations of clay, the permeabilities are relatively high in sandstones (1200–23,000 mD) and moderate in siltstones (400 mD). The porosities of the sandstones range from 32% to 35% with the exception of a sample that is cemented by patches of hematite reducing porosity to 6%, whereas the permeability remained on a high level (Figure 32). The siltstones are very porous (<42%) and cemented by patches of hematite that probably reduces the permeability. Accumulations of clay probably plugged the previous sediments in the bauxitic top layers and permeability is limited to a minimum.

Similar to the data of the Biyadh aquifer, the horizontal and vertical permeability of the Wasia aquifer exhibits almost no anisotropy (Figure 33). The samples consist of mainly uncemented, friable, and cross-bedded sandstones that are only slightly influenced by bioturbation. The sandstones and the intensively silicified samples of the Majma Formation are rather isotropic. The data of the Huraysan samples

Table 8. Porosity and permeability data for the Malihah Formation.

Sample ID	Sample Name	Lithology	Z [mD]	X/Y -Average [mD]	Total Perm. [mD]	Intrinsic Perm. [mD]	Porosity %
178	F-1	Qtz Sdst.	12930.58	14100.27	13710.37	2645.8	32.34%
179	F-1/1	Qtz Sdst.	27504.76	21578.29	23553.78	2802.5	32.78%
180	F-1/2	Qtz Sdst.	9294.13	13621.87	12179.29	3205.5	25.91%
181	F-2	Qtz Siltstone.	854.9	176.71	402.77	96.93	41.77%
182	F-3	Qtz Sdst.	2165.5	1.56	1083.53	2264.6	35.30%
183	F-3/1	Qtz Sdst.	7289.69	14609.77	12169.74	*n.m.*	34.46%
184	F-4	Qtz Sdst.	6609.74	8496.59	7867.64	4352.1	33.41%
185	F-4/1	Qtz. Sdst.	3933.79	6830.82	5865.14	5891.2	31.94%
219	KR-2	Bauxite.	0.18	1.39	0.98	4.63	28.39%
220	KR-2/1	Bauxite.	*n.m.*	*n.m.*	*n.m.*	*n.m.*	17.65%

show a slight increase in vertical permeability probably caused by vertical pathways along coarser laminae of foresets. On the contrary, the permeability for siltstones that occur in the upper parts of the Malihah Formation appears to be more anisotropic (Figure 33). Whereas siltstones cemented by clay minerals or hematite exhibit a slight increase of horizontal values, the siltstones without significant cementation show a higher vertical permeability. This anisotropy is probably caused by fossil burrows of roots, plants, or animals that penetrate the deposits. Most of these burrows are filled with overlying sandy sediments or incrusted roots containing hollows, offering suitable flow paths and therefore increased permeabilities.

The porosity and permeability for deposits of the Qibah Formation are primarily relatively low due to the high content of clay and dolomite. However, intercalations of fine-grained sandstones show practicable values, especially in vertical permeability (Figure 33) caused by vertical burrows. Very low permeability and porosity were measured for a dolomite sample of the upper part of the formation (Figure 32). However, these dolomites are laterally not persistent (only up to 300 m [985 ft] wide). Moldic porosity is very abundant in these rocks so that connected molds possibly provide good pathways for fluids. Although of limited lateral extend, these features are most likely also present in other areas, where dolomites occur in the Qibah Formation.

Aquifer Properties

Table 4 is a compilation of data on different properties of the aquifer. From these data and the present results, the Wasia aquifer represents a confined porous sandstone aquifer with a permeability varying on a high level, depending on the sedimentary facies.

However, in the western part along the outcrop area of the Wasia Group, the aquifer exhibits unconfined conditions (GTZ/Dornier, 2011). It is composed of relatively poorly cemented, porous sandstones, containing a largely preserved primary intergranular porosity. Secondary porosity caused by fractures and bedding planes seems to be of minor importance. The suitability of the aquifer is decreasing from the western part of the study area, where the outcrops of the Wasia Formation are located, toward the eastern margin of the Arabian Peninsula. First, this is caused by facies changes into shales and carbonates on the distal Arabian platform; only locally (Burgan Sands, Kuwait) did siliciclastic detritus prograde that far east. The complex facies changes and the concomitant resulting stratigraphic nomenclature are documented by Christian (1997, 1998) and Ziegler (2001).

Second, while the quality of groundwater is generally good (TDS <1,500 ppm) near the recharge areas in the western part of the study area, it deteriorates toward the extreme eastern part, where values almost a hundred times higher (>150,000 ppm) are present. There, brines associated with oil field structures prevail within the aquifer. The gradient of increasing salinity of the groundwater is estimated to be about 50–1000 ppm/km (0.15–0.3 ppm/ft; GTZ/Dornier, 2011).

Aruma Aquifer

The Aruma aquifer is composed of deposits of the Late Cretaceous and constitutes a regional source for groundwater. The Aruma aquifer represents a secondary aquifer of predominantly carbonates with subordinate shales (Khanasir and Hajajah formations) that passes upward into the shaly and marly deposits of the Lina Formation, which originated in the early Paleogene. The lower boundary of the aquifer is the uppermost shaly deposits of the Wasia Group (Malihah Formation). At the top, the aquifer is bounded by the rather impermeable shales and marls of the Lina Formation that unconformably rests upon the older formations of the Aruma Group. The lithology of the Aruma Group is laterally largely uniform in the central and northern parts of the study area; however, its southern sandy facies is part of the Cretaceous sands aquifer.

Diagenesis

Only one sample from the still siliciclastically influenced lowermost part of Khanasir Formation was studied for diagenesis. This sandy dolomite is crystalline and bears floating quartz grains of reworked subjacent deposits (Figure 35C, D). The floating of quartz grains indicates a very early diagenetic formation of the dolomite. The dolomite crystals are developed as rhombohedra and reflect a multicycled formation as documented by various zones of intracrystalline secondary porosity. However, interparticle porosity is poor and the fabric is very dense, resulting in low porosity (10%) and permeability (0.75 mD).

Porosity and Permeability

The Aruma aquifer is a thick succession built of two calcareous formations (Khanasir and Hajajah formations) that is capped by an impermeable layer of

predominantly shales (Lina Formation). The aquifer itself is mainly composed of limestones and dolomitic limestones with subordinate intercalations of shales. Since the carbonates of these formations are predominantly dense and solid, the drilling and cutting of samples was unproblematic. Thus, a wealth of data was obtained for the entire aquifer regarding porosity and permeability. Since in carbonate rocks, fracturing and karstification are often, but not always exclusively the dominant factors controlling aquifer yield, the data on permeability and porosity reflect the primary sedimentologic and "early" diagenetic components of reservoir quality.

Eighty-one samples were taken from rocks of the aquifer, 42 from the Khanasir Formation (Table 9) and 39 from the Hajajah Formation. Additional 14 samples were measured from dolomites of the Lina Formation to control the hydraulic properties of this aquitard as well.

Except for a transitional facies of sand and sandy dolomite at the base of the formation, the Khanasir Formation comprises mainly limestones and dolomitic limestones with only differences of small-scale in porosity and permeability. The carbonates are classified as mud-, wacke-, and local packstones with a dense fabric constituting porosities up to 17% (Figure 32). The permeability averages about 1 mD (0.01–4 mD), except some samples of nodular and clayey limestones reaching 10–75 mD probably due to secondary openings. It is conspicuous that most of the samples showing higher values for both porosity and permeability are from dolomitic limestones, thus indicating a possible interrelation between dolomitization, pore space geometry, and permeability.

The sandy facies at the base of the formation is only a few meters (a few feet) thick but shows some distinct differences in hydraulic properties compared to the overlying carbonates (Figure 32). The presence of detrital quartz grains causes intergranular pore spaces resulting in porosities between 30% and 35%. Although the sand- and siltstones are mainly agglutinated by patches of dolomitic cements, the permeability reaches a level of almost 6000 mD. The overlying dolomitic quartz sandstone is entirely cemented with a porosity of only 14% and permeability of 3 mD. The quartz bearing crystalline dolomite is relatively dense with a porosity of 6–21% and permeabilities between 0.7 and 14 mD. However, on a macro-scale, the dolomite contains abundant dissolution vugs that are partly filled with calcite and probably could multiply the total permeability about a thousand times.

Regarding the porosity and permeability, the Hajajah Formation is very similar to the Khanasir Formation as its hydraulic properties are also controlled by the different textures of the carbonates (Figure 32, Table 10). The formation is composed of limestones, dolomitic limestones, dolomites, and subordinate shales. The carbonates are predominantly mud-, wacke-, pack-, and grainstones with subordinate float- or rudstones. Locally, the limestones represent biostromes with a baffle- or framestone texture. On average, the porosity tends to be higher in the Hajajah Formation, possibly due to the presence of more coarse-grained carbonates and a higher degree in dolomitization. The values range between 1% and 4% for dense mudstones, 8% and 14% for grainstones, and reach about 24% for porous framestones (Figure 32). The values of the other carbonate types are irregularly spread ranging between 5% and 21%. Higher values usually correspond to dolomitic limestones. The permeability ranges on a low level between 0.1 and 14 mD and seems to be rather independent of the carbonate type with exception of the framestone reaching about 40 mD.

The anisotropy of the permeability seems to be similar for both the Khanasir and Hajajah formations (Figure 33). The most data measured for the vertical permeability approximate the horizontal permeability indicating a more isotropic behavior. A few exceptions show aberrations of higher flow rates in vertical and horizontal directions probably caused by the presence of cracks or fissures that probably originated as a result of burial and diagenesis. These secondary openings in turn are mostly sealed by precipitated calcite or clay minerals in the course of pressure solution and stylolite formation. On a macro-scale, sedimentary structures like bedding planes and cross-beds in grainstones as well as nodular fabrics might influence the isotropy of permeability.

The Lina Formation overlies the Aruma aquifer and is considered to be an aquitard separating the older Aruma sediments from the Paleocene Umm Er Radhuma aquifer. The Lina Formation mainly consists of dolomitic shales with subordinate intercalations of dolomitic limestones and dolomites (Table 11). The carbonates are mainly fine-grained mudstones and wackestones with a relative dense fabric. Porosities range between 4 and 21%, probably according to the degree of dolomitization, and the permeability does not exceed 28 mD (Figure 32). The permeability seems to be mainly higher in horizontal directions possibly influenced by bedding planes or diagenetic processes (Figure 33).

Because the shale deposits are laterally persistent throughout the formation, the very poor hydraulic properties of the carbonate intercalations can be neglected and the Lina Formation can be assumed to be an impermeable layer of regional extent.

Table 9. Porosity and permeability data for the Khanasir Formation.

Sample ID	Sample Name	Lithology	Z [mD]	X/Y -Average [mD]	Total Perm. [mD]	Intrinsic Perm. [mD]	Porosity %
186	F-5	Dolom. qtz-sdst.	4.21	5.17	4.85	0.977	13.81%
187	F-6	Sandy dolomite	0.76	0.74	0.75	0.502	9.82%
188	F-6/1	Sandy dolomite	35.26	3.735	14.24	1.718	6.28%
189	F-7	Limestone	3.25	2.905	3.02	0.417	12.07%
190	F-7/1	Limestone	*n.m.*	*n.m.*	*n.m.*	*n.m.*	*n.m.*
225	K-1/1	Limestone	0.13	0.03	0.06	0	1.20%
226	K-2/2	Limestone	0.05	0.085	0.07	0.001	9.53%
227	K-3	Limestone	0.25	0.14	0.18	0.455	11.28%
228	K-3/1	Chalky limestone	0.2	3.475	2.38	0.018	9.85%
229	K-4/1	Chalky limestone	21.28	16.16	17.87	1.353	12.77%
230	K-5	Limestone	5.24	5.3	5.28	2.216	12.49%
231	K-6/3	Chalky limestone	0.25	0.24	0.25	0.007	12.48%
294	K-2/1	Limestone	0.21	0.415	0.35	0.006	8.63%
239	C-1	Marly limestone	0.8	1.505	1.27	29.307	11.55%
240	C-1/1	Marly limestone	12.01	11.43	11.63	5.5178	6.59%
241	C-2	Dolom. claystone	*n.m.*	*n.m.*	*n.m.*	*n.m.*	37.68%
242	C-3	Dolom. limestone	*n.m.*	*n.m.*	*n.m.*	*n.m.*	*n.m.*
243	C-4	Dolom. limestone	*n.m.*	*n.m.*	*n.m.*	*n.m.*	11.38%
248	D-1	Limestone	0.16	2.975	2.04	0.001	1.62%
249	D-1/1	Limestone	0.53	0.025	0.2	5.787	2.29%
250	D-2	Limestone	0.21	0.105	0.14	0.002	2.65%
251	D-2/1	Limestone	0.12	0.665	0.48	0.001	2.55%
252	D-2/2	Limestone	0.17	5.86	3.97	0.007	5.26%
253	D-2/3	Limestone	0.17	0.11	0.13	0.006	3.56%
254	D-3	Limestone	0.32	0.245	0.27	0.285	8.70%
255	D-3/1	Limestone	1.93	2.725	2.46	1.844	9.88%
256	D-3/2	Limestone	0.17	0.38	0.31	0.032	4.01%
281	P-1	Limestone	6.7	8.87	8.14	21.8	5.11%
282	P-2	Limestone	0.45	0.83	0.7	150.24	10.57%
283	P-3	Marly limestone	0.76	1.745	1.42	0.587	9.46%
284	P-4	Dolom. limestone	0.5	1.64	1.26	0.236	9.79%
285	P-5	Dolom. limestone	0.32	0.975	0.76	0.06	9.79%
286	P-6	Chalky limestone	0.53	1.285	1.03	0.04	11.09%
287	P-7	Limestone	1.23	2.78	2.27	0.745	14.64%
288	P-8	Dolom. limestone	0.56	0.585	0.58	0.341	7.77%
289	P-9	Dolom. limestone	4.27	1.735	2.58	0.383	12.57%
290	P-10	Limestone	2.07	5.41	4.3	0.277	16.57%
291	P-11	Limestone	0.38	0.245	0.29	0.003	7.25%
292	P-12	Dolomite	1.87	3.16	2.73	1.743	16.17%
293	P-13	Sandy dolomite	1.5	8.98	6.48	2.141	20.67%

Table 10. Porosity and permeability data for the Hajajah Formation.

Sample ID	Sample Name	Lithology	Z [mD]	X/Y -Average [mD]	Total Perm. [mD]	Intrinsic Perm. [mD]	Porosity %
232	K-7	Dolom. limestone	0.17	0.2	0.19	0.005	5.38%
233	K-7/1	Dolom. limestone	0.71	1.09	0.96	0.41	6.76%
234	K-8	Dolom. limestone	0.54	0.25	0.34	0.005	1.25%
235	K-9/2	Limestone	0.17	8.76	5.89	0.001	0.91%
236	HA-1	Chalky framestone	20.98	47.46	38.63	15.93	23.48%
237	HA-1/1	Chalky limestone	2.5	6.04	4.86	0.42	13.46%
238	HA-1/2	Chalky limestone	*n.m.*	*n.m.*	*n.m.*	1.2941	15.72%
244	C-5	Dolom. limestone	1.45	3.39	2.74	1.33	19.78%
245	C-5/1	Dolom. limestone	6.11	1.945	3.33	0.37	17.87%
246	C-6	Dolom. limestone	1.12	4.71	3.51	0.354	16.55%
247	C-6/1	Dolom. limestone	0.99	12.075	8.38	0.14	16.58%
257	L-1	Limestone	0.17	0.46	0.36	0.025	9.95%
258	L-1/1	Limestone	7.13	5.075	5.76	0.27	18.16%
259	L-2	Limestone	3.36	1.145	1.88	7.86	11.74%
260	L-2/1	Limestone	0.52	0.715	0.65	0.12	10.14%
261	L-3	Limestone	0.44	0.33	0.36	0.47	9.50%
262	L-3/1	Limestone	0.59	0.47	0.51	0.94	6.16%
263	L-4	Dolom. limestone	0.12	0.2	0.18	0.001	3.11%
264	L-4/1	Dolom. limestone	0.25	3.58	2.47	0.057	1.47%
265	L-6	Limestone	18.16	12.74	14.54	16.39	13.00%
266	L-6/1	Limestone	10.06	10.54	10.37	8.61	8.41%
267	H-1	Dolom. limestone	0.36	0.415	0.4	6838.5	14.93%
268	H-2	Limestone	2.59	4.4	3.8	1.85	20.91%
269	H-3	Limestone	0.03	0.24	0.17	0.04	3.20%
270	H-3/1	Limestone	0.42	0.44	0.43	0.007	6.73%
272	H-5/1	Limestone	*n.m.*	*n.m.*	*n.m.*	0.23	9.20%
273	H-5/2	Limestone	2.55	2.23	2.33	0.001	1.05%
274	H-6	Limestone	0.29	0.5	0.42	0	1.82%
275	H-7/1	Limestone	0.86	1.33	1.18	0.6	13.52%
276	H-8/1	Limestone	0.35	0.49	0.44	0.047	6.23%
277	H-8/2	Limestone	0.11	0.18	0.16	6.62	6.95%
278	H-8/3	Limestone	0.7	2.59	1.96	1.9	11.65%
279	H-9	Limestone	1.77	1.03	1.27	0.04	6.85%
280	H-9/3	Limestone	0.42	0.32	0.35	1.88	2.13%
305	S-9	Limestone	2.16	4.82	3.93	8.67	5.28%
306	S-10	Limestone	0.69	1.66	1.33	0.25	6.03%
307	S-11	Limestone	0.18	0.35	0.29	0.009	4.67%
308	S-12	Limestone	1.33	3.05	2.47	2.35	8.46%
309	S-13	Limestone	1.33	2.29	1.97	3.39	7.71%

Table 11. Porosity and permeability data for the Lina Formation.

Sample ID	Sample Name	Lithology	Z [mD]	X/Y -Average [mD]	Total Perm. [mD]	Intrinsic Perm. [mD]	Porosity %
173	HL-1	Dolom. limestone	0.45	2.86	2.05	0.15	6.96%
174	HL-2	Dolom. limestone	1.93	2.06	2.01	0.53	17.03%
175	HL-3	Limestone	0.74	1.31	1.12	7.83	3.62%
176	HL-4	Limestone	0.36	1.315	1	0.02	21.49%
177	HL-5	Dolom. limestone	14.48	2.77	6.67	0.08	16.64%
295	S-1	Dolom. limestone	0.28	0.5	0.43	0.002	3.86%
296	S-2	Chalky limestone	0.5	0.33	0.38	0.005	16.85%
297	S-3	Limestone	0.45	0.82	0.69	0.003	11.88%
298	S-4	Dolomite	0.57	1.81	1.39	0.1	14.82%
300	S-5	Dolomite	1.37	0.97	1.1	0.3	7.79%
301	S-5/1	Dolom. limestone	0.3	0.52	0.45	0.02	12.80%
302	S-6	Dolom. limestone	0.56	5.84	4.08	0.02	4.15%
303	S-7	Dolom. limestone	52.05	37.27	42.2	13.18	11.29%
304	S-8	Dolom. limestone	0.71	6.39	4.5	3.393	11.15%

(Hydro-) Stratigraphic Architecture of the Cretaceous and Conclusions

Stratigraphic Architecture of the Biyadh Formation

In the Ath Thumama area (Figure 4), section BWA-1 (Figure 12) consists of fine- to medium-grained, well sorted, and rounded quartz sandstones with planar and subordinate trough cross-bedding. Dominantly of fluvial origin, there is additionally a coastal flood plain–tidal influence in this area, indicated by an abundance of reactivation surfaces, mud drapes, and vertical burrows. Only some minor channels are present in this outcrop, draining toward the northeast. The flood plain deposits and their characteristic SGR expression are used to correlate this section (Figure 36) to section B-1 northeast of Ar Riyadh (Figure 4). The lithology of the middle part of the formation exposed there consists of medium- to fine-grained sandstones with subordinate silt- and claystone. A large system of amalgamated and stacked channels with lag deposits is developed. The channels are stacked in a cyclic way. Whereas the lower part of the succession shows mainly complete cycles of fluvial meandering systems, the upper part of the succession is dominated by tidal conditions as evidenced by sigmoidal-shaped cross-beds, reactivation surfaces between bed sets, and mud drapes covering foresets. Cycles are mostly incomplete through channel migration. The sandstones are tabular and trough cross-bedded indicating a paleo flow direction toward the northeast. They are predominantly well sorted and only consist of subrounded to rounded quartz grains.

It is conspicuous throughout these sections that almost no cementation is present, resulting in a very friable consistence of the rocks. Secondary porosity, observed in thin sections and SEM photographs, indicates dissolution of earlier calcareous cement (Figure 31C, D, G, H). However, some horizons of intensively silicified sandstones extend throughout the outcrop area and are probably bound to distinct horizontal surfaces. The detrital quartz grains are completely covered by silica overgrowths that almost entirely plug the pore space of the grain fabric (Figure 31A, B). Permeability is very low in these layers, which might act as regional aquicludes if they are of lateral extent. The exact origin of this multicyclic cementation is not clear at present and awaits further studies.

Some of the fine-grained units of the flood plain environment extend throughout the entire outcrop and might influence the aquifer properties if they are laterally persistent. In both sections, the upper part of the Biyadh Formation is truncated by the pre-Majma unconformity. Tracing the unconformity to the Khashm Wisi area (Figure 37), the Biyadh Formation reappears in section BKD-1 (Figure 11). Here, the upper part of the formation and its conformable transition into the Sallah Formation are exposed. The upper Biyadh deposits consist of fine-grained siliciclastic rocks of a coastal floodplain and a few carbonates of the adjacent marine tidal flat.

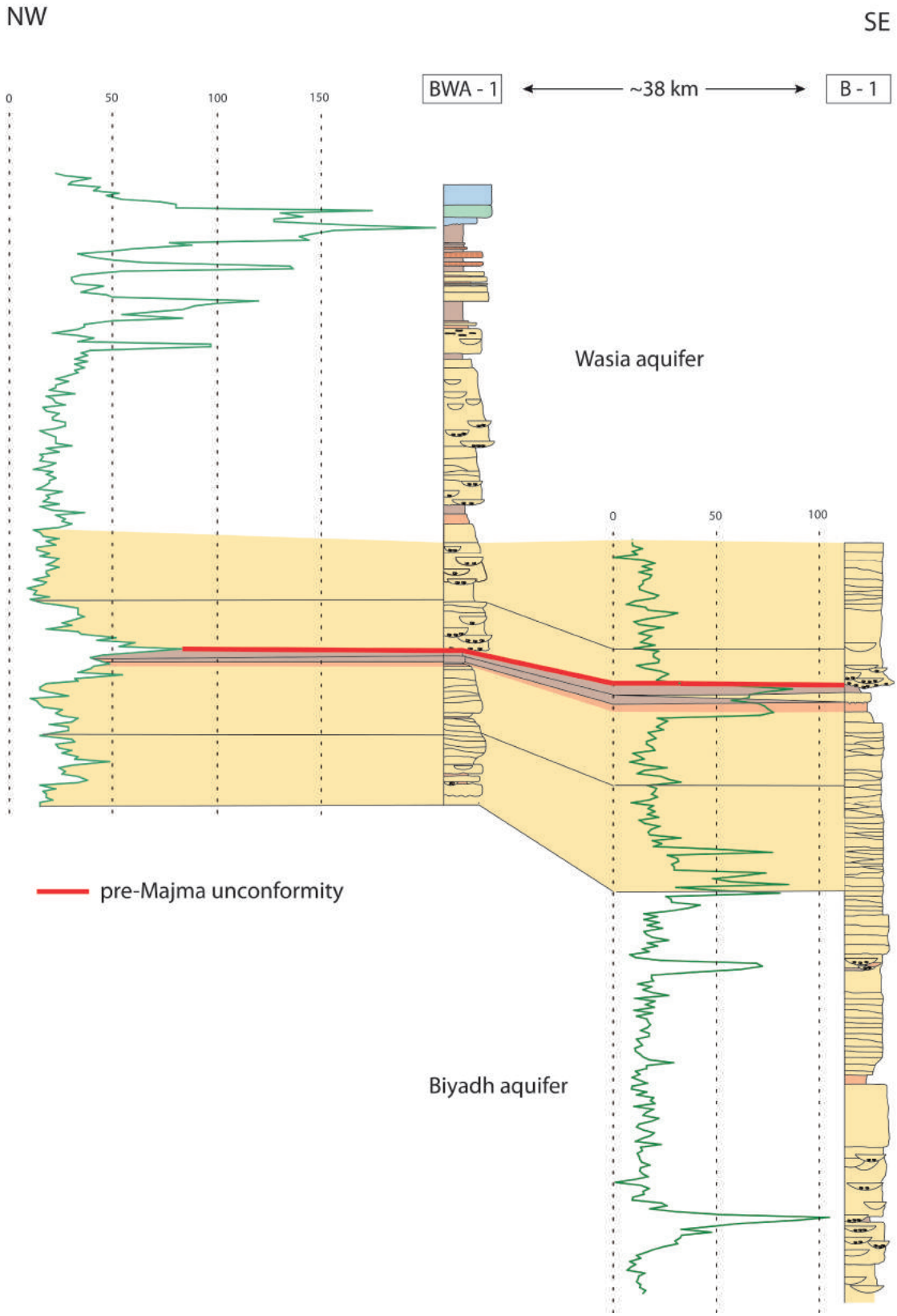

Figure 36. Correlation of the Biyadh and Wasia aquifers (red line) in sections BWA-1 (Figure 12) and B-1 (Figure 9) and corresponding gamma-ray logs (green, in API). Localities as in Figure 2.

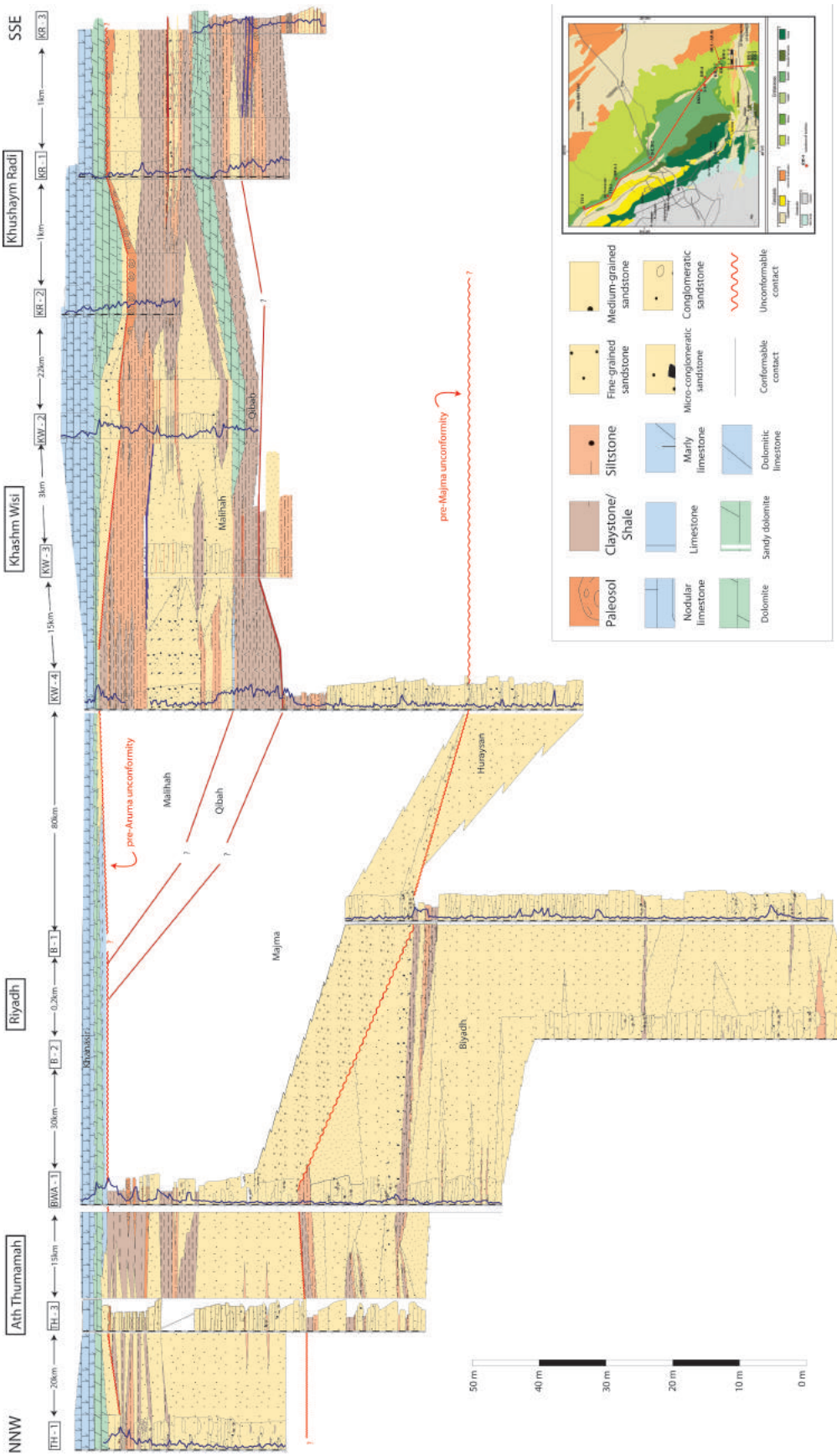

Figure 37. Stratigraphic architecture of the Cretaceous strata in the study area. Localities as in Figure 2.

Hydraulic Properties of the Biyadh Aquifer

The hydraulic properties of the Biyadh Formation are excellent (Table 3). Porosity of the sandstones ranges between 20% and 30% and permeability locally exceeds 10,000 mD. The pore space of the grain fabric is mainly free of hindering cementation except some areas where intensive silicification or infiltration by clayey material was found and reduce porosity and permeability of the rocks (Figure 38). Especially the almost impermeable silicified layers could have an influence on the aquifer's properties if they are of regional extent. Silica overgrowths almost close the pore space completely, reducing the porosity as well as permeability to a minimum (<10%, <20 mD). However, sandstones with high porosity and permeability prevail within the Biyadh Formation (Figure 38).

In contrast, the top deposits of the Biyadh Formation (Figures 11, 37) are mainly fine-grained silt- and claystones that represent transition to the shallow-marine deposits of the Sallah Formation. Although no samples were taken and measured from this section, the hydraulic properties of these sediments can be estimated to be poor. Hence, the upper Biyadh Formation and the Sallah Formation together form a regional aquitard to aquiclude (Figure 39).

Stratigraphic Architecture of the Wasia Group

The Wasia aquifer comprises deposits of the Huraysan and Majma formations. Outcrops of the Huraysan Formation are restricted to the southern study area (Figure 15); the Majma Formation occurs throughout the entire study area progressively truncating subjacent formations toward the north where it directly overlies the Biyadh Formation (Figure 37).

Huraysan Formation—In section KW-4 (Figure 15), the upper part of the Huraysan Formation is composed of medium- to coarse-grained, poor to moderately sorted sandstones that consist of angular to subrounded quartz grains. The predominantly poor sorting of grains and their angular shape indicate an environment of broad fluvial plains with braided rivers, located relatively near to the source area. The sandstones are arranged in stacking patterns of planar cross-beds that show incomplete fining-upward cycles to fine-grained ripple cross-bedded sandstones and only occasionally an uppermost thin bed of clay. The successions are amalgamated and slightly truncate each other at the boundary of the sequences. As rates of dune migration and accumulation are orders of magnitude faster than rates of subsidence, the amalgamation likely relates to (high rates of) vigorous sediment flux (Le Nindre et al., 2008). The sandstones are very friable and porous (30%; Figure 32) due to lack of cementation. Only some traces of hematite occur within the grain fabric (Figure 31C, D) resulting in wide-opened pores and high permeability (2000–4000 mD). Similar conditions and even coarser-grained sandstones were reported for the area south of Al Kharj, where the deposits of the Huraysan Formation correspond to a broad fluvial braided fan (Le Nindre et al., 2008).

Majma Formation—Deposits of the Majma Formation were observed in eight different sections from Khushaym Radi in the south of the study area toward Ath Thumamah in the north. The formation progressively truncates subjacent deposits toward the north where it directly overlies the Biyadh Formation (Figure 37). The thickness of the formation seems to increase proportional to the truncation toward the north where it comprises about 40 m (131 ft) of predominantly sandstone in section BWA-1 (Figure 9), TH-3 (Figure 8), and TH-1 (Figure 16). In this area, the Majma Formation dominantly represents the fill of an ancient fluvial valley, whose architecture has been described by Moshrif (1979, 1980, 1983) and Le Nindre et al. (2008). Toward the top of the formation, the lithology becomes finer-grained in the northern sections, where silt- and claystones containing abundant fragments of roots and plants point to the development of ancient soils. The Khanasir Formation of the Aruma Group truncates the top of the formation and a bauxitic horizon was observed beneath the unconformity.

In the area of Khashm Wisi (Figure 37), the Majma Formation still consists of a thick succession of fluvial siliciclastic rocks. The sandstones are mainly coarser than in the northern sections and the sorting and rounding of quartz grains is less distinct. In section KW-4 (Figure 15), the formation comprises about 30 m (98 ft) of deposits. The lower and middle parts of the formation reflect incomplete fining-upward cycles of mainly trough cross-bedded sandstones that often are arranged in channels containing coarse lag deposits at the bottom of troughs. Analog to sandstones of the subjacent Huraysan Formation, cementation is lacking in these deposits resulting in high porosity and permeability (Figures 32, 38). Toward the top of the Majma Formation, the sandstones grade into a finer-grained succession of silt- and claystones that reflecting heavily rooted paleosols. The top of the formation represents the transition to a fine-grained succession of the Qibah Formation, which locally shows evidence of marine ingression. The lithology

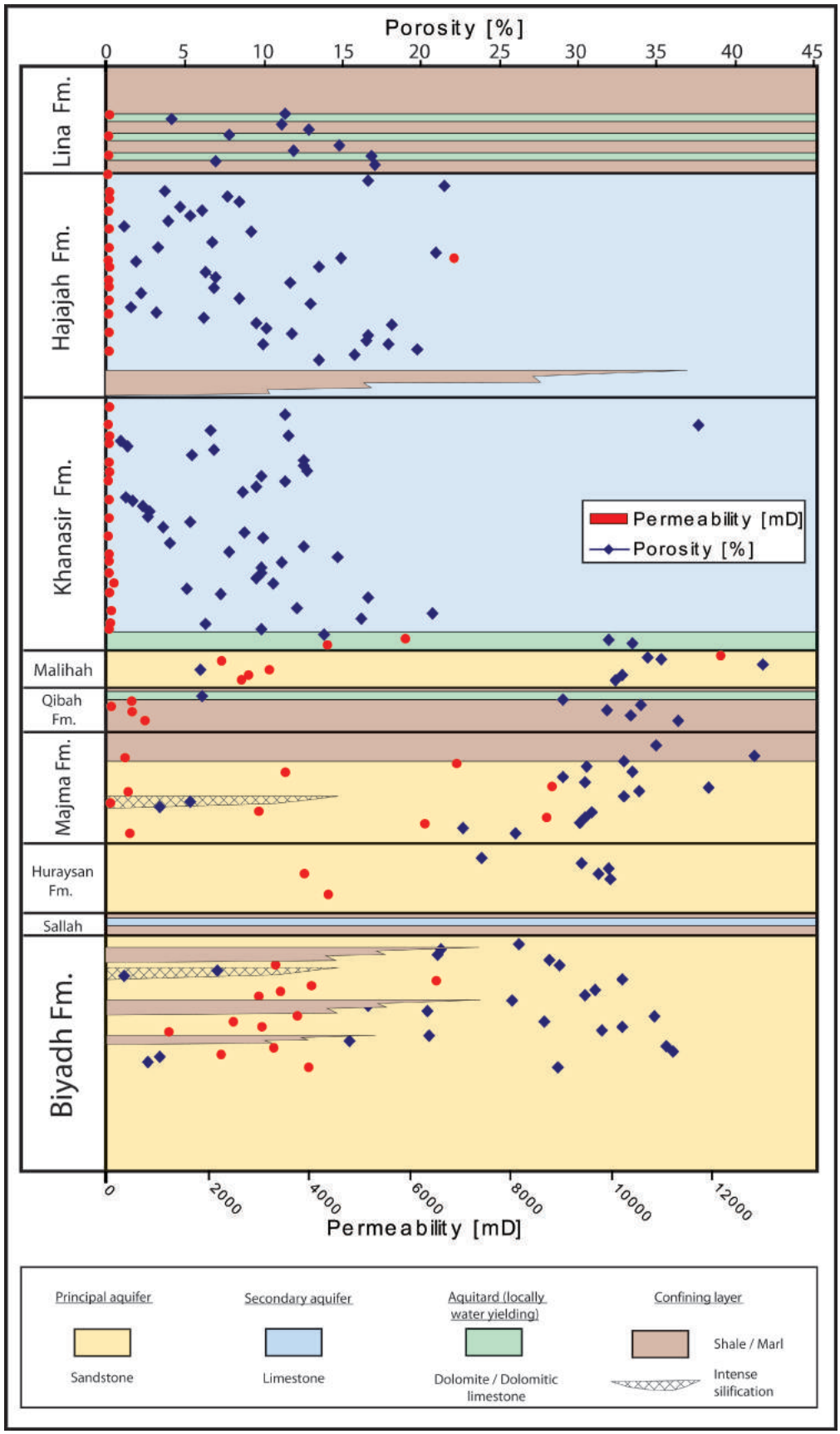

Figure 38. Simplified lithostratigraphy and hydraulic properties of the Cretaceous strata in the study area.

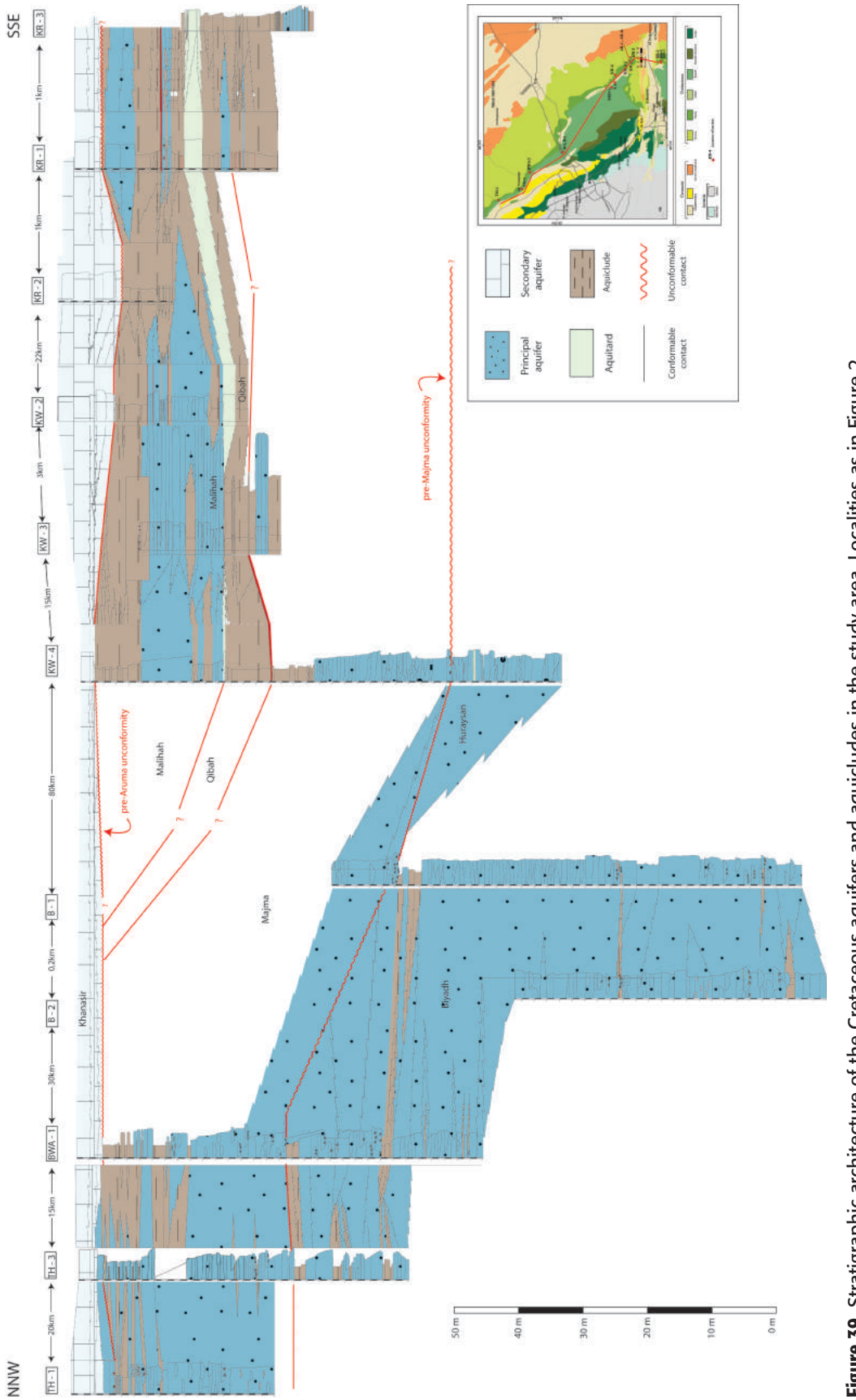

Figure 39. Stratigraphic architecture of the Cretaceous aquifers and aquicludes in the study area. Localities as in Figure 2.

of the Majma Formation seems to be rather uniform toward the area of Khushaym Radi (Figures 17, 18) in the south, where only slight differences in depositional style were observed. Here, the development of paleosols is more distinct and the deposits are finer grained (Figure 37).

Hydraulic Properties of the Wasia Aquifer

The sandstones of the Wasia aquifer usually possess a high visible intergranular porosity that remained open due to lack of cementation (Figure 31E, F). Secondary porosity caused by dissolution of earlier calcareous cements additionally increases the porosity to an average of 30%. Only locally, occurrence of patchy hematite and relicts of silica cement were observed during the study. These factors result in high permeability for the sandstones ranging from 4000 mD to locally more than 10,000 mD. In section B-1 (Figure 9), a horizon of intensive cementation by silica overgrowths is developed reducing the porosity and permeability to a minimum for this sandstone (Figure 31G, H). This phenomenon seems to be rather local, but if laterally extending, the horizon might act as an impermeable layer.

In the central parts of the study area, the siliciclastic rocks of the Huraysan Formation are directly overlain by the sandstones of the Majma Formation without an impermeable or confining unit separating them. Because the deposits of these two formations are rather similar in lithology and their hydraulic properties, the succession can be treated as a single-storey aquifer of very good quality (Figure 39; Table 4). Similarly, in the northern parts of the study area, the Majma Formation unconformably overlies the sandstones of the Biyadh Formation. The aquifers are locally separated by a fine-grained succession of the Biyadh Formation but are probably connected through hydraulic windows (Figure 39).

Toward the south, the upper part of the Majma Formation decreases slightly in grain size and probably loses its excellent qualities as aquifer in this part of the area.

Quality of the Aruma Aquifer

The Aruma aquifer is predominantly composed of shallow-marine carbonates of the Upper Cretaceous Khanasir and Hajajah formations. The lithology shows no significant changes in the studied sections and seems to be rather uniform throughout the study area (Figure 40).

The carbonates are predominantly mud-, wacke-, and packstones with a dense micritic fabric and very less intergranular porosity. The porosity (Figure 32) averages between 10 and 15% and permeability is mainly very low (0.01–100 mD; Figure 32). Locally, some grainstones, framestones, and dolomitic limestones occur that reach porosities up to 20% and moldic porosity occurs. However, the pores seem to be unconnected as the permeability of these rocks also remains very low. Additionally to the limestone successions, some intercalations of clayey deposits were observed in several parts of the formations resulting in impermeable and probably confining layers that further decrease the quality of this aquifer. The uppermost part of the Aruma Group is composed of shales with subordinate carbonates of the Lina Formation that acts as regional aquiclude overlying the Aruma aquifer (Figures 37, 39).

Regarding the porosity and permeability measured in samples taken from this aquifer, its hydraulic properties and therefore qualities as principal aquifer are poor (Figure 38). However, a high degree in fracturing and strong karstification of the calcareous formations result in abundant pathways for fluids and cause good storage capacities for the aquifer. Therefore, the Aruma aquifer can be treated as secondary aquifer.

ACKNOWLEDGMENTS

This chapter is part of the diploma thesis of D. Bohnsack as part of the aquifer study of the Wasia–Biyadh–Aruma aquifer system, carried out on behalf of the Ministry of Water and Electricity (MoWE, Saudi Arabia) by GTZ/DCo (now GIZ/DCo) in cooperation with the Technical University of Darmstadt and the Friedrich-Alexander University Erlangen–Nürnberg (Germany). We would like to thank the Ministry of Water and Electricity and its Dr. Mohammad Al-Saud, for his unlimited support. We would like to thank R. Rausch and J. Döhler (GTZ/DCo) for the logistic support provided. Thanks also to all personnel of GTZ/DCo, especially J. Karpiel, I. Abdul Qader, A. Al Noor, and A. Habte, who participated in field work and gave other support. Thanks also to the technicians at TU Darmstadt and FAU Erlangen for their help and stimulation and the lasting interest in the progress of the work. Special thanks to Y.-M. Le Nindre for his meticulous review, which helped to clarify many issues and to improve the manuscript considerably. Similarly, the thoughtful review of Ron Steel is gratefully acknowledged. Finally, we would like to thank Homoud Anzi (ARAMCO) for his encouragement to write this chapter and to continue with the process of review in busy times.

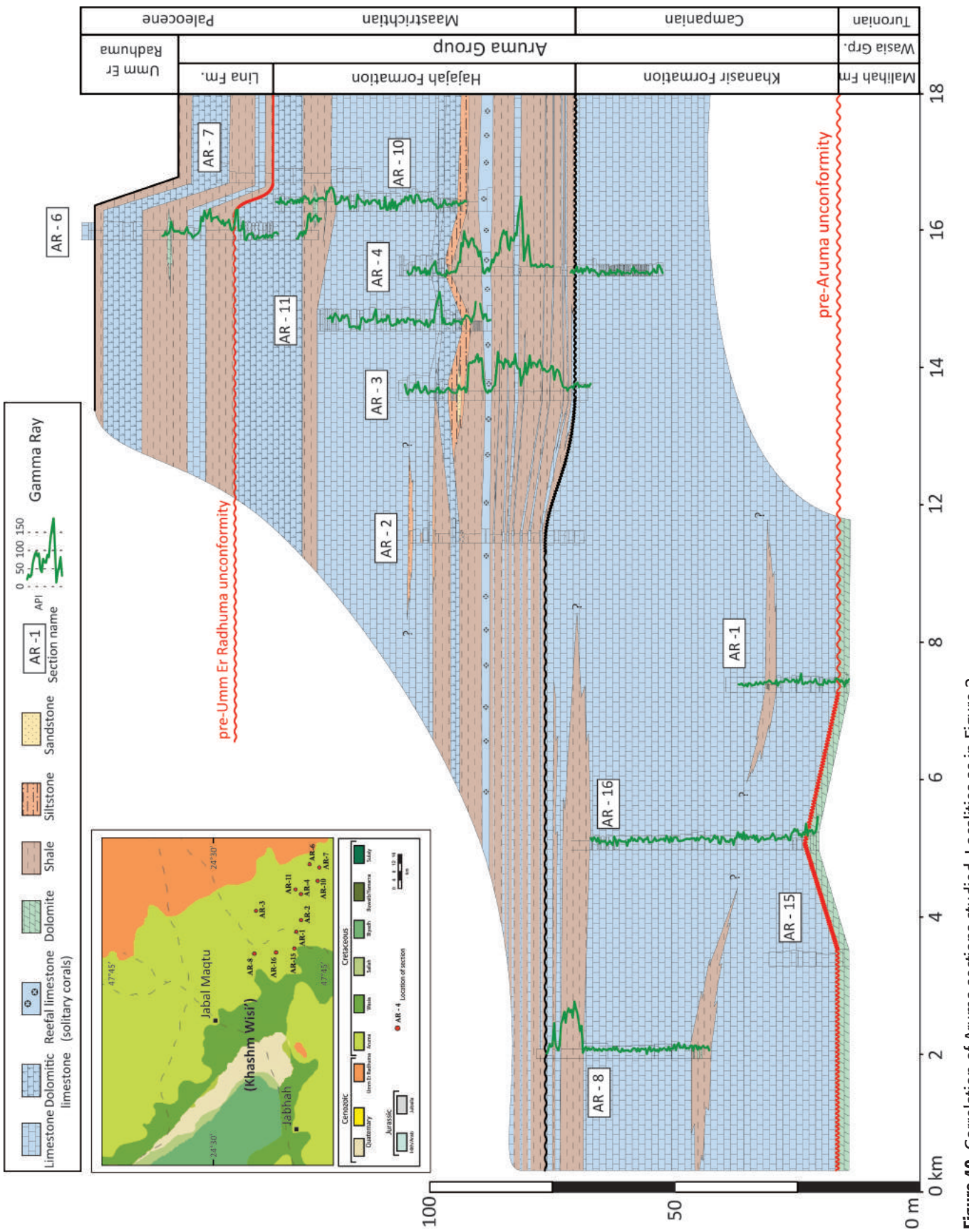

Figure 40. Correlation of Aruma sections studied. Localities as in Figure 2.

REFERENCES

Al-Alawi, J., and M. Abdul Razzak, 1994, Water in the Arab peninsula: Perspectives and prognoses, *in* P. Rogers and P. Lydon, eds., Water in the Arab world: Perspectives and prognoses: Cambridge, Massachusetts, Harvard University Press, p. 3–28.

Al-Husseini, M. I., 2000, Origin of the Arabian Plate structures: Amar Collision and Najd Rift: GeoArabia, v. 5, p. 527–542.

Al-Husseini, M. I., 2008, Middle East geological time scale 2008: Launch of the Middle East geologic time scale: GeoArabia, v. 13, p. 11 and p. 185–188.

Alsharhan, A. S., and A. E. M. Nairn, 1990, A review of the Cretaceous formations in the Arabian Peninsula and Gulf: Part III. Upper Cretaceous (Aruma Group) stratigraphy and paleogeography: Journal of Petroleum Geology, v. 13, p. 247–266.

ARAMCO, 1975, Eastern Arabia and adjacent areas, *in* J. F. Aubert, E. Couve de Murville, C. Dadrian, and H. Edmundson et al., eds., Well Evaluation Conference: Arabia, Services Techniques Schlumberger, p. 9–25.

Christian, L., 1997, Cretaceous subsurface geology of the Middle East region: GeoArabia, v. 2, p. 239–256.

Christian, L., 1998, Middle East Geological Map Series "MEGMaps": Manama, GulfPetrolink.

Davies, R. B., D. M. Casey, A. D. Horbury, P. R. Sharland, and M. D. Simmons, 2002, Early to mid-Cretaceous mixed carbonate-clastic shelfal systems: Examples, issues and models from the Arabian Plate: GeoArabia, v. 7, p. 541–598.

Davies, S. J., and T. Elliott, 1996, Spectral gamma ray characterization of high resolution sequence stratigraphy: Examples from Upper Carboniferous fluvio-deltaic systems, County Clare, Ireland, *in* A. Howell and F. Aitken, eds., High resolution sequence stratigraphy: Innovations and applications: Geological Society (London) Special Publication 104, p. 25–35.

Di Naccio, D., P. Boncio., S. Cirilli., F. Casaglia, E. Morettini, G. Lavecchia, and F. Brozzetti, 2005, Role of mechanical stratigraphy on fracture development in carbonate reservoirs: Insights from outcropping shallow-water carbonates in the Umbria–Marche Apennines, Italy: Journal of Volcanic and Geothermal Research, v. 148, p. 98–115.

Edgell, H. S., 1997, Aquifers of Saudi Arabia and their geological framework: Arabian Journal for Science and Engineering, v. 22, p. 3–31.

Ehrenberg, S. N., and T. A. Svånå, 2001, Use of spectral gamma-ray signature to interpret stratigraphic surfaces in carbonate strata: An example from the Finnmark carbonate platform (Carboniferous–Permian), Barents Sea: AAPG Bulletin, v. 85, p. 295–308.

El-Asaad, G. M., 1983a, Bio- and chronostratigraphy of the Aruma Formation in central Saudi Arabia, *in* A. Abed, and M. Khaled, eds., Proceedings of the First Jordanian Geological Conference: Jordanian Geologists Association Special Publication 1, p. 72–86.

El-Asaad, G. M., 1983b, Lithostratigraphy of the Aruma Formation in central Saudi Arabia, *in* A. Abed and M. Khaled, eds., Proceedings of the First Jordanian Geological Conference: Jordanian Geologists Association Special Publication 1, p. 87–111.

El-Asaad, G. M., 1989, *Loftusia arabica sp. nov.* (Foraminifera) from the Maastrichtian of central Saudi Arabia: Journal of Micropaleontology, v. 8, no. 1, p. 49–54.

Ellis, D. V., and J. M. Singer, 2007, Well logging for earth scientists: Springer, Dordrecht.

GTZ/Dornier, 2011, Detailed water resources studies of Wasia–Biyadh and Aruma aquifers: Riyadh, Ministry of Water and Electricity of the Kingdom of Saudi Arabia.

Goldstein, J. I., 2003, Scanning electron microscopy and X-ray microanalysis: New York City, Kluwer Academic, 689 p., DOI: 10.1007/978-1-4615-0215-9.

Gross, M. R., 2003, Mechanical stratigraphy: The brittle perspective: Geological Society of America, Abstracts with Programs, v. 35, p. 641.

Gross, M. R., M. P. Fischer, T. Engelder, and R. J. Greenfield, 1995, Factors controlling joint spacing in interbedded sedimentary rocks: Interpreting numerical models with field observations from the Monterey Formation, USA, *in* M. S. Ameen, ed., Fractography: Fracture topography as a tool in fracture mechanics and stress analysis: Geological Society of America Special Publication 92, p. 215–233.

Hiscock, K. M., 2005, Hydrogeology: Malden, Massachusetts, Blackwell Publishers, 408 p.

Hornung, J., and T. Aigner, 1999, Reservoir- and aquifer characterisation of fluvial architectural elements: Stubensandstein, Upper Triassic, South-West Germany: Sedimentary Geology, v. 129, p. 215–280.

Hornung, J., and T. Aigner, 2002a, Reservoir architecture in a terminal alluvial plain: An outcrop analogue study (Upper Triassic, Southern Germany). Part 1: Sedimentology and petrophysics: Journal of Petroleum Geology, v. 25, p. 11018.

Hornung, J., and T. Aigner, 2002b, Reservoir architecture in a terminal alluvial plain: An outcrop analogue study (Upper Triassic, Southern Germany). Part 2: Cyclicity, controls and models: Journal of Petroleum Geology, v. 25, p. 151–178.

Hornung, J., and T. Aigner, 2004, Sedimentäre Architektur und Poroperm-Analyse fluviatiler Sandsteine: Fallbeispiel Coburger Sandstein, Franken: Hallesches Jahrbuch für Geowissenschaften, Reihe B, v. 18, p. 121–138.

Koehrer, B., T. Aigner, H. Forke, and M. Pöppelreiter, 2012, Middle to Upper Khuff (Sequences KS1 to KS4) outcrop-equivalents in the Oman Mountains: Grainstone architecture on a subregional scale: GeoArabia, v. 17, p. 59–104.

Konert, G., A. M. Afifi, S. A. Al-Hajri, and H. J. Droste, 2001, Paleozoic stratigraphy and hydrocarbon habitat of the Arabian Plate: GeoArabia, v. 6, p. 407–442.

Le Nindre, Y. M., J. Manivit, H. Manivit, and D. Vaslet, 1990, Stratigraphie séquentielle du Jurassique et du Crétacé en Arabie Saoudite: Bulletin Société Geologique France, v. 8, p. 1025–1034.

Le Nindre, Y. M., D. Vaslet, S. S. Maddah, and M. I. Al-Husseini, 2008, Stratigraphy of the Valanginian? to Early Paleocene succession in central Saudi Arabia outcrops: Implication for regional Arabian sequence stratigraphy: GeoArabia, v. 13, p. 51–86.

Lebret, P., M. A. Halawani, A. Memesh, C. Bourdillon, D. Janjou, Y.-M. Le Nindre, J. Roger, H. Shorbaji, and

H. Kurdi, 1999, Explanatory notes to the geologic map of the Turubah Quadrangle, Kingdom of Saudi Arabia: Geoscience Map GM-139, scale 1:250.000, sheet 28F, 46 p.

MEWA, 2017a, Detailed water resources studies of the Khuff–Jilh–Minjur–Dhruma and overlying aquifers—main report: Riyadh, Ministry of Environment, Water and Agriculture, 79 p.

MEWA, 2017b, Detailed groundwater resources studies in the Rub' Al Khali Desert—main report: Riyadh, Ministry of Environment, Water and Agriculture, 61 p.

Miall, A. D., 1996, The geology of fluvial deposits, Springer, Berlin, 582 p., DOI: 10.1007/978-3-662-03237-4.

MoEP, 2010, Assessment and strategic plan of the water sector: Riyadh, Kingdom of Saudi Arabia, Ministry of Economy and Planning, 159 p.

Moshrif, M. A., 1979, Depositional environments of the Buwaib–Biyadh–Wasia rocks deduced by X-ray diffraction analysis: Journal of Faculty of Science, King Saud University, Riyadh, v. 10, p. 123–141.

Moshrif, M. A., 1980, Recognition of fluvial environments in the Biyadh–Wasia sandstones (Lower-Middle Cretaceous) as revealed by textural analysis: Journal of Sedimentary Petrology, v. 50, p. 603–612.

Moshrif, M. A., 1983, Fining-upward cycles in the Biyadh–Wasia Sandstones (Lower–Middle Cretaceous) in central Saudi Arabia: Journal of College of Science, Riyadh, v. 14, p. 145–156.

Navidtalab, A., H. Rahimpour-Bonab, A. Nazari-Badii, and M. Sarfi, 2014, Challenges in deep basin sequence stratigraphy: A case study from the Early–Middle Cretaceous of SW Zagros: Facies, v. 60, p. 195–215, doi: 10.1007/s10347-013-0377-x.

North, C. P., and M. Boering, 1999, Spectral gamma-ray logging for facies discrimination in mixed fluvial-eolian successions: A cautionary tale: AAPG Bulletin, v. 83, p. 155–169.

Obermaier, M., T. Aigner, and H. C. Forke, 2012, Facies, sequence stratigraphy and reservoir/seal potential of a Jilh Formation outcrop equivalent (Wadi Sahtan, Triassic, Upper Mahil Member, Sultanate of Oman): GeoArabia, v. 17, p. 85–128.

Obermaier, M., N. Ritzmann, and T. Aigner, 2015, Multilevel stratigraphic heterogeneities in a Triassic shoal grainstone, Oman Mountains, Sultanate of Oman: Layercake or shingles?: GeoArabia, v. 20, p. 115–142.

Pettijohn, F. J., 1983, Sedimentary rocks: New York, Harper and Row, 628 p.

Philip, J. M., J. Roger, D. Vaslet, F. Cecca, S. Gardin, S., and A. M. S. Memesh, 2002, Sequence stratigraphy, biostratigraphy and paleontology of the Maastrichtian-Paleocene Aruma Formation in outcrop in Saudi Arabia: GeoArabia, v. 7, p. 699–718.

Pöppelreiter, M., C. Schneider, M. Obermaier, H. C. Forke, B. Koehrer, B., and T. Aigner, 2011, Seal turns into reservoir: Sudair equivalents in outcrops, Al Jabal al-Akhdar, Sultanate of Oman: GeoArabia, v. 16, p. 69–108.

Powers, R. W., 1968, Saudi Arabia (excluding Arabian Shield): Lexique stratigraphique international Asie, p. 1–177.

Powers, R. W., L. F. Ramirez, C. D. Redmond, and E. L. Elberg Jr., 1966, Geology of the Arabian Peninsula: U.S. Geological Survey, Professional Paper 560-D, 147p.

Reineck, H., and I. B. Singh, 1980, Depositional sedimentary environments: Berlin, Springer, 549 p.

Robelin, C., M. S. Al-Muallem, J. M. Brosse, J. Fourniget, M. Garcin, J. F. Gouyet, M. A. Halawani, D. Janjou, and Y. M. Le Nindre, 1994, Geologic Map of the Qibah quadrangle, sheet 27G: Geoscience Map GM-136, scale 1:250.000: Explanatory notes, 33 p.

Schlumberger, 1982, Natural gamma-ray spectrometry: Essentials of N. G. S. interpretation: Houston, Texas, Schlumberger, 69 p.

Sharland, P. R., P. Archer, D. M. Casey, R. B. Davies, S. H. Hall, A. P. Heward, A. D. Horbury, and M. D. Simmons, 2001, Arabian Plate sequence stratigraphy: GeoArabia Special Publication 2, 371 p.

Sharland, P. R., D. M. Casey, R. B. Davies, M. D. Simmons, and O. E. Sutcliffe, 2004, Arabian Plate Sequence Stratigraphy—Revision to SP2: GeoArabia, v. 9, p. 199–214.

Thomas, H., M. Roger, M. A. Halawani, M. Memesh, P. Lebret, C. Bourdillon, E. Buffetaut, et al., 1999, Late Paleocene to Early Eocene marine vertebrates from the uppermost Aruma Formation (northern Saudi Arabia, implications for the K-T transition: Comptes Rendus de l'Académie des Sciences de Paris, v. 329, p. 905–912.

Vaslet, D., C. Pellaton, J. Manivit, Y.-M. Le Nindre, J.-M. Brosse, and J. Fourniguet, 1985, Geologic map of the Sulayyimah Quadrangle, Kingdom of Saudi Arabia: Geoscience Map GM-100C, scale 1:250,000, sheet 21H: Explanatory notes, 31 p.

Vaslet, D., M. S. Al Muallem, S. S. Maddah, J. M. Brosse, J. Fourniguet, J. Breton, and Y. M. Le Nindre, 1991, Geologic map of the Ar Riyad quadrangle: Geoscience Map GM-121, scale 1:250.000, sheet 24I: Explanatory notes, 54 p.

Ziegler, M. A., 2001, Late Permian to Holocene paleofacies evolution of the Arabian Plate and its hydrocarbon occurrences: GeoArabia, v. 6, p. 445–504.

Zötl, J. G., 2006, Der geologische Aufbau der Arabischen Halbinsel, *in* W. Dostal, ed., Tribale Gesellschaften der südwestlichen Regionen des Königreiches Saudi Arabien: Verlag der Österreichischen Akademie der Wissenschaften, p. 481–516.